

UC San Diego

UC San Diego Electronic Theses and Dissertations

Title

Ligand specificity and conformational states of the acetylcholine binding protein, a nicotinic receptor surrogate

Permalink

<https://escholarship.org/uc/item/49p5m05v>

Author

Hansen, Scott B.

Publication Date

2005

Peer reviewed|Thesis/dissertation

UNIVERSITY OF CALIFORNIA, SAN DIEGO

Ligand Specificity and Conformational States of the Acetylcholine Binding Protein, a
Nicotinic Receptor Surrogate

A dissertation submitted in partial satisfaction of the
requirements for the degree Doctor of Philosophy

in

Chemistry and Biochemistry

by

Scott B Hansen

Committee in charge:

Professor Palmer Taylor, Chair
Professor Elizabeth A. Komives, Co-chair
Professor Roger Y. Tsien
Professor Mauricio Montal
Professor Kyriacos C. Nicolaou

2005

Copyright

Scott B Hansen, 2005

All rights reserved

The dissertation of Scott B Hansen is approved, and it is
acceptable in quality and form for publication on microfilm:

K.C. Nicolazzo

M. Monroe

Roger Tyson

Elizabeth A. Kerie

Co-Chair

John J. ...

Chair

University of California, San Diego

2005

TABLE OF CONTENTS

	Signature Page.....	iii
	Table of Contents.....	iv
	List of Abbreviations.....	viii
	List of Figures.....	xi
	List of Tables.....	xiv
	Acknowledgments.....	xv
	Vita, Field of Study, and Publications.....	xvii
	Abstract of the Dissertation.....	xx
I.	Introduction to the Nicotinic Acetylcholine Receptor.....	1
	A. Historical Development.....	1
	B. Nicotinic Receptor Subtypes.....	3
	C. Agonists and Antagonists of Nicotinic Receptors.....	3
	1. Agonists.....	5
	2. Antagonists.....	5
	D. The Acetylcholine Binding Protein.....	7
	E. Fluorescence Spectroscopy.....	10
	1. Intrinsic Tryptophan Fluorescence.....	10
	2. Fluorescence Resonance Energy Transfer (FRET).....	10
	F. X-ray crystallography.....	11
	1. Crystallization.....	11
	2. X-ray Diffraction.....	13
	3. Structure Assembly and Refinement.....	13
	G. Dissertation Objective.....	17
	H. References.....	18
II.	Gene Synthesis, Protein Production, Subunit Assembly and Ligand Binding of the Acetylcholine Binding Protein.....	20
	A. Synthesis of AChBP Genes (cDNA) from Synthetic Oligonucleotides.....	20
	1. <i>Lymnaea</i> AChBP Gene.....	22
	2. <i>Aplysia</i> AChBP Gene.....	22
	B. Mammalian Expression and Purification of Secreted AChBP.....	22

1.	AChBP Gene Stably Transfected into HEK 293 Cells.	22
2.	AChBP Gene Stably Transfected into GnTI HEK Cells.....	23
3.	Immuno-affinity Purification of Secreted AChBP.....	26
C.	AChBP Gating of an AChBP/5HT _{3A} Chimera	26
D.	Discussion.....	27
E.	References.....	31
III.	Tryptophan Fluorescence Reveals Conformational Changes in the Acetylcholine Binding Protein.....	32
A.	Abstract.....	32
B.	Introduction.....	32
C.	Experimental Procedures.....	33
1.	Gene Synthesis and Protein Expression.....	33
2.	Fluorescence Assays.....	34
3.	Stopped-flow Kinetics.....	34
D.	Results and Discussion.....	35
E.	Acknowledgements.....	45
F.	References.....	46
IV.	Structural and Ligand Recognition Characteristics of an Acetylcholine Binding Protein from <i>Aplysia californica</i>	48
A.	Abstract.....	48
B.	Introduction.....	48
C.	Experimental Procedures.....	50
1.	Construction of an Expression Vector cDNA.....	50
2.	Fast Protein Liquid Chromatography.....	51
3.	Sedimentation Equilibrium Analysis.....	51
4.	Estimation of Binding Parameter from Fluorescence Signals.....	52
5.	pH Stability of AChBP's.....	52
6.	Stopped-flow Kinetics.....	53
D.	Results.....	53
1.	Expression of the Acetylcholine Binding Protein from a Synthetic Gene.....	53
2.	Characterization of the Binding Protein.....	54
3.	Ligand Binding Properties.....	63
E.	Discussion.....	67
1.	Synthesis, Assembly and Stability of the Acetylcholine Binding Protein.....	69
2.	Determinants of Ligand Specificity.....	71
F.	Acknowledgments.....	73
G.	References.....	74

V.	Insights into Intrinsic Tryptophan Fluorescence of the Acetylcholine Binding Protein.....	76
	A. Abstract.....	76
	B. Background.....	76
	C. Methods.....	77
	1. Mutagenesis.....	77
	2. Expression and Purification of AChBP.....	77
	3. Radioligand Binding Assay.....	78
	4. Fluorescence Emission.....	78
	5. Crystallization.....	79
	6. Structure Refinement.....	79
	D. Results.....	79
	1. Tryptophan Mutations.....	79
	2. Radioligand Competition Assays.....	82
	3. Emission of Intrinsic Tryptophan Fluorescence.....	82
	4. Crystal Structure of Apo <i>Aplysia</i> Y55W.....	86
	E. Discussion.....	86
	1. Expression of <i>Lymnaea</i> AChBP Tryptophan Mutants.....	92
	2. Ligand Binding of <i>Lymnaea</i> vs. <i>Aplysia</i> AChBP.....	92
	3. Tryptophan Fluorescence.....	93
	F. Conclusion.....	95
	G. References.....	96
VI.	Structures of <i>Aplysia</i> AChBP Complexes with Nicotinic Agonists and Antagonists Reveal Distinct Binding Interfaces and Conformations.....	98
	A. Abstract.....	98
	B. Introduction.....	98
	C. Results and Discussion.....	101
	1. Determination and Quality of the Structure.....	101
	2. Structure of A-AChBP in the Apo Form.....	102
	3. Apo A-AChBP versus the Muscle-type $\alpha 1$ Subunit.....	109
	4. Antagonist Binding.....	110
	a. The α -Conotoxin ImI-AChBP Complex.....	110
	b. The Methyllaconitine-AChBP Complex.....	115
	5. Agonist Binding.....	116
	a. The Lobeline-AChBP Complex.....	116
	b. The Epibatidine-AChBP Complex.....	118
	6. Conformational Fit for Antagonists and Agonists.....	119
	7. Ligand Selectivity.....	122
	D. Concluding Remarks.....	125

E.	Materials and Methods.....	125
1.	Protein Expression and Purification.....	125
2.	Ligand Binding.....	126
3.	Crystallization and Data Collection.....	126
4.	Structure Determination and Refinement.....	127
F.	Acknowledgments.....	129
G.	References.....	130
VII.	Summary and Implications.....	133
A.	Protein Expression.....	133
1.	Gene Synthesis.....	133
2.	Mammalian Expression and Glc-NAc Transferase I deficient Cells.....	133
3.	<i>Aplysia</i> vs. <i>Lymnaea</i> AChBP as a Surrogate.....	134
B.	Ligand Binding Assays.....	135
1.	Steady-state Equilibrium.....	135
2.	Stopped-flow Fluorescence.....	136
C.	Frequency Resonance Energy Transfer (FRET) to the dansylcholine acceptor.....	136
D.	Contributions to Receptor Knowledge.....	138
E.	The nAChR as a Drug Target.....	138
1.	Structural Basis of Agonism and Antagonism.....	139
2.	Competitive Ligand Binding Pocket-Energetics.....	139
F.	Conformations and Receptor Activation.....	142
G.	Structural Basis of Partial Agonism.....	143
H.	Future Implications.....	146
I.	References.....	147

LIST OF ABBREVIATIONS

AChE	acetylcholinesterase
A-AChBP	<i>Aplysia californica</i> acetylcholine binding protein
ab	antibody
AChBP	acetylcholine binding protein
AMoRe	molecular replacement program
bgtx	α -bungarotoxin
BSA	bovine serum albumin
cbtx	α -cobratoxin
CMV	cytomegalovirus
Ctx or ImI	α -conotoxin ImI
Dansyl	Dansylcholine
EPI	epibatidine
FRET	fluorescence resonance energy transfer
HEK	human embryonic kidney
L-AChBP	<i>Lymnaea stagnalis</i> acetylcholine binding protein
LBD	ligand binding domain
LOB	lobeline
MAD	multiwavelength anomalous diffraction
MLA	methyllycaconitine
nAChR	nicotinic acetylcholine receptor

NIC	nicotine
PBS	phosphate buffered saline
PCR	polymerase chain reaction
PO	phosphate buffer
PPT	preprotrypsin
REFMAC	macromolecular refinement program
SDS-PAGE	Sodium dodecyl sulfate polyacrylamide gel electrophoresis
<i>sp</i>	<i>species</i>
TBS	Tris buffered saline
TD	transmembrane domain

Amino Acid Residues

Ala or A	alanine
Arg or R	arginine
Asn or N	asparagine
Asp or D	aspartate
Cys or C	cysteine
Glu or E	glutamate
Gln or Q	glutamine
Gly or G	glycine
His or H	histidine
Ile or I	isoleucine

Lys or K	lysine
Leu or L	leucine
Met or M	methionine
Phe or F	phenylalanine
Pro or P	proline
Ser or S	serine
Thr or T	threonine
Trp or W	tryptophan
Tyr or Y	tyrosine
Val or V	valine

LIST OF FIGURES

Chapter I	
I.1	Phylogenetic relationship of nAChR subtypes..... 4
I.2	Structures for some common nicotinic agonists and antagonists..... 6
I.3	Sequence alignment of mollusk AChBPs with nicotinic acetylcholine receptor subtypes..... 8
I.4	Crystal structure of <i>Lymnaea</i> AChBP..... 9
I.5	Tryptophan and dansyl FRET partners..... 12
I.6	Hanging drop method of crystallization..... 14
I.7	Schematic of X-ray diffraction 15
I.8	X-Ray diffraction 16
Chapter II	
II.1	Schematic of AChBP gene synthesis 21
II.2	Structure of N-linked glycosylation in GnTI HEK cells..... 24
II.3	SDS-PAGE and FPLC profiles of GnTI expressed AChBP..... 25
II.4	Coupling of AChBP to the 5HT-3 ion pore..... 28
II.5	AChBP/5HT-3 chimera gating currents..... 29
Chapter III	
III.1	Characterization of acetylcholine binding protein (AChBP)..... 36
III.2	Equilibrium titration of AChBP with α -bungarotoxin and epibatidine 37
III.3	Kinetics of ligand association with AChBP..... 39
III.4	Docking of gallamine to the AChBP using DOT..... 44
Chapter IV	
IV.1	Protein sequence alignments 55
IV.2	AChBP cDNA constructs used to characterize the acetylcholine

	binding protein.....	56
IV.3	FPLC of AChBP's	59
IV.4	SDS-PAGE of the purified acetylcholine binding proteins.....	60
IV.5	Analytical ultracentrifugation of <i>Aplysia</i> AChBP.....	61
IV.6	pH Stability of the AChBP's	62
IV.7	Steady state of ligand binding to AChBP's.....	64
IV.8	Titration of ligand stoichiometry	68
Chapter V		
V.1	Sequence alignment showing tryptophans	80
V.2	Location of <i>Lymnaea</i> AChBP tryptophans	81
V.3	Scintillation proximity assay of wild type <i>Aplysia</i> AChBP	84
V.4	Steady-state fluorescence emissions of wt <i>Aplysia</i> and <i>Lymnaea</i> AChBP.....	87
V.5	Steady-state fluorescence emissions of mutant <i>Aplysia</i> and <i>Lymnaea</i> AChBP.....	88
V.6	Crystal structure of apo <i>Aplysia</i> Y55W	90
V.7	Aromatic binding pocket with agonist bound to wild type <i>Aplysia</i> and <i>Lymnaea</i> AChBP	91
Chapter VI		
VI.1	Sequence alignment of A-AChBP with ligand selective side chains highlighted.....	103
VI.2	Schematic view of the organic ligands.....	104
VI.3	Overall view of the Apo A-AChBP structure and structural comparisons.....	105
VI.4	The A-AChBP subunit interface in the antagonist and agonist complexes.....	112

VI.5	Expanded views of the bound ligands.....	113
VI.6	Conformational fit mechanism and ligand selectivity	120
Chapter VII		
VII.1	Fluorescence competition with limiting volumes.....	137
VII.2	Alignment of nAChR subtypes with AChBP and potential selective residues.....	140
VII.3	The competitive ligand binding pocket.....	141
VII.4	Residue and loop positions in AChBP	144
VII.5	Model for partial agonism.....	145

LIST OF TABLES

Chapter III	
III.1	AChBP ligand binding kinetics..... 40
Chapter IV	
IV.1	Properties of the acetylcholine binding proteins from <i>Lymnaea</i> and <i>Aplysia</i> 57
IV.2	Dissociation constants for ligand binding to the <i>Aplysia</i> and <i>Lymnaea</i> acetylcholine binding proteins..... 65
IV.3	Kinetic constants for association and dissociation of various ligands for the acetylcholine binding proteins..... 66
Chapter V	
V.1	Expression of AChBP tryptophan mutants in HEK 293 cells..... 83
V.2	Dissociation constants for various ligands with wild-type and mutant AChBP..... 85
V.3	Fractional Fluorescence at 340nm of various ligands complexes with wild type and mutant AChBP's..... 89
Chapter VI	
VI.1	Ligand dissociation constants for the two AChBP species..... 106
VI.2	Data collection and refinement statistics..... 107

ACKNOWLEDGMENTS

I thank my mentor and advisor, Dr. Palmer Taylor. This work is a reflection of his patience, guidance, and wisdom. Dr. Taylor provided every means necessary to accomplish this work. In particular, I am grateful for his confidence and generous means to complete these studies. I credit Dr. Taylor for my personal development as a scientist. Dr Taylor exemplifies hard work, humility, generosity, patience, and scientific insightfulness. He consistently asks the important questions with a spark of brilliance. Without exception, I have trusted his advice. I will always cherish my opportunity to work under his tutelage.

I thank all members of the Taylor lab past and present who contributed to this work. I especially recognize Zoran Radić for his skill and contribution with the fluorescence studies. I thank Todd Talley for innumerable discussions, both scientific and social. Todd contributed in most aspects of this work in particular by finding a reliable radioligand assay. I thank Ryan Hibbs for daily contributions to experiments and discussion, Lori Jennings and Jian Shi for mass spectrometry data, Meghan Miller and Jessie Coward with mutagenesis experiments, and Davide Comoletti for assistance with analytical centrifugation. I thank Shelley Camp for help with molecular biology and organizing the lab and Pam Tetu for her clerical assistance. Others contributing are Brian Molles, Warren Lewis, Igor Tsigelny, Sventja Von Daake and Robyn Flynn.

I am grateful to Yves Bourne and Pascale Marchot for allowing me to work in their laboratories in Marseille, France; and to Gerlind Sulzenbacher for her hard work refining structures and teaching me crystallography. I thank Tom Huxford in the

laboratory of Gourisanker Ghosh for materials and teaching protein me crystallization and crystallography. I thank Choel Kim and Susan Taylor for providing synchrotron time and in aiding X-ray data collection and processing. I am grateful to Steven M. Sine at the Mayo Clinic for fruitful collaborations including the coupling of the acetylcholine binding protein to an ion pore.

Lastly I thank my family. First, I am grateful to my mother who taught me math at a young age; instilling a confidence and a foundation for the sciences. Later, my parents with little means, sacrificed greatly to support me through a bachelors of science degree. I am grateful to my brother Andrew for many hours of discussion and for preparing of the intellectual property related to this work. I feel my family and the successes of this thesis have been blessings given to me.

Chapter III, in full, is a reprint of the material as it appears in *Journal of Biological Chemistry* 2002, Hansen SB, Radic Z, Talley TT, Molles BE, Deerinck T, Tsigelny I, and Taylor P., American Society for Biochemistry and Molecular Biology, 2002. Chapter IV, in full, is a reprint of the material as it appears in *The Journal of Biological Chemistry* 2004, Hansen SB, Talley TT, Radic Z, and Taylor P. American Society for Biochemistry and Molecular Biology, 2004. Chapter VI, in full, is a reprint of the material as it appears in *European Molecular Biology Organization* 2004, Hansen SB, Talley TT, Radic Z, and Taylor P. Nature Publishing Group 2005. The dissertation author was the primary investigator and single author of these papers.

VITA

- 1999 B.S., Utah State University
- 2001-2005 Research Associate, University of California, San Diego
- 2003-2005 Dissertation Research Fellow, Tobacco Related Disease Research Program
- 2005 Ph.D., University of California, San Diego

FIELD OF STUDY

Major Field: Chemistry and Biochemistry

Studies in Protein Structure-Function Relationships
Professor Palmer W. Taylor

PUBLICATIONS

Hansen SB et al. "Insights into Intrinsic tryptophan Fluorescence of the Acetylcholine Binding Protein" in preparation

Gao F, Mer G, Tonelli M, Hansen SB, Burghardt TP, Taylor P, and Sine SM "Solution NMR Spectroscopy Demonstrates Agonist-mediated Conformational Change of the C-loop in Acetylcholine Binding Protein" submitted *J Biol Chem.* 2005

Hibbs RE, Johnson DA, Shi J, Hansen SB, and Taylor P "Structural Dynamics of the α -Neurotoxin-Acetylcholine Binding Protein Complex: Hydrodynamic and Fluorescence Anisotropy Decay Analyses" *Biochemistry* 2005 in press

Bourne Y., Hansen S.B., Sulzenbacher G., Talley T.T., Huxford T., Taylor P., & Marchot P. (2005) Comparaison structurale de trois complexes entre une toxine peptidique et une proteine synaptique liant l'acetylcholine. [Review in french; abstract in english]. In *Toxines et Douleur* (Bon C., Goudey-Perrière F., Goyffon M., & Sauviat M-P., eds.) Coll. *Rencontres en Toxinologie*, Editions Lavoisier, Paris, 2005, pp. 213-216

Hansen SB, Sulzenbacher G, Huxford T, Marchot P, Taylor P, and Bourne Y "Structures of *Aplysia* AChBP complexes with agonists and antagonists reveal distinctive binding interfaces and conformations" *Embo J* 2005, 24:3635-46

Bourne Y, Talley TT, Hansen SB, Taylor P and Marchot P "Crystal structure of a Cbtx-AChBP complex reveals essential interaction between snake α -neurotoxins and nicotinic receptors" *Embo J* 2005, 24: 1512-22

Bouzat C, Gumilar F, Spitzmaul G, Wang HL, Rayes D, Hansen SB, Taylor P, and Sine SM "Coupling of agonist binding to channel gating in an ACh-binding protein linked to an ion channel" *Nature* 2004 Aug 19:430:896-900

Hansen SB, Talley TT, Radic Z, and Taylor P. "Structural and ligand recognition characteristics of an acetylcholine binding protein from *Aplysia californica*" *J Biol Chem.* 2004 Jun 4:279(23):24197-202

Taylor P, Hansen SB, Talley TT, Hibbs RE, and Radic Z. "Contemporary paradigms for cholinergic ligand design guided by biological structure" *Bioorg Med Chem Lett.* 2004 Apr 19;14(8):1875-7.

Gao F, Bern N, Little A, Wang HL, Hansen SB, Talley TT, Taylor P, and Sine SM. "Curariform antagonists bind in different orientations to acetylcholine-binding protein" *J Biol Chem.* 2003 Jun 20;278(25):23020-6.

Hansen SB, Radic Z, Talley TT, Molles BE, Deerinck T, Tsigelny I, and Taylor P. "Tryptophan fluorescence reveals conformational changes in the acetylcholine binding protein" *J Biol Chem.* 2002 Nov 1;277(44):41299-302.

ABSTRACTS

Hansen SB, Sulzenbacher G, Huxford T, Marchot P, Bourne Y, and Taylor P (*Society of Neuroscience*, Washington DC, 2005) "Crystal Structure of *Aplysia* AChBP Agonists-antagonists complexes reveals distinctive nAChR surfaces and conformations"

Hansen SB, Sulzenbacher G, Huxford T, Marchot P, Bourne Y, and Taylor P (*XIVth International Symposium on Cholinergic Mechanisms*, Alicante Spain, 2005) "Crystal structures of *Aplysia* AChBP Complexed with Nicotinic Agonists and Antagonists"

Hansen SB and Taylor P (*Experimental Biology*, San Diego, CA 2005) "Structure/function of the Acetylcholine Binding Protein from *Aplysia californica*."

Hansen SB and Taylor P (*Society of Neuroscience*, San Diego, CA 2004) "Structure/function of the acetylcholine binding protein from *Aplysia californica*: a nicotinic receptor surrogate"

Hansen SB, Talley TT, Radic Z, and Taylor P (*Experimental Biology*, Washington DC 2004) "Structure/function of the acetylcholine binding protein from *Aplysia californica*"

Hansen SB and Taylor P (*Western Pharmacology Society*, Honolulu, HI 2004) "Characterization of a Conotoxin ImI Specific Acetylcholine Binding Protein from *Aplysia californica*"

Hansen SB, Radic Z, Talley TT, Taylor P (*Experimental Biology*, San Diego, CA 2003) "Ligand Binding Characteristics of the Acetylcholine Binding Proteins from *Lymnaea stagnalis* and *Aplysia californica*"

US PATENTS

Hansen SB, Radic Z, and Taylor P "Fluorescent Ligand Binding Assay of the Acetylcholine Binding Protein and Analogs of Ligand-gated Ion Channels" USPTO 2005 June 30, Pub. No. US-2005-0143285-A1.

ABSTRACT OF THE DISSERTATION

Ligand Specificity and Conformational States of the Acetylcholine Binding Protein, a
Nicotinic Receptor Surrogate

by

Scott B Hansen

Doctor of Philosophy in Chemistry and Biochemistry

University of California, San Diego, 2005

Professor Palmer Taylor, Chair

The acetylcholine binding protein (AChBP) is a structural and functional surrogate of the nicotinic acetylcholine receptor (nAChR) ligand binding domain (LBD). AChBP is a natural truncation of the nAChR. The soluble protein is secreted into the cholinergic synapse of mollusks as a primitive synaptic modulator. The solubility of AChBP is amenable to fluorescence spectroscopy and X-ray crystallography and provides an opportunity to investigate ligand related conformational changes and structural determinants of ligand binding.

Material for studying *Lymnaea* and *Aplysia* AChBP was obtained by chemically synthesizing genes (cDNA) encoding for the proteins. A mammalian expression system was devised in combination with a FLAG-antibody immunopurification protocol. A single FLAG tag on the N-terminus was optimal for

expression of both proteins. Ligand binding of most agonists and antagonists resulted in a substantial change in intrinsic tryptophan fluorescence. Kinetic measurements by stopped-flow techniques showed rapid rates of association and dissociation for agonists and slow rates for the α -neurotoxins. Equilibrium dissociation constants for ligands with rates beyond the detection of stopped-flow were measured in a fluorescent plate reader at equilibrium.

AChBP from *Aplysia californica* was shown to have five orders of magnitude higher affinity for α -conotoxin Iml. Crystal structures were determined for agonists and antagonists bound to AChBP. Antagonists included α -conotoxin Iml, α -cobratoxin, and methyllycaconitine. Antagonist binding was compared to that of the agonists epibatidine and lobeline. Ten side chains were associated with all bound ligands delineating the competitive hydrophobic binding pocket. Antagonists occupied two additional non-overlapping binding surfaces; one on the apical side of the C loop the another on the ‘membrane’ side under the C loop. Changes in conformational states of AChBP were investigated by comparing a crystal structure of apo *Aplysia* AChBP with those of antagonists and agonists. The C loop undergoes a large conformational change to cap the binding pocket when agonists are bound. Antagonists extend the C loop radially up to 11 Å when compared to agonists. Knowledge of structural determinants for binding selective ligands and associated conformational changes should facilitate rational drug design and the understanding of nAChR function.

Chapter I

Introduction to the Nicotinic Acetylcholine Receptor

Receptors are important proteins with recognition capacity in signal transduction, particularly in neurons. Cholinergic neurons in the central and peripheral nervous system are defined by storage, release and stimulation of neurotransmitter acetylcholine (ACh). At the neuromuscular junction, the release of acetylcholine from presynaptic neurons into the synaptic cleft triggers activation through channel opening of the nicotinic acetylcholine receptor (nAChR) in the postsynaptic membrane. The associated conductance of the open channel leads to depolarization at the motor endplate and stimulation of muscle contraction. ACh is rapidly removed from the neuromuscular junction through catalysis by acetylcholinesterase. A central role of cholinergic receptors in signal transduction, particularly that involved in motor activity of fish and mammals, is evident from a host of natural toxins such as α -cobratoxin, α -bungarotoxin, α -conotoxin, lophotoxin, and *d*-tubocurarine that target nAChRs for predation or defense against predation. Likewise, nAChRs have a major pharmacological target for treating pain, epilepsy, nicotine addiction, myasthenia gravis, and Alzheimer's disease. nAChRs has been and continues to be the prototypic receptor for the entire cys-loop family of pentameric ligand-gated ion-channels including GABA, serotonin, and glycine receptors.

A. Historical Development

In 1914, Sir Henry Dale described the first neurotransmitter, a choline ester that stimulated components of the cholinergic nervous system (1). Details of receptor

function began to emerge with the advent of microelectrode technology followed by the voltage clamp. By 1952 Huxley and Hodgkin, using the voltage clamp, developed a full quantitative model for the ionic basis of a neuronal action potential (2). Knowledge about nAChR structural composition likewise advanced during this period in large part due to tools provided by nature. In 1940 Feldberg et al. discovered mg quantities of nAChRs in the electric organ of the *Torpedo* ray (3). And in 1966 Lee and Chang showed an α -toxin from the snake venom of *Bungarus multicinctus* to bind virtually irreversibly to nAChRs (4). This soon led to the identification of a 250-kDa pentameric protein with subunits α , β , γ , and δ (5,6). Two copies of the α subunit correlate with two binding sites per pentameric molecule (7). Theories of activation led to the identification of three receptor states, resting and activatable, open channel and desensitized.

Detection of individual channel opening events with the patch clamp (8) and molecular cloning dawned a new era in the early 1980s. Cloning confirmed 4 subunits in a pentameric $\alpha_2\beta\gamma\delta$ arrangement (9-11) and revealed the receptor topology containing a large N-terminal extracellular domain, 4 transmembrane spanning domains, and a large cytoplasmic domain between transmembranes 3 and 4 (12). Extensive site directed mutagenesis and cysteine labeling experiments showed the site of agonist binding to be comprised of multiple loops in the extracellular domain at the subunit interface (13). The nAChR family in the nervous system expanded to included 16 receptor subunits (14) capable of assembly in multiple combinations and regulating innumerable functions throughout the nervous system. Serendipity struck again when in 2001 Brejc et al. identified and solved a high resolution X-ray structure of a naturally-soluble homologous protein from the fresh water snail *Lymnaea stagnalis* (15).

B. Nicotinic Receptor Subtypes

Seventeen different subtypes of nAChRs have been described (Figure I.1). Nicotinic acetylcholine receptors were first subclassed by their ability to block at the neuromuscular junction or at autonomic ganglia. It was later found α -neurotoxins from snake, such as α -bungarotoxin, showed selectivity for nicotinic receptors at the neuromuscular junction. Two muscle receptors are known consisting of 4 subunits. Embryonic muscle receptors form a pentamer of γ , δ , $\beta 1$, and two $\alpha 1$ subunits. Mature innervated muscle consists of ϵ , δ , $\beta 1$, and two $\alpha 1$ subunits. Binding sites are formed at the subunit interfaces of the two alpha subunits. Therefore, muscle receptors have two binding sites per pentamer. The remaining 12 subtypes are neuronal being found in the central and peripheral nervous systems. Of those only the homomeric $\alpha 7$ pentamer binds α -bungarotoxin. Four neuronal receptors are homomeric; $\alpha 7$, $\alpha 8$, $\alpha 9$, $\alpha 10$ and have 5 binding sites. The remaining 8 are thought to form pentamers of 2 α and 3 β subunits consisting of two binding sites per pentamer. Several possible combinations of α and β subtypes exist many of which are known. The diversity of receptors coupled with their varied expression in tissues is complex and provides an opportunity for detailed understanding of the neuronal function and signaling. Distinctions in subtype provide a basis for potential drug intervention in neuronal disease; however, limited progress has been made developing subtype specific ligands for therapeutic intervention.

C. Agonists and Antagonists of Nicotinic Acetylcholine Receptors

Most nicotinic ligands have been isolated from natural products. Hundreds of ligands are known and reviewed (16). The ligands described here are among the more common

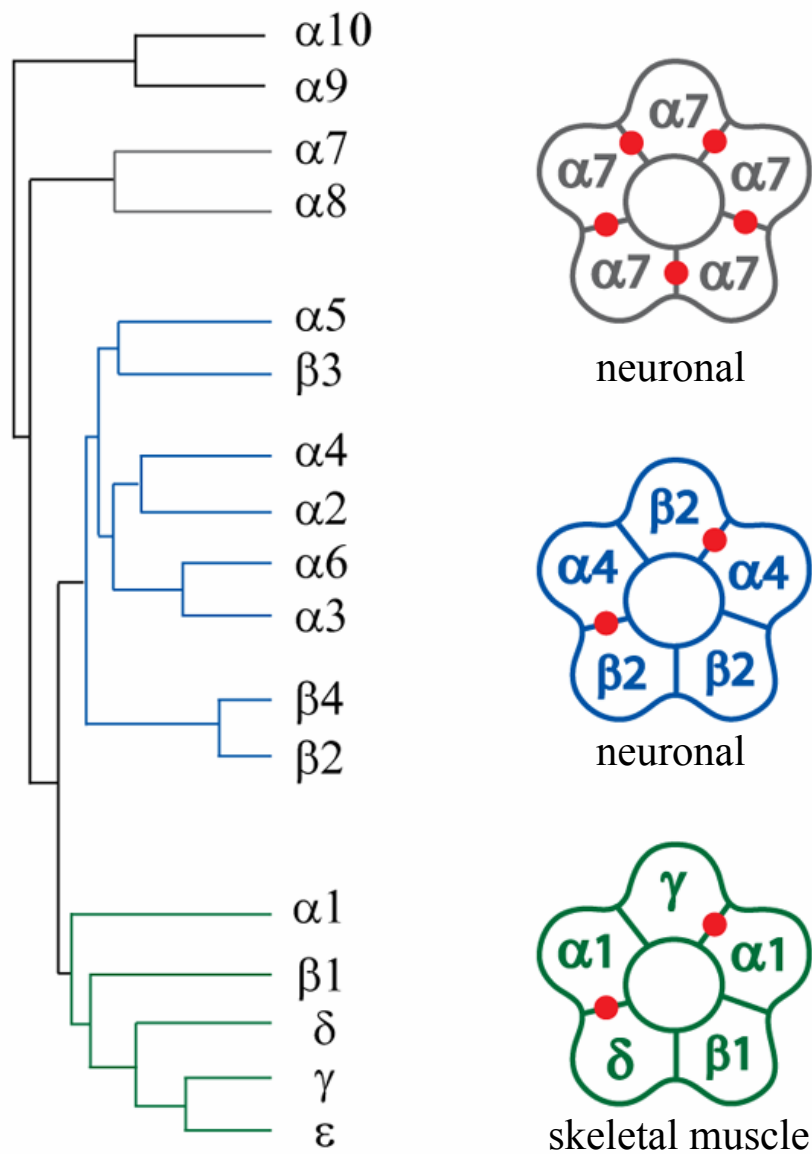


Figure I.1: Phylogenetic Relationship of nAChR subtypes. Receptor subtypes $\alpha 7$ -10 are homomeric. Neuronal $\alpha 2$ -6 and $\beta 2$ -4 are heteromeric with 2 α and 3 β . Muscle receptors are 2 $\alpha 1$, $\beta 1$, δ , and γ or ϵ . Examples of subunit composition are shown as cartoon and are color coded the phylogenetic diagram. Solid red circles indicate a binding site at the subunit interface. (Figure adapted from Novère and Changeux et al. 2002)

and relate directly to the work described in the thesis (Figure I.2)

1. Agonists

The receptor is named after the natural agonist nicotine which was first isolated from the *Nicotiana tabacum* plant in 1826 and its pharmacologic selectivity studied in 1893. Humans have been conducting *in vivo* experiments with nicotine for centuries by smoking leaves of nicotine containing plants. (Such behaviors are currently out of vogue in the US and hazardous to human health. A Tobacco Related Disease Research dissertation fellowship to SBH supports research of this thesis.) The endogenous agonist acetylcholine was discovered later in 1907 (16). In 1992 epibatidine was isolated from an *Epipedobates tricolor* tree frog and became an instant research tool with an unprecedented picomolar dissociation constant (17). Another natural product lobeline isolated from the *Lobelia* is intermediate in its action with some agonist and some antagonist properties (i.e.: a partial agonist). (Figure I.2)

2. Antagonists

Nicotinic antagonist can be divided into two categories as small molecules or large peptides. *d*-Tubocurarine (Figure I.2) is commonly known as the South American arrow poison and has been in use in paralysis of game since the 1600s. More recently *d*-tubocurarine and its analogs have been employed as neuromuscular blocking agents in anesthesia. Another alkaloid antagonist methyllycaconitine (MLA) was isolated from the Larkspur plant *Delphinium* in 1982. For centuries the plant was toxic and fatal to livestock in the western US. In 1916 physostigmine ,an AChE inhibitor, was reported as an effective antidote to larkspur poisoning.

Snakes and cone snails use nAChR toxins to paralyze their prey. α -Bungarotoxin

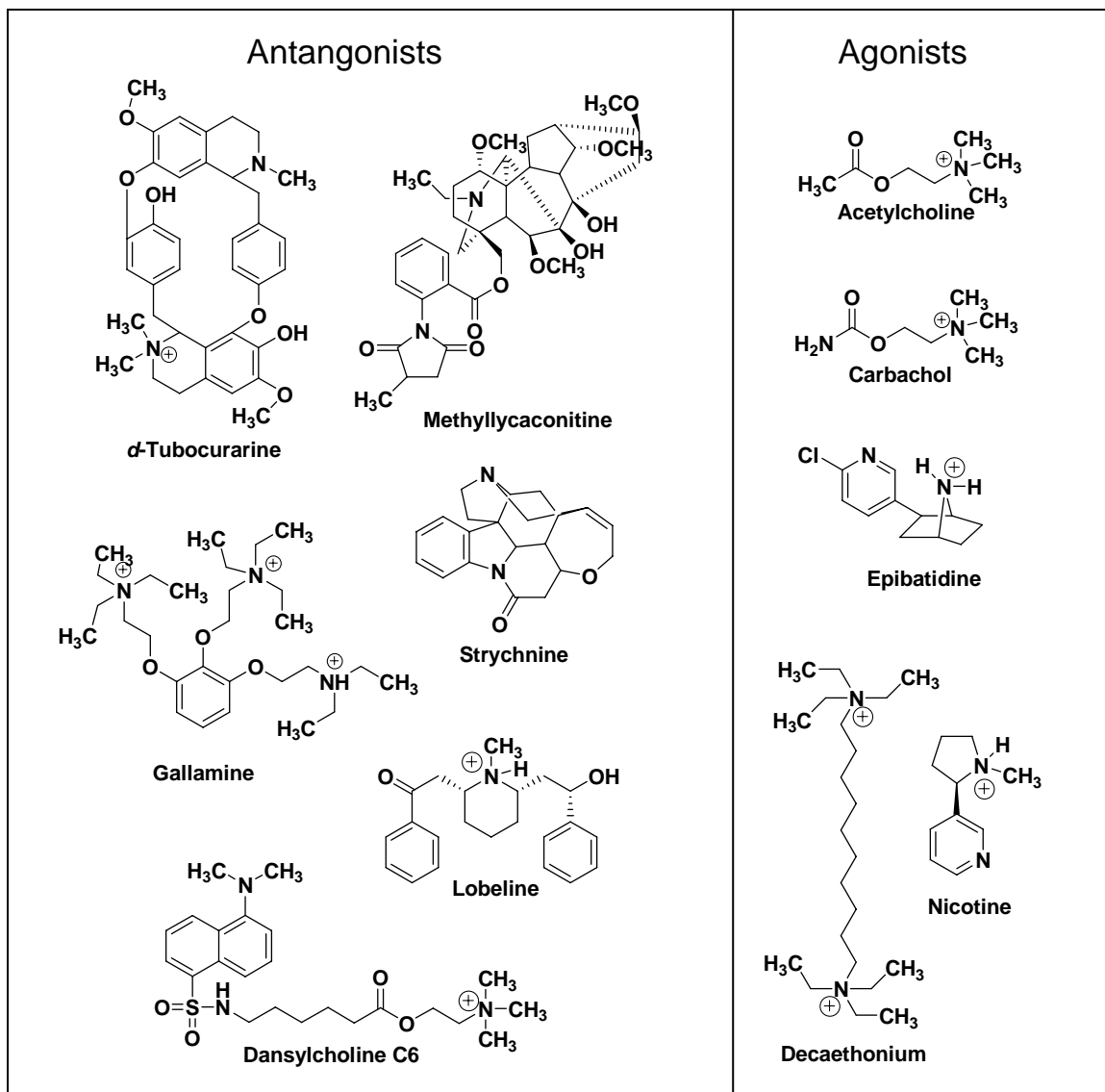


Figure I.2: Structures for select nicotinic agonists and antagonists.

(bgtx) from *Bungarus multicinctus* is historically the most important; it binds virtually irreversibly, and led to the first purification of the nAChR (18). Bgtx is an 8 kDa protein with three disulfide linkages forming a 3 finger like structure. α -Cobratoxin from *Naja naja* is homologous and binds similarly to nAChRs. Other snake toxins known to affect nicotinic receptors are the short three fingered α -neurotoxins toxins and waglerin from the viper family. Cone snails make small compact peptidic toxins that bind to nAChR, also with subtype specificity. In particular α -conotoxin ImI from the cone snail *Conus imperialis* binds specifically neuronal $\alpha 7$ and $\alpha 3\beta 2$ subtypes (19). α -conotoxin ImI is a twelve amino acid peptide with two sets of disulfides.

D. The Acetylcholine Binding Protein

The Acetylcholine Binding Protein (AChBP) was first discovered by Smit et al in the glia of the fresh water mollusk *Lymnaea stagnalis* (20). They proposed that AChBP is released by glial cells into the synaptic cleft of cholinergic neurons as a primitive mechanism of synaptic modulation. Smit et al showed AChBP to be soluble and bind α -bungarotoxin with high affinity. Other nicotinic agonists and antagonists exhibit dose-response curves similar to those of the nAChR (20). AChBP is most similar to nAChR $\alpha 7$ subtype showing 24% sequence identity (Figure I.3). In a parallel study, Brejc et al determined the three dimensional structure of AChBP (15) revealing the nicotinic fold for the Cys loop family of pentameric ligand gated ion channels (Figure I.4). The structure shows virtually all of the features predicted from a host of affinity labeling, site-specific mutagenesis, and subunit assembly studies conducted on the nicotinic receptor for over two decades (22-24).

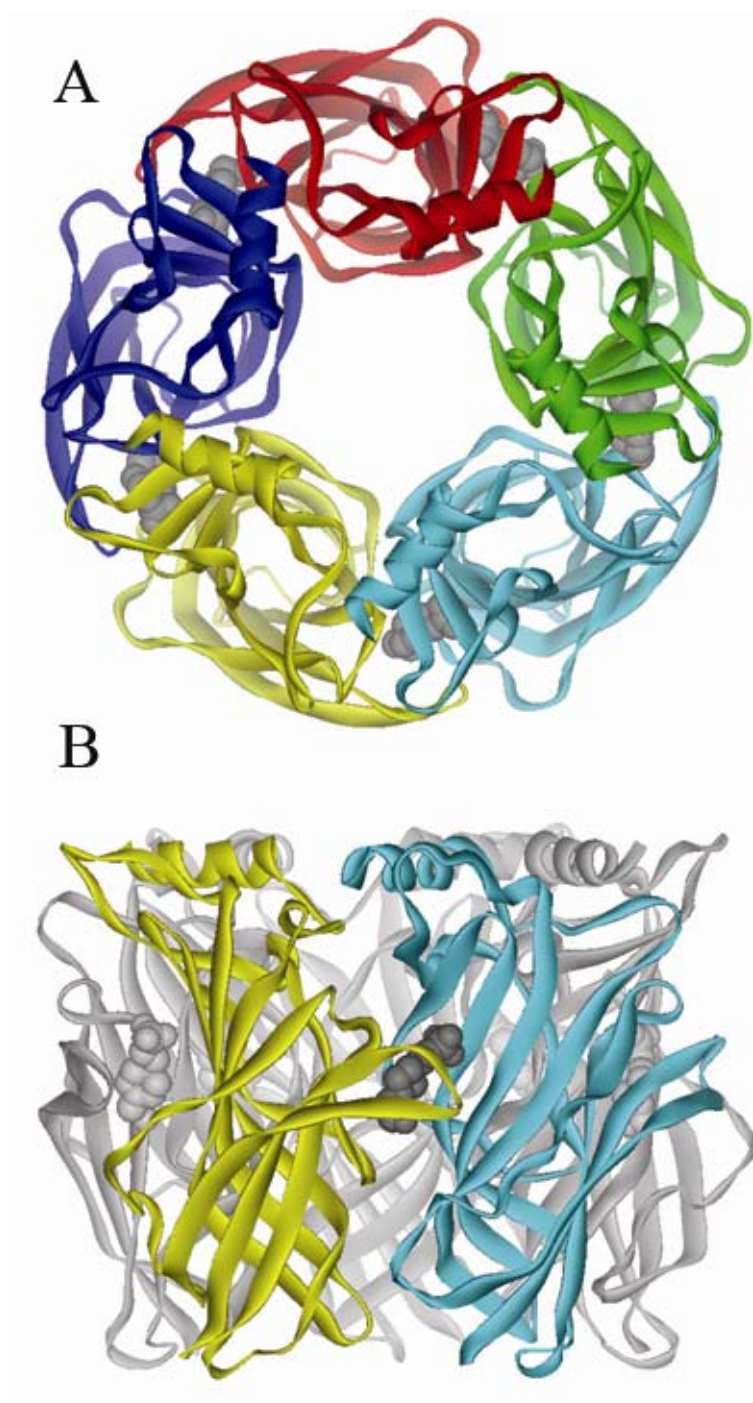


Figure I.4: Crystal structure of *Lymnaea* AChBP **A** top view of AChBP looking down a five-fold symmetry axis. All five protomers are colored with a grey space filling buffer molecule in the binding site between subunits. **B** Side view of the pentamer with two protomers colored revealing the subunit interface (15).

E. Fluorescence Spectroscopy

Fluorescence spectroscopy is a technique whereby light is absorbed by a molecule that then emits the light at a longer wavelength. Fluorescence is a powerful technique that can be used to monitor reaction in real time by stopped-flow. Draw backs are that the sample must be pure and made soluble without detergents. Light scatter by detergents reduces the sensitivity of the detection. The solubility and homogeneity requirements are applicable to the acetylcholine binding protein.

1. Intrinsic Tryptophan Fluorescence

Aromatic amino acids in proteins produce ultraviolet fluorescence. Tryptophan dominates by absorbing at the longest wavelength, having the largest extinction coefficient and quantum yield (25). In proteins where tryptophans make up the ligand binding site, quenching of intrinsic tryptophan fluorescence has been used as a means of monitoring ligand binding (25) for example, in the cholinesterase (26). When protein is excited at 280nm, although both tyrosine and tryptophans contribute to fluorescence, tryptophan is the major contributor to changes in fluorescence upon binding of a ligand. Tryptophan fluorescence can be more selectively excited at wavelengths between 295-305 nm light (25). In general, when solvent is occluded tryptophan fluorescence is enhanced. Solvent or electron withdrawing atoms such as in a cationic interaction with a tryptophan quenches fluorescence.

2. Fluorescence Resonance Energy Transfer (FRET)

Resonance energy transfer is widely used for monitoring associations of biomolecules. FRET occurs when a fluorescent donor molecule transfers energy from an excited state to an acceptor molecule depopulating the excited state by resonance energy

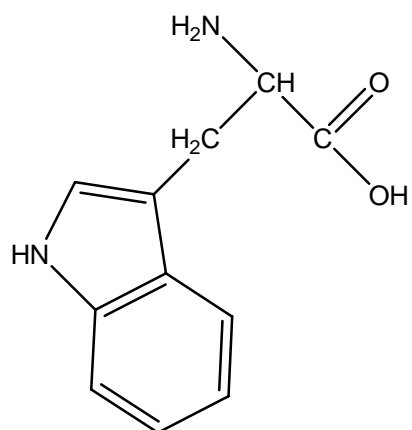
transfer (27). The donor and the acceptor molecule must have proper spectral overlap for energy transfer and have an alignment of excited state dipoles for maximal transfer. For example, the amino acid tryptophan has fluorescent properties and is capable of serving as a donor for FRET with a dansyl (5-dimethylaminonaphthylsulfonyl) acceptor (Figure I.5). Tryptophan is excited by light at 280nm and emits maximally at 340nm. Dansyl absorbs light at 340 and emits at 535nm. When in close proximity, tryptophan in its excited state will transfer its energy to the dansyl moiety through FRET instead of emitting the light. Since the dansyl moiety is also fluorescent, it can emit the light at 535nm. In practice, one would excite tryptophan with 280nm light and then observe fluorescence at 535nm.

F. X-ray Crystallography

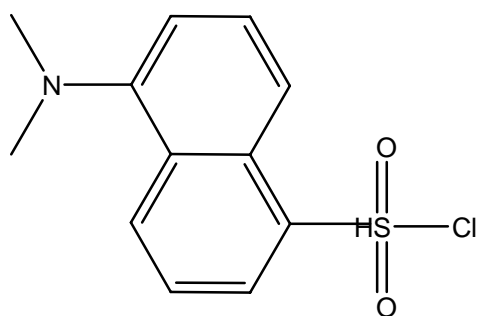
Atomic resolution of macromolecular structure plays an important role in assessing structure/function relationships and in drug discovery. Crystallography is the most widely used technique to obtain such information at atomic levels of resolution. However, well ordered crystals are required, and obtaining crystals in the absence of detergents or for disordered proteins is difficult. Full length nAChR containing the membrane associating domain have not yet been crystallized likely due to their requirements for detergents. Consequently, the acetylcholine binding protein is a necessary surrogate for obtaining suitable structures.

1. Crystallization

Protein crystallization consists of allowing the protein to nucleate and crystallize from solution in such a way that the protein molecules form an ordered crystal lattice. In the hanging drop method a reservoir solution is made consisting of salt, buffer, and a



Tryptophan



Dansyl Chloride

Figure I.5: Tryptophan and dansyl Fluorescence Resonance Energy Transfer (FRET) partners. When in an excited state and with proper proximity and orientation, donor tryptophan is capable of transferring energy to an acceptor dansyl by energy resonance transfer.

precipitant. Typically, one to two micro liters of pure concentrate (~10mg/ml) protein is placed on a cover slip, inverted, sealed over a reservoir solution, and allowed to equilibrate

(Figure I.6). Water slowly diffuses into the reservoir solution causing the protein to precipitate. Crystals may form with days or months. The cover slip is then detached, inverted, and the crystals removed with a nylon loop. The crystals are flashed cooled in liquid nitrogen and a cryoprotectant.

2. X-Ray Diffraction

A single protein crystal attached to a nylon loop is placed in front of an X-ray beam under cryogenic conditions (Figure I.7). The crystal causes the beam to diffract and the resulting X-rays are exposed onto the surface of an X-ray sensitive detector. Typical diffraction can be seen in Figure I.8. The crystal is rotated and exposed up to 180 degrees. The resulting spots are assigned a space group and each spot location and intensity are cataloged in three-dimensional space.

3. Structure Assembly and Refinement

The diffraction spots can be described as vectors with a magnitude of their intensity and related by a phase angle. This angle is unknown and must be estimated from molecular replacement or solved for using techniques such as MAD phasing. A Fourier transformation can then be applied to describe an electron density. Atoms with their proper geometric constraints are then built into the electron density using automated software(29) or manually into a graphical representation of the electron density(30). The structure is then refined using software packages that sample likely atomic position and validate them by comparing expected diffraction from the observed diffraction. The

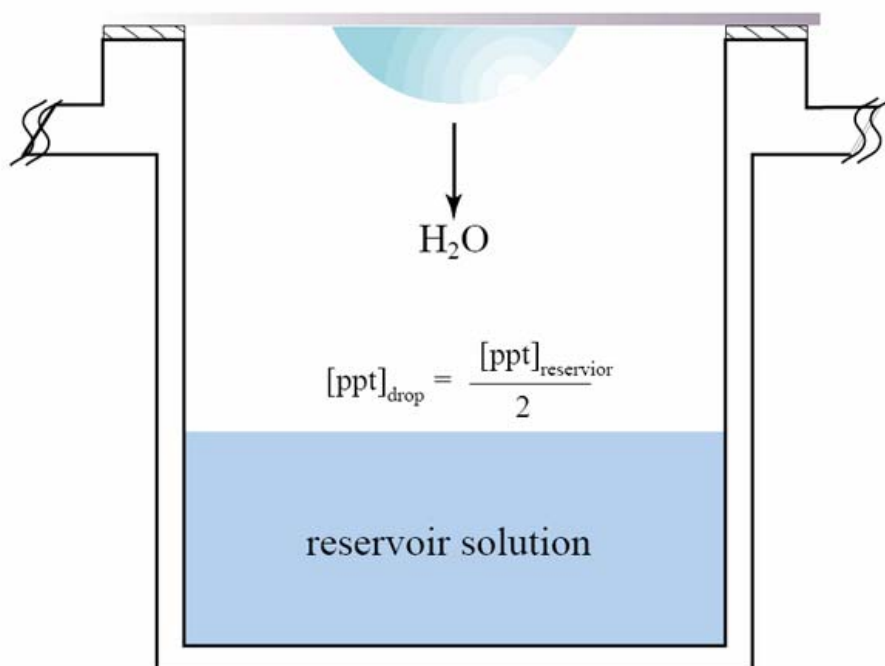


Figure I.6: Hanging drop method of crystallization (28). A reservoir solution (blue) contains salt, buffer, and a precipitant. The semi-sphere represents a 2 μ l hanging drop of protein in solution. Precipitant in the reservoir solution causes the protein drop to dehydrate and the protein to precipitate. Crystals that form are removed from the drop with a nylon loop and flash cooled in liquid nitrogen.

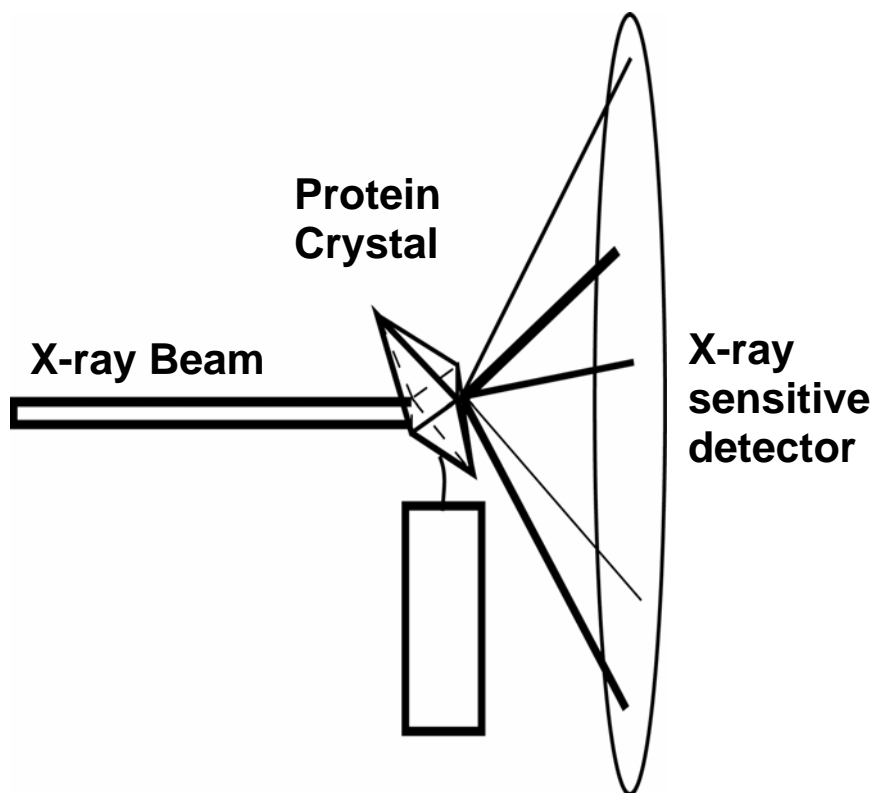


Figure I.7: Schematic of X-ray diffraction

A single protein crystal is exposed to an X-Beam. Diffracting X-rays are exposed onto the surface of an X-ray sensitive detector.

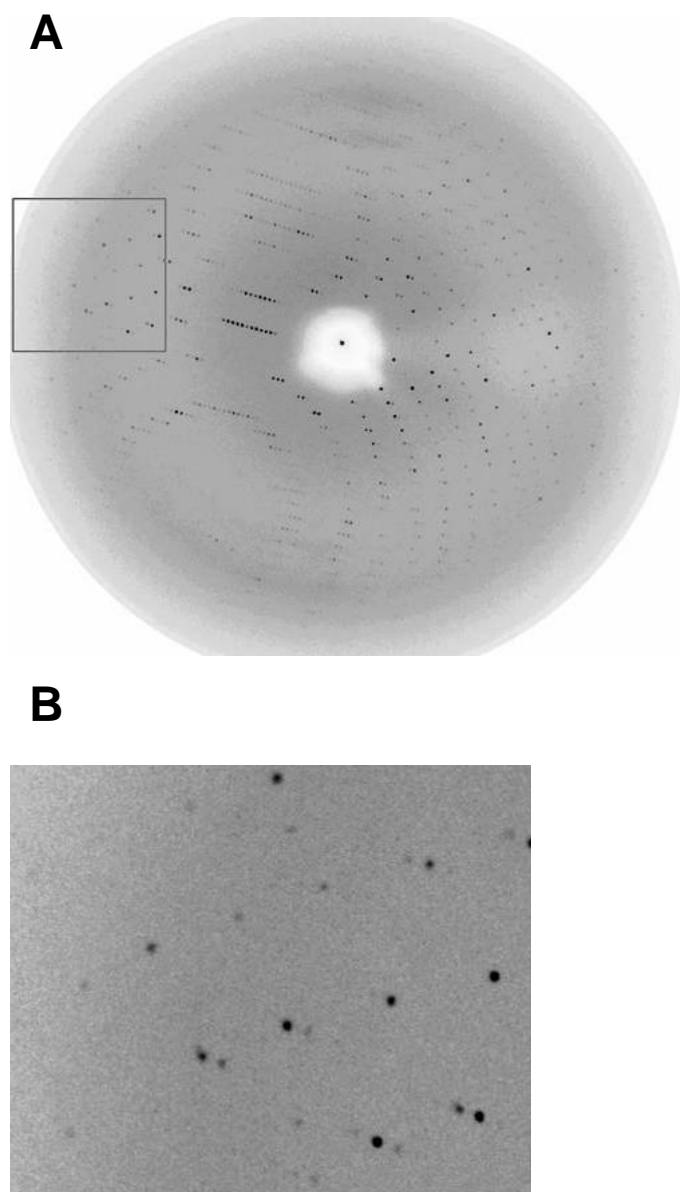


Figure I.8: X-Ray diffraction

A Diffraction of AChBP 2.7 Å resolution **B** Zoom of boxed region in **A**. X-rays from a diffracting crystal form patterns of spots with varying degrees of intensity. Spot intensity reveals contains the information for structure determination.

expected diffraction is calculated from the working atomic model. The R factor is a comparison of the observed vs. calculated structure factors.

G. Dissertation Objective

The objectives of this dissertation are: (a) to identify chemical determinants in proteins of ligand binding, in particular, those giving rise to nicotinic acetylcholine receptor (nAChR) subtype specificity, and (b) to identify ligand induced conformational changes that couple ligand binding to ion channel gating. Specific experimental aims are: First through oligonucleotide synthesis form a gene (cDNA in an expression vector); employ the gene to express secreted acetylcholine binding protein (AChBP) in a mammalian expression system, and purify the expressed protein to homogeneity. Second, develop assays for steady state and kinetic monitoring of ligand binding using intrinsic tryptophan fluorescence and radioligand competition assays. Characterize additional AChBPs to serve as surrogates for receptor subtypes with distinct ligand specificities. Establish from the characterized ligand specificity that the AChBPs found in mollusks are suitable surrogates of the nAChR ligand binding domain. Obtain atomic structures of bound species-selective ligands by x-ray crystallography and investigate ligand selectivity and structural determinants by site-directed mutagenesis. Show conformational changes in the ligand binding domain by comparing crystal structures of AChBP in the apo form and bound to nicotinic agonists and antagonists.

H. References

1. Dale, H. H. (1914) *J Pharmacol Exp Ther* **6**, 147-190
2. A. L. Hodgkin, A. F. H., and B Katz. (1952) *J. Physiol. Lond.* **116**, 424-448
3. Feldberg W, F. A., Nachmansohn D. (1940) *J Physiol* **97**, 3-4
4. Lee, C. Y., and Chang, C. C. (1966) *Mem Inst Butantan* **33**, 555-572
5. Reynolds, J. A., and Karlin, A. (1978) *Biochemistry* **17**, 2035-2038
6. Lindstrom, J., Walter, B., and Einarson, B. (1979) *Biochemistry* **18**, 4470-4480
7. Neubig, R. R., and Cohen, J. B. (1979) *Biochemistry* **18**, 5464-5475
8. Neher, E., and Sakmann, B. (1976) *Nature* **260**, 799-802
9. Raftery, M. A., Hunkapiller, M. W., Strader, C. D., and Hood, L. E. (1980) *Science* **208**, 1454-1456
10. Noda, M., Takahashi, H., Tanabe, T., Toyosato, M., Furutani, Y., Hirose, T., Asai, M., Inayama, S., Miyata, T., and Numa, S. (1982) *Nature* **299**, 793-797
11. Ballivet, M., Patrick, J., Lee, J., and Heinemann, S. (1982) *Proc Natl Acad Sci U S A* **79**, 4466-4470
12. Claudio, T., Ballivet, M., Patrick, J., and Heinemann, S. (1983) *Proc Natl Acad Sci U S A* **80**, 1111-1115
13. Prince, R. J., and Sine, S. M. (1996) *J Biol Chem* **271**, 25770-25777
14. Le Novere, N., and Changeux, J. P. (1995) *J Mol Evol* **40**, 155-172
15. Brejc, K., van Dijk, W. J., Klaassen, R. V., Schuurmans, M., van Der Oost, J., Smit, A. B., and Sixma, T. K. (2001) *Nature* **411**, 269-276
16. Daly, J. W. (2005) *Cell Mol Neurobiol* **25**, 513-552
17. Qian, C., Li, T., Shen, T. Y., Libertine-Garahan, L., Eckman, J., Biftu, T., and Ip, S. (1993) *Eur J Pharmacol* **250**, R13-14

18. Changeux, J. P., Kasai, M., and Lee, C. Y. (1970) *Proc Natl Acad Sci U S A* **67**, 1241-1247
19. McIntosh, J. M., Santos, A. D., and Olivera, B. M. (1999) *Annu Rev Biochem* **68**, 59-88
20. Smit, A. B., Syed, N. I., Schaap, D., van Minnen, J., Klumperman, J., Kits, K. S., Lodder, H., van der Schors, R. C., van Elk, R., Sorgedragger, B., Brejc, K., Sixma, T. K., and Geraerts, W. P. (2001) *Nature* **411**, 261-268
21. Thompson, J. D., Higgins, D. G., and Gibson, T. J. (1994) *Nucleic Acids Res* **22**, 4673-4680
22. Karlin, A. (2002) *Nat Rev Neurosci* **3**, 102-114
23. Corringer, P. J., Le Novere, N., and Changeux, J. P. (2000) *Annu Rev Pharmacol Toxicol* **40**, 431-458
24. Taylor, P. (2000) in *Handbook Exp. Pharm* (Clementi F, Guthon M, and Gotti C, ed) Vol. 144, pp. 79-100, Springer-Verlag Berlin
25. Lakowicz, J. R. (1999) in *Principles of Fluorescence Spectroscopy*, Second Ed., pp. 445-486, Kluwer Academic/ Plenum Publishers, New York, Boston, Dordrecht, London, Moscow
26. Radic, Z., and Taylor, P. (2001) *J Biol Chem* **276**, 4622-4633
27. Lakowicz, J. R. (1999) in *Principles of Fluorescence Spectroscopy*, pp. 386-394, Kluwer Academic/ Plenum Publishers, New York, Boston, Dordrecht, London, Moscow
28. Hampton (2003) in *Crystallization Research Tools* Vol. 13, 1 Ed., pp. 202-203, Hampton Scientific, Laguna Niguel
29. Perrakis, A., Morris, R., and Lamzin, V. S. (1999) *Nat Struct Biol* **6**, 458-463
30. McRee, D. (1992) *J. Molecular Graphics* **10**, 44-46
31. Le Novere, N., Corringer, P. J., and Changeux, J. P. (2002) *J Neurobiol* **53**, 447-456

Chapter II

Gene Synthesis, Protein Production, Subunit Assembly and Ligand Binding for the Acetylcholine Binding Protein

To study the ligand binding in the nicotinic acetylcholine receptor, soluble ligand binding domains from mollusks were employed. Genes encoding the protein were synthesized chemically as a cDNA and codon usage was optimized for expression in a mammalian expression system. Unique restriction sites and cassette regions were conveniently placed to facilitate mutagenesis at various points in the open reading frame.

A Synthesis of AChBP Genes (cDNA) from Synthetic Oligonucleotides

Gene sequences for acetylcholine binding proteins from *Lymnaea Stagnalis* and *Aplysia californica* were located using the entrez protein databases (<http://www.ncbi.nlm.nih.gov>). Unique restriction sites were engineered using Webcutter 2.0 (1997 Max Heiman).

1. *Lymnaea* AChBP Gene

The *Lymnaea* gene was previously identified and its gene product expressed as a soluble surrogate of the extracellular ligand binding domain of the nAChR in a yeast expression system. (1) In my study, mollusk codon usage was changed to reflect that of mammals using a table of mammalian codon frequency. Long oligonucleotides (80-126 bp) were ordered from Proligo (San Diego, CA) with random overlap of 25-30 bp. Sets of either 4 or 6 oligonucleotides (Figure II.1) were annealed by heating to 98° C and allowed to cool to room temperature. Regions with resisting secondary structure were cycled in a thermal cycler varying the temperature by 5-10° and decreasing temperature

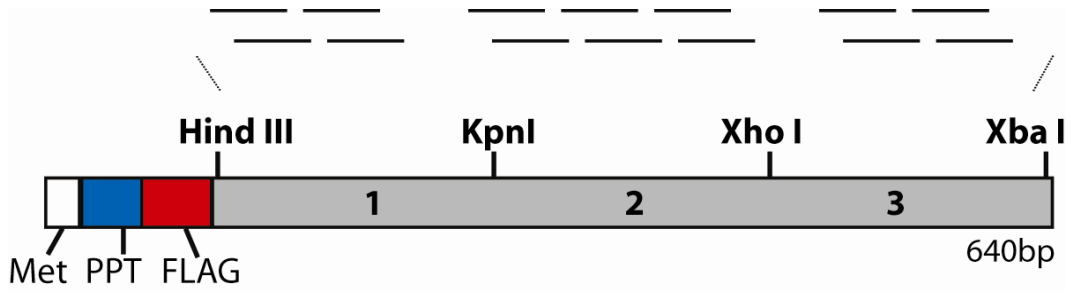


Figure II.1: Schematic of AChBP gene synthesis

Long oligonucleotides were ligated into the FLAG CMV-9 vector (Sigma) containing preprotrypsin-PPT leader sequence and the FLAG epitope (DYKDDDDYK). Enzyme restriction sites are part of the multiple cloning site. Three regions labeled 1-3 were ligated in separate reactions with complimentary cDNAs (shown as lines) coding for the acetylcholine binding protein (AChBP) from *Lymnaea stagnalis*

from 98° to 15° over 10 hours. Alternatively, (in a third case) annealed nucleotides were subjected to polymerase chain reaction and with appropriate oligonucleotides for restriction site cleavage. PCR products were analyzed by gel electrophoresis, and bands of appropriate molecular weight were selected and enzymatically cleaved for ligation. All annealed or DNAs produced by PCR were ligated into the FLAG-CMV-9 expression vector (Sigma USA).

2. *Aplysia* AChBP Gene

A search of the Entrez Protein database revealed a protein sequence termed the soluble acetylcholine receptor from *Aplysia californica* (gi:17225107) with sequence similarity to *Lymnaea* AChBP. A sequence alignment of the two proteins showed sequence similarity in regions of the *Lymnaea* protein thought to contribute to its solubility. Mammalian codon usage was introduced by reverse translating from protein to DNA using Bioedit (1999 Hall T.) A scheme similar to that described for the *Lymnaea* gene was employed for the first 400bp of the *Aplysia* gene (Figure II.1). The remaining 250bp were synthesized as a separate unit (Bionexus, USA). Fragments were ligated into the CMV-9 expression vector (Sigma USA).

B. Mammalian Expression and Purification of Secreted AChBP

1. AChBP Gene Stably Transfected into HEK 293 Cells

Human embryonic kidney (HEK 293) cells were purchased from American Type Culture Collection (Atlanta, GA). Cells were plated in Dulbecco's modified Eagle's medium (DMEM) supplemented with 10% fetal bovine serum (FBS) at a density of 1.5×10^6 cells per 10 cm dish, 24 hours prior to transfection. Twenty micrograms of plasmid DNA were added per plate of cells using standard HEPES/calcium phosphate

precipitation methods. Stable transfectants were selected by G418 (Gemini Bio-Products, Inc., Calabasas, CA) resistance following cotransfection of the AChBP genes and a neomycin resistance gene. Untransfected cells did not survive 800 µg/ml G418 and within 3-7 days were sloughed from the plate. Stable transfectants were expanded in 10cm dishes and split at least two times, while maintaining G418 in the media. Triple layer flasks with a surface area of 500cm² (Nalge Nunc International, Rochester, NY) were inoculated with 10 cm dishes. After cells grew to confluence, the percentage of FBS was reduced from 10 to 2%. The media containing the secreted AChBP was collected every 1-3 days, and the adherent cells replenished with fresh media for 3 to 5 weeks. Media was centrifuged to remove dead cells, and 0.02% azide was added to preserve the media.

2. AChBP Gene Stably Transfected into GnTI⁻ HEK Cells

In order to obtain AChBP with restricted oligosaccharide processing and greater homogeneity, cDNAs of genes encoding the AChBP's were transfected into an N-acetylglucosaminyltransferase I-negative (GnTI⁻) (HEK293S) cell line from Reeves and Khorana (2) (Figure II.2). Stable transfectants were obtained following standard calcium phosphate transfection methods as described above. However, GnTI⁻ cells were more sensitive to G418, and selection of resistant cells was done with 200µg/ml of the aminoglycoside. In general, GnTI⁻ cells were less robust and needed media to be replenished more frequently. Medium of triple layer flasks required replenishing daily. Expression levels of GnTI⁻ cells were equal or greater than that of wild type HEK expression levels. SDS PAGE analysis showed a homogeneous band ~2500 Da less than protein expressed in wild type HEKs (Figure II.3A). Mass spectroscopy of GnTI⁻

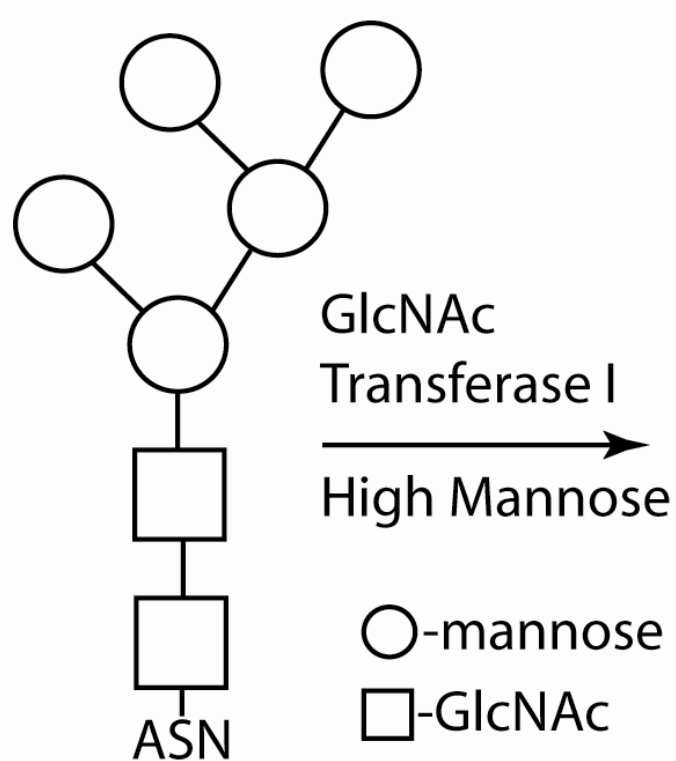


Figure II.2 Structure of N-linked glycosylation in GNTI HEK cells. In the endoplasmic reticulum sugars added to proteins en bloc are trimmed to 2 N-acetylglucosamine and 5 or 3 mannose residues. In the Golgi phase of the secretory pathway N-acetylglucosaminyltransferase is a key branching enzyme that leads to complex glycosylation. Cells deficient in this enzyme should yield the product shown.

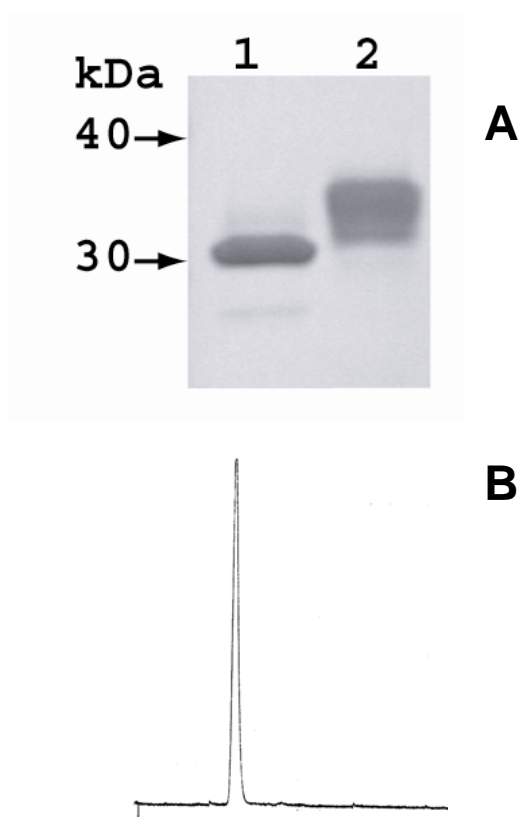


Figure II.3 (A) SDS-PAGE and (B) FPLC profiles of GnTI expressed AChBP. A lane 1 AChBP purified from GnTI cells of HEK origin (2) Lane 2 AChBP purified from standard HEK 293 cells. B Fast protein liquid chromatography (FPLC) profile of purified protein from GnTI cells. A single peak is seen at the characteristic elution volume of a pentamer (3,4).

produced AChBP showed a single peak with a mass corresponding to the peptide molecular mass plus two mannose and 5 N-acetylglucosamine (GlcNAc) residues. Processing pathways allow for the possibility of only 3 GlcNAc, but this oligosaccharide was not observed in the AChBP product. Fast protein liquid chromatography showed a homogeneous peak corresponding to a pentamer (Figure II.3B)

3. Immuno-affinity Purification of Secreted AChBP

Immuno-affinity chromatography was employed to purify AChBP and mutants. Anti-FLAG resin (Sigma, USA) in 1-5cm diameter column was stripped by application of 0.1 M glycine, pH 3.5, by gravity flow for 15 min. Resin was immediately equilibrated in 50mM Tris HCl, pH 7.4, 150mM NaCl containing 0.02% Azide. AChBP protein was adsorbed to the resin overnight by slow gravity flow ~0.5ml/min. The resin was washed with 50-100 times the column volumes of the above buffer. AChBP protein was eluted by application of two packed resin volumes of 50-100 µg/ml FLAG (DYKDDDDYK) peptide in TBSA. Fractions containing protein estimated by Bradford protein assay (Bio-Rad) were collected and concentrated in centricon spin column (Millipore) with a molecular cut off of 50,000 or 100,000. Concentrated protein 1-5 mg/ml was buffer exchanged 2-3 times with 10-fold excess buffer to remove contaminating elution peptide. For crystallography, purified samples were further concentrated to 10-15 mg/ml in a micron spin column YM50 (Millipore).

C. AChBP Gating of an AChBP/5HT_{3A} Chimera

In collaboration with Cecilia Bouzat and Steven M. Sine at Mayo, *Lymnaea* AChBP was replaced for the ligand binding domain of the 5HT_{3A} serotonin receptor (5)

demonstrating AChBP to be a functional surrogate of the nicotinic acetylcholine receptor.

Linking AChBP N-terminal to the 5HT_{3A} transmembrane domain (TD) did not result in a functional receptor. Several loops from the ligand binding domain (LBD) make contact with the TD (Figure II.4A). Many of the mutations are hydrophilic residues in AChBP that are conserved hydrophobic residues in transmembrane spanning receptors. It is reasonable that hydrophobic residues at the LBD and TD interface would not be conserved in the soluble binding protein. When these regions were mutated to residues found in the 5HT receptor (Figure II.4B), channel gating was observed in response to acetylcholine (figure II.5). These results are of importance for two reasons. First, they give insight into the residues whereby the LBD communicates to the gate ions in the TD. Second, these results demonstrate AChBP is capable of changing conformation manifested in channel opening following agonist addition.

D. Discussion

The acetylcholine binding protein can be produced as a stable soluble secreted protein in respectable quantities from a transfected mammalian cell line. This is the first member of the Cys loop family of protein to have such characteristics, enabling structural studies that employ X-ray crystallography, fluorescence spectroscopy, hydrogen-deuterium exchange, and nuclear magnetic resonance.

Mammalian expression systems are particularly amenable to membrane and extracellular proteins with endogenous glycosylation. Inherent heterogeneity of glycosylation can prove limiting in many studies; for example, crystallographic analysis. Removal of the glycosylation site in AChBP results in severely decreased protein

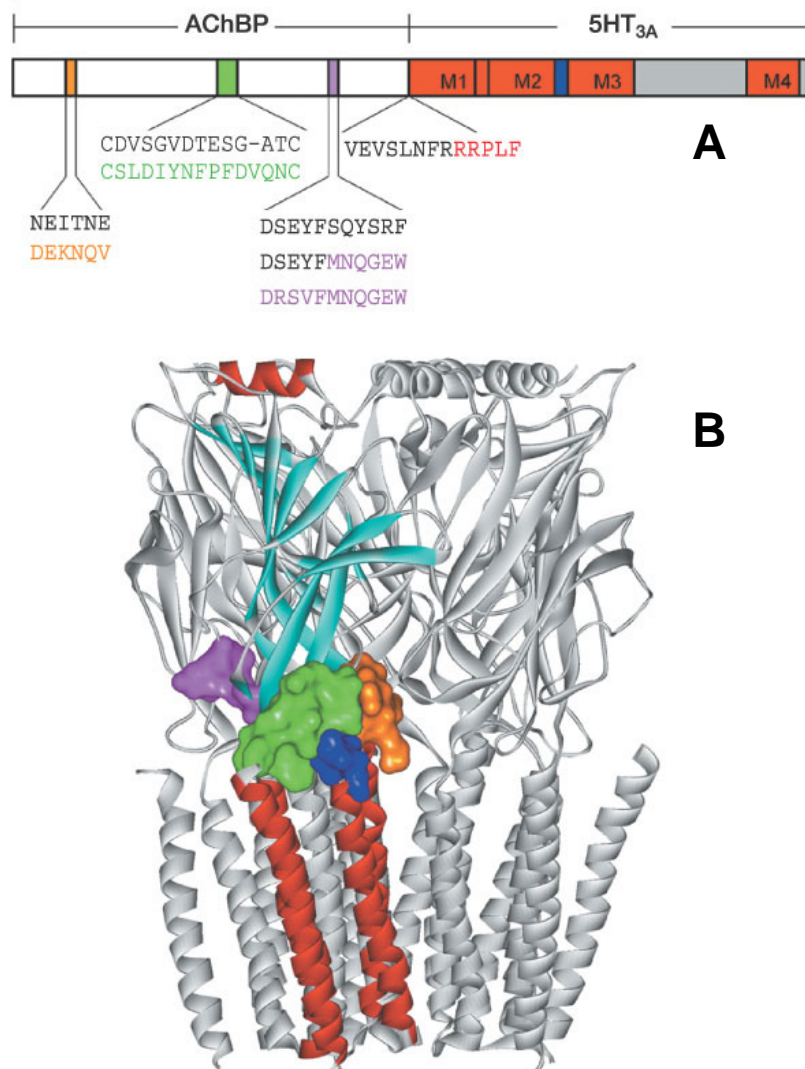


Figure II.4: Coupling of AChBP to the 5HT-3 ion pore. **A** Schematic diagram of a subunit composed of AChBP and 5-HT_{3A} sequences. The amino terminus contains AChBP (white bars and black font) and 5-HT_{3A} sequences (loop β 1- β 2, orange; Cys-loop, green; β 8- β 9 loop, magenta). The 5-HT_{3A} pore domain follows, with transmembrane helices M1-M4 (red) and the M2-M3 linker (blue). Red font indicates the start of the M1 domain. **B** Homology model of the chimeric receptor (C3, Table 1) with key regions of one subunit color-coded as in **A**.

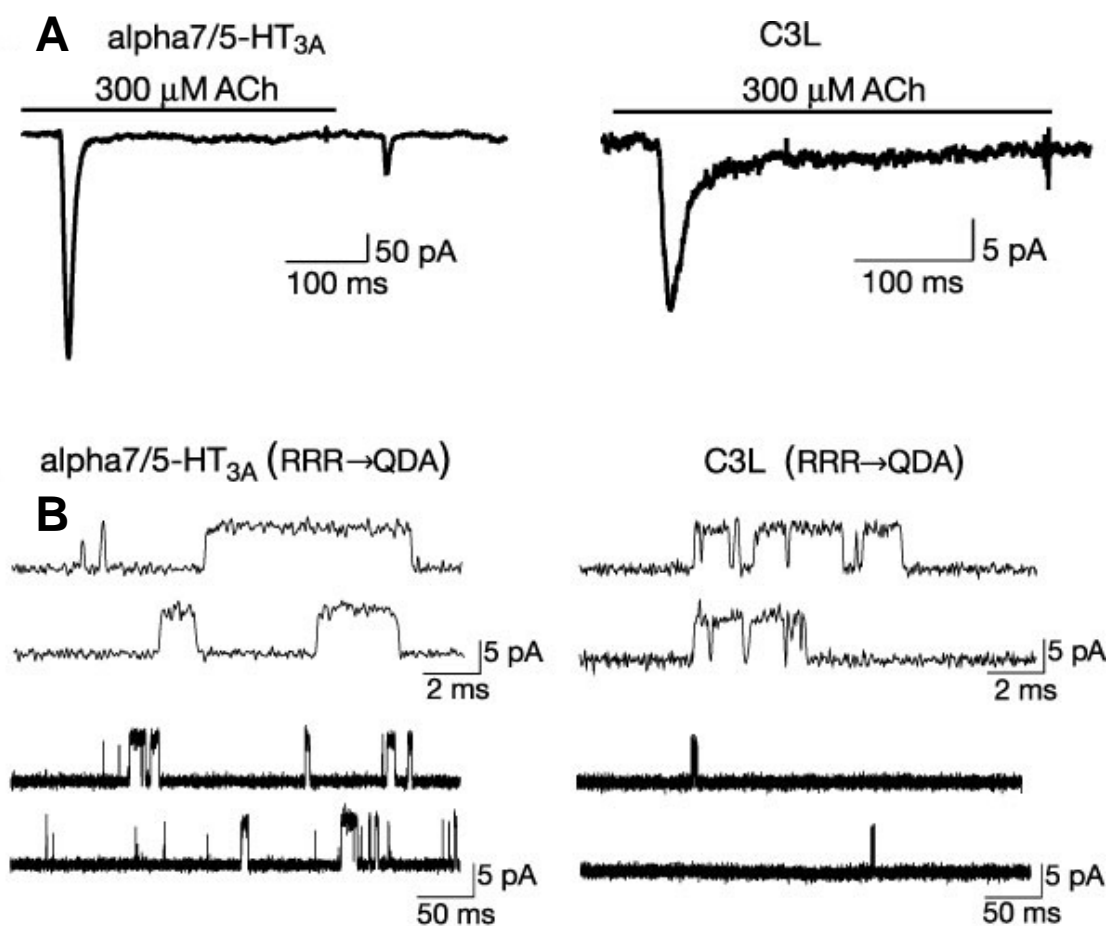


Figure II.5: AChBP/5HT-3 chimera gating currents **A** Whole-cell currents through alpha7/5-HT_{3A} or C3L chimaeras (300 μM ACh). Each trace represents the average of 4 to 8 ACh applications. Decay time constants are 12 ms (alpha7/5-HT_{3A}) and 15 ms (C3L). Holding potential, -50 mV. **B** Single-channel currents through alpha7/5-HT_{3A} and C3L chimaeras from cell-attached patches (1 mM ACh). Chimaeras contain the triple mutation (RRR →QDA) to increase conductance(6). Currents are displayed at 9 kHz bandwidth with channel openings as upward deflections. Membrane potential, -70 mV.

expression, improper folding and loss of binding activity. A more moderate approach was taken to attenuate glycosylation to a homogenous population of two mannose and five N-acetylglucosamine using HEK 293S cells deficient in N-acetylglucosaminyltransferase I (2).

AChBPs lack of the transmembrane spanning domain is crucial to these methods, but also limits the study to that of the ligand binding domain. In collaboration with Cecilia Bouzat and Steven M. Sine, this protein was modified by mutagenesis at three locations. The mutated region was constructed as a chimera with a transmembrane spanning domain of a related pentameric receptor (5HT-3) to produce a functional receptor(5). AChBP's ability to communicate acetylcholine binding to a full length receptor demonstrates that AChBP is capable of conformational changes observed in the full length receptors. The frequency of open events and their conductance appears to vary among the chimeric constructs, but it is likely the conformational states are very similar.

E. References

1. Smit, A. B., Syed, N. I., Schaap, D., van Minnen, J., Klumperman, J., Kits, K. S., Lodder, H., van der Schors, R. C., van Elk, R., Sorgedrager, B., Brejc, K., Sixma, T. K., and Geraerts, W. P. (2001) *Nature* **411**, 261-268
2. Reeves, P. J., Callewaert, N., Contreras, R., and Khorana, H. G. (2002) *Proc Natl Acad Sci U S A* **99**, 13419-13424
3. Hansen, S. B., Radic, Z., Talley, T. T., Molles, B. E., Deerinck, T., Tsigelny, I., and Taylor, P. (2002) *J Biol Chem* **277**, 41299-41302
4. Hansen, S. B., Talley, T. T., Radic, Z., and Taylor, P. (2004) *J Biol Chem* **279**, 24197-24202
5. Bouzat, C., Gumilar, F., Spitzmaul, G., Wang, H. L., Rayes, D., Hansen, S. B., Taylor, P., and Sine, S. M. (2004) *Nature* **430**, 896-900

Chapter III

Tryptophan Fluorescence Reveals Conformational Changes in the Acetylcholine Binding Protein

A. Abstract

The recent characterization of an acetylcholine binding protein (AChBP) from the fresh water snail, *Lymnaea stagnalis*, shows it to be a structural homolog of the extracellular domain of the nicotinic acetylcholine receptor (nAChR). To ascertain whether the AChBP exhibits the recognition properties and functional states of the nAChR, I have expressed the protein in milligram quantities from a synthetic cDNA transfected into human embryonic kidney (HEK) cells. The protein secreted into the medium shows a pentameric rosette structure with ligand stoichiometry approximating five sites per pentamer. Surprisingly, binding of acetylcholine, selective agonists and antagonists ranging from small alkaloids to larger peptides, results in substantial quenching of the intrinsic tryptophan fluorescence. Using stopped-flow techniques, I demonstrate rapid rates of association and dissociation of agonists and slow rates for the α -neurotoxins. Since agonist binding occurs in msec time frames and the α -neurotoxins may induce a distinct conformational state for the AChBP-toxin complex, the snail protein shows many of the properties expected for receptor recognition of interacting ligands. Thus, the marked tryptophan quenching not only documents the importance of aromatic residues in ligand recognition, but establishes that the AChBP will be a useful functional as well as structural surrogate of the nicotinic receptor.

B. Introduction

Ligand-gated ion channels, of which the nicotinic acetylcholine receptor is a prototypic structure, are composed of five subunits, each of which traverses the membrane four times (1,2); their hydrophobicity and size preclude conventional structural studies at atomic resolution by X-ray crystallography or nuclear magnetic resonance spectrometry. Recently, an acetylcholine binding protein (AChBP) from the fresh water snail, *Lymnaea stagnalis*, has been characterized, crystallized and its structure determined (3,4). The crystal structure shows virtually all of the features predicted from a host of affinity labelling, site-specific mutagenesis, and subunit assembly studies conducted on the nicotinic receptor for over two decades (1,2,5). Although the isolated protein shares ligand recognition characteristics with its closest mammalian homolog, the pentameric $\alpha 7$ receptor (4), details on its ligand specificity, binding kinetics and conformational changes remain unknown. These questions are critical to ascertaining whether the snail protein has the recognition properties and conformational states to serve as a functional as well as a structural surrogate of the extracellular domain of the nicotinic receptor. To this end, I have expressed the binding protein in a mammalian system from a chemically synthesized cDNA of 637bp. The cDNA contains restriction sites at various locations to allow for substitution of encoding receptor segments into the cDNA template of the binding protein. Upon ligand binding, AChBP shows major changes in fluorescence emitted from five tryptophans on each subunit, providing an intrinsic detection system to monitor the stoichiometry and kinetics of ligand binding.

C. Experimental Procedures

1. Gene Synthesis and Protein Expression

I synthesized 7 double stranded oligonucleotides between 80 and 126 bp reflecting codon usage in mammalian cells and containing appropriate overhangs for ligation (6). These were assembled into three ligation products that were then inserted into construction vectors and their sequence confirmed by automated sequencing. After digestion with appropriate restriction enzymes followed by band isolation, the inserts were ligated into a p3xFLAG-CMV-9 expression vector (Sigma) containing a preprotrypsin leader peptide followed by an N-terminal 3xFLAG epitope¹. The expression plasmid also contained neomycin acetyltransferase for clonal selection. Transfection of the plasmid into human embryonic kidney cells produced an epitope-attached glycoprotein secreted primarily into the medium. Selection with G418 yielded a stable cell line secreting AChBP. Ultraculture media (Bio Whittaker) was collected at 3-day intervals from multi-tier flasks for several weeks. Adsorption onto a flag antibody column followed by elution with the 3xFLAG peptide yielded purified protein in quantities between 1 and 2.5 mg/L.

2. Fluorescence Assays

Fluorescence measurements were performed on a Jobin Yvon-Spex Fluoromax 2 fluorometer (Instruments S.A., Inc., Edison, NJ). AChBP was excited at 280 nm and emission intensity monitored for 0.1 s intervals at unitary wavelengths between 337 and 343 nm.

3. Stopped-flow Kinetics

Stopped-flow measurements were obtained using an Applied Photophysics SX.18MV (Leatherhead, UK) stopped-flow spectrofluorometer. Excitation was at 280 nm and a cut off filter at 305 nm was used to collect the fluorescence signal.

Measurements of binding of the dansyl choline analogues employed 280 nm excitation and measured the enhanced fluorescence using a 420 nm cut off filter. Rates of association and dissociation were estimated from the slope and ordinate intercept of plots of overall rate of fluorescence change versus ligand concentration. Dissociation rates were also estimated in several cases by reacting the preformed complex with a large excess of gallamine in the stopped-flow instrument and observing the time course of the increase in fluorescence.

D. Results and Discussion

Purification of AChBP secreted into the media produced a single band on SDS gels migrating at ~ 35 kDa (Fig. 1a). Treatment with PNGase to remove N-linked oligosaccharides enhances the migration rate considerably. N-terminal sequencing and MALDI mass spectrometry after deglycosylation yielded a sequence and mass consistent with cleavage of the leader peptide. Negative staining electron microscopy showed a typical rosette structure expected of a pentameric subunit assembly (Fig. 1b and c). Hydrodynamic analysis revealed a Stokes radius of 57 \AA from gel filtration and a sedimentation coefficient of 4.9 S from sucrose density gradients, values also consistent with pentamer formation.

Stoichiometry of ligand binding was estimated from AChBP tryptophan quenching through titration by high affinity ligands (Fig. 2). In separate preparations, this yielded values of 4.7 to $5.6 \text{ } \mu\text{moles}/\mu\text{mole}$ or $0.94 - 1.12 \text{ } \mu\text{moles}$ per $26,551 \text{ Dalton}$ subunit based on quantitative amino acid analysis. These data show approximately 50% quenching of the intrinsic tryptophan fluorescence with epibatidine as a high affinity

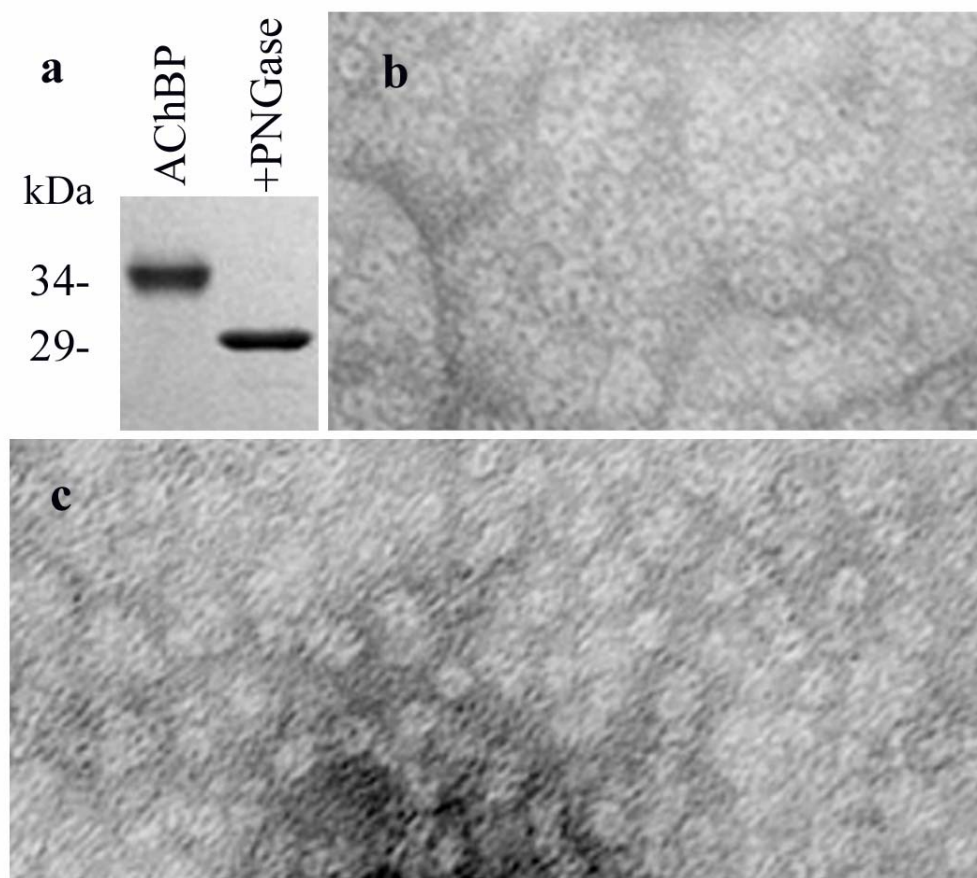


Figure III.1: Characterization of acetylcholine binding protein (AChBP). a, SDS Page electrophoresis showing apparent molecular weight of untreated and PNGase F treated AChBP (1 μ g each lane). Electron micrographs of b, *Torpedo californica* nAChR in isolated membrane vesicles prepared by density gradient centrifugation (27) and c, AChBP by negative staining with 2% uranyl acetate.

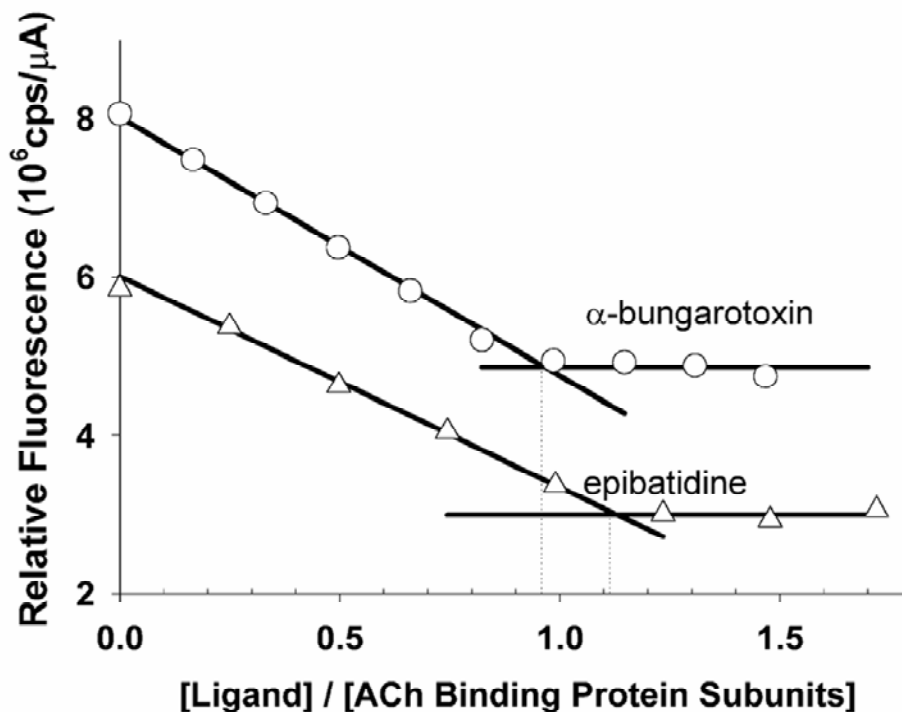


Figure III.2: Equilibrium titration of AChBP with α -bungarotoxin and epibatidine. AChBP at 300 nM was titrated in a 4 mm x 4 mm cuvette with incremental quantities of the peptide antagonist and the alkaloid agonist. Since quenching by α -bungarotoxin is only 15-20% of the unliganded receptor fluorescence, a receptor-gallamine complex was formed by addition of 2 μ M gallamine to enhance fluorescence prior to the α -bungarotoxin addition. The contribution of the fluorescence from the added α -bungarotoxin was subtracted from the titration curve. The single tryptophan in α -bungarotoxin has less than 2% of the emission intensity at 335 nm of the tryptophans in the receptor-gallamine complex, so only a small correction is necessary. Fluorescence was recorded in a SPEX Fluoromax2 spectrofluorometer at 25 °C. Protein content was determined by quantitative amino acid analysis with a subunit molecular weight of 26,551. Fluorescence excitation at 280 nm; emission maxima were measured over the range of 337 to 343 nm.

ligand, typical quenching values for most of the quaternary and tertiary amines used as ligands in this study. Since these ligands, with the exception of the dansyl choline derivatives, lack the spectral overlap with tryptophan emission necessary for fluorescence resonance energy transfer (FRET) (7), the precise mechanism of quenching is unknown. However, at least two (Trp 53 and Trp 143) and perhaps a third (Trp 82) of the 5 tryptophans are found in proximity to the bound ligand (3). The organic cation in fitting into this aromatic nest of tryptophans and tyrosines may disrupt aromatic connectivity established between the side chains (8). Upon binding of ligands lacking the capacity for FRET, tryptophan fluorescence quenching has also been observed for acetylcholinesterase (9); its binding site is at the base of a narrow gorge whose base and walls are lined with aromatic residues (10). In the muscle and $\alpha 7$ nAChR, residue substitution of tryptophans homologous to residues 53 and 143 reduces ligand affinity, but does not eliminate binding (11,12), and a charge transfer – complex involving one or more tryptophans has been proposed to stabilize various ligand complexes (13,14). Systematic substitution of other aromatic residues for the five tryptophans should enable one to delineate further their individual contributions to quenching of fluorescence.

Stopped-flow kinetic studies of ligand association are shown in Figure III.3; data for several ligands, monitored by AChBP fluorescence quenching, are tabulated in Table I. Rates of association and dissociation approach the time resolution of the stopped-flow technique (~ 1 msec). A comparison of agonists shows that the bimolecular rates of agonist binding approach the diffusion limitation and the rate constants found in single channel or voltage-current relaxation analyses for the muscle or neuronal nicotinic receptor (15-20). Rates of dissociation are slower than dissociation of ligand from the

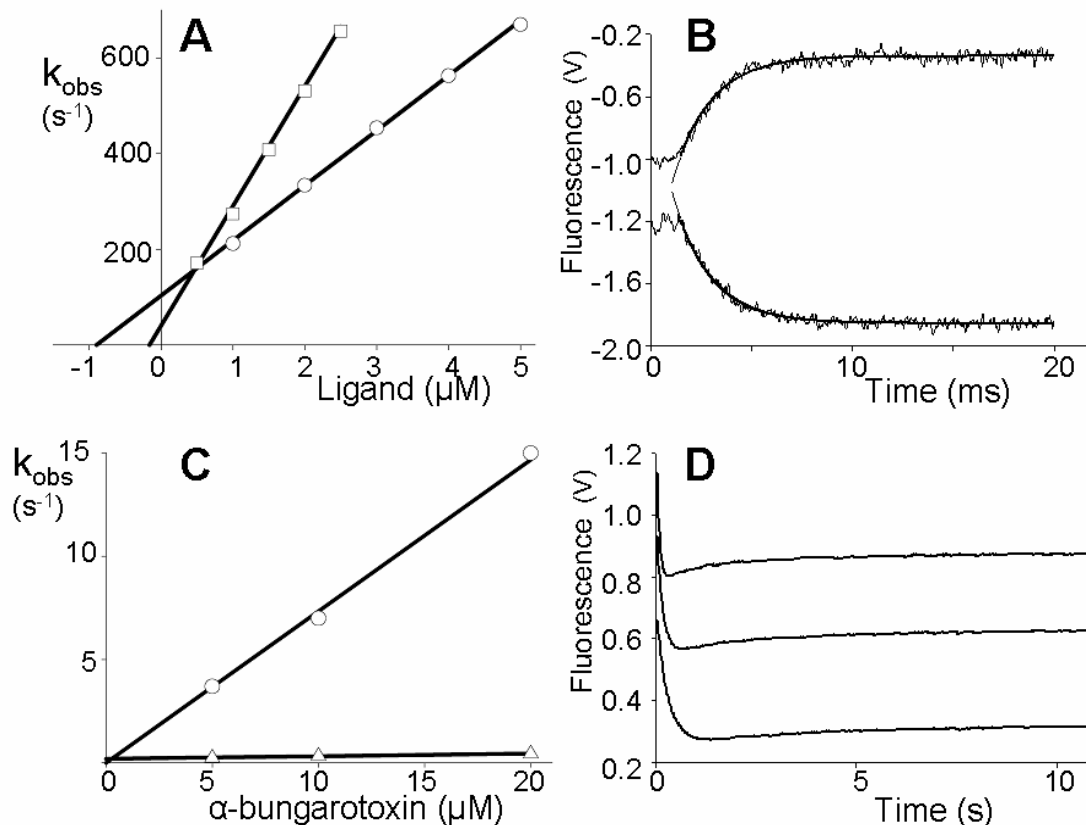


Figure III.3: Kinetics of ligand association with AChBP. A. Gallamine (\square) and acetylcholine (\circ) at the designated concentrations were reacted with 20 nM AChBP in an Applied Photophysics SX.18MV stopped-flow spectrofluorometer and the fluorescence signal recorded. Excitation was at 280 nm and a cut-off filter at 305 nm was used on the emission side. The first order rate constant k_{obs} was plotted against ligand concentration. The individual rate constants were obtained from $k_{\text{obs}} = k_1[L] + k_{-1}$, where k_1 is the slope and k_{-1} the ordinate intercept. B. Typical traces showing the observed fluorescence during and after stoppage of flow. The flow time between the mixing and observation chambers is ~ 1 msec. The increase in fluorescence associated with gallamine binding and decrease associated with acetylcholine binding are shown in the top and bottom traces. C. Kinetics of the fast and slow phases of α -bungarotoxin association with unliganded AChBP. Kinetics for the fast phase (\circ) were calculated as described above, whereas the apparent concentration independence of the slow phase (Δ) yields a limiting value of 0.34 sec^{-1} . D. Traces for the three bungarotoxin concentrations shown in panel C.

Table III.1
AChBP ligand binding kinetics

Ligand	k_1 ($\times 10^8 \text{ M}^{-1}\text{s}^{-1}$)	k_{-1} (s^{-1})	K_d (nM)
Decamethonium	3.2 ± 0.17	120 ± 17	380
Dansyl-C ₂ -choline*	2.1	2.9	14
Gallamine	2.5 ± 0.14	36 ± 6.5	140
α -Tubocurarine	2.0	30	150
(+)-Epibatidine	1.7 ± 0.26	0.027 ± 0.037	0.16
(-)-Nicotine	1.5	5.7	38
Dansyl-C ₆ -choline**	1.3	7.6	58
Acetylcholine	1.1 ± 0.12	120 ± 16	1000
Waglerin-1	0.048	31	6500
α -Cobratoxin	0.033	0.011	3.2
α -Bungarotoxin	0.0097 ± 0.002	0.0017 ± 0.0003	1.8

k_1 and k_{-1} were determined from rate measurements at various ligand concentrations according to $k_{\text{obs}} = k_1[\text{L}] + k_{-1}$ (cf. Fig. 2) and K_d was calculated from k_{-1}/k_1 . Standard errors reflect values from three or more measurements. Where standard errors are not shown, values reflect an average of two measurements.

* 5-dimethyl aminonaphthyl sulfonamidoethyl trimethylammonium

** 5-dimethyl aminonaphthyl sulfonamidoethyl trimethylammonium

activatable receptor, but of nearly the same magnitude as dissociation from the open channel state, and more rapid than dissociation from the presumed desensitized state (15-20). Hence, agonists bind and dissociate with rates expected from electrophysiologic studies for an open channel state of the receptor. In fact, certain residues in the transmembrane span of the receptor have been shown to enhance dissociation of ligands from the activatable, closed channel state of the receptor (21). Moreover, the AChBP structure may resemble more closely the open channel conformation of the *Torpedo* acetylcholine receptor (22).

Given the proposed role for AChBP in scavenging the neurotransmitter in synapses (4), an association rate for acetylcholine similar to that found for the receptor would be expected in order to achieve efficient function. Also, the kinetic constants for the antagonist, *d*-tubocurarine, are of comparable magnitude to those found electrophysiologically for the receptor (23). No evidence for appreciable cooperativity of binding was found in the kinetic profiles.

Epibatidine and α -bungarotoxin have equilibrium dissociation constants for AChBP that differ by only an order of magnitude, yet the rate of association for the peptide antagonist is ~ 200 -fold slower than for the nicotinic agonist (Table I). If the association reactions for α -bungarotoxin are run at higher concentrations, two steps in the reaction are evident with the rapid step being bimolecular and concentration dependent. The unimolecular step ($k_2 = 0.34 \text{ sec}^{-1}$) shows a small enhancement in fluorescence that diminishes, but does not eliminate, the overall fluorescence quenching. The slower α -neurotoxin kinetics of association, which also has been well documented in nicotinic receptors from several species (24-26), and the linked unimolecular step seen here are

suggestive of the α -bungarotoxin locking the AChBP into a distinctive conformational state. The single tryptophan in α -bungarotoxin has approximately 2% of the fluorescence intensity of the 5 tryptophans in each AChBP subunit. The fluorescence change in the slow step could emerge from enhanced fluorescence of the single tryptophan of the toxin in the complex or a slight enhancement of the AChBP tryptophans after formation of the initial complex. Irrespective of the tryptophans contributing to the signal differences, the slower unimolecular isomerization points to differing positions of the tryptophans in the initial complex and the final equilibrium state.

The *tris*-quaternary antagonist, gallamine, when associated with the receptor results in an enhancement of the tryptophan fluorescence suggesting that the stabilization of this ligand may differ from the other agonists and antagonists studied. The three triethylammonioethyl groups that emanate from the pyrogallol ring probably preclude full insertion of the ring into the aromatic pocket. Rather stabilization involving the quaternary ammonium ligands and anionic moieties at the subunit interface account for the different binding orientation of gallamine resulting in fluorescence enhancement (Figure III.4). Since gallamine binding appears mutually exclusive with the other agonists and antagonists listed in Table I, reaction of the various ligand - AChBP complexes with gallamine by stopped-flow provided a valuable means of confirming the dissociation rates of the various antagonists (Table I), as well as measuring the stoichiometry of ligand binding for ligands that quench to a lesser extent than epibatidine (Figure III.2).

Quite apart from establishing ligand specificity for the AChBP, intrinsic tryptophan fluorescence quenching affords a universal means of directly following ligand binding to

the AChBP without the necessity of developing competition studies with radioactive or fluorescent ligands. Substitution of sequences unique to particular receptor subtypes may allow one to examine selectivity of various AChBP-receptor chimeric sequences fashioned after the neuronal or muscle subtypes of receptor. The ligand binding kinetics seen with the AChBP reveals similarities to kinetics anticipated for ligand binding to the many subtypes of nicotinic receptor. Physical measurements in solution should enable one to correlate conformation with kinetic parameters of ligand recognition, and add another dimension to investigating specificity of this unique binding protein in relation to the larger family of receptor-related offspring.

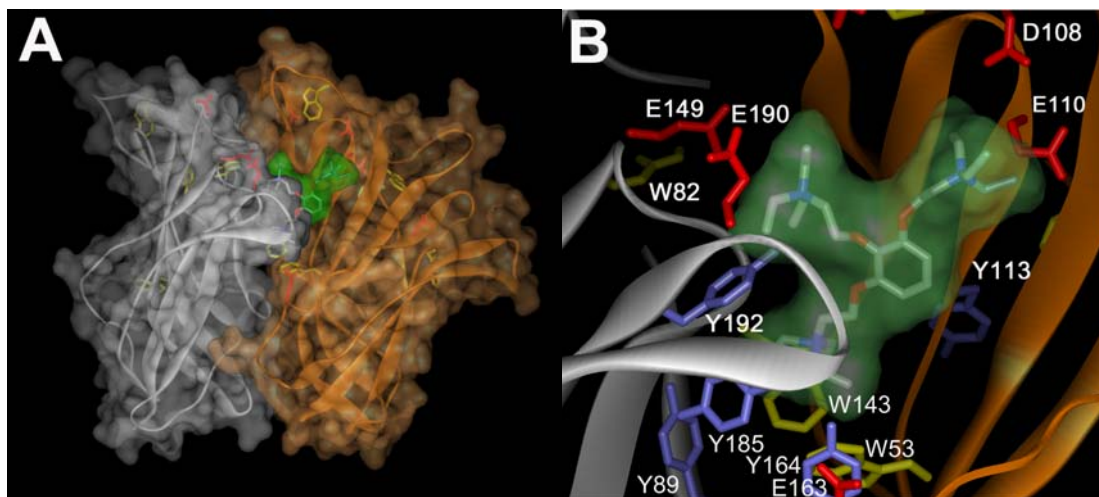


Figure III.4: Docking of gallamine to the AChBP using DOT (28). A. Crystal structure of the subunit interface (3) showing the α carbon chain and the space filling residues for two subunits. The exposed portion of the docked gallamine is shown in green, tryptophan side chains in yellow and selected anionic side chains in red. B. Expanded view of the alpha carbon chain with the tryptophan side chains in yellow, tyrosine in blue and anionic residues in red. Note the positioning of the triethylammonio moieties near the anionic side chains (Glu 110,149,163,190; Asp 108) at the binding site. The pyrogallol ring is sandwiched between the vicinal cysteines at 187 and 188 and isoleucine 112 side chain on the neighboring subunit. The position of gallamine docked by computation may be contrasted with HEPES found in the crystal structure (3).

E Acknowledgments

This chapter is material as it appears in:

Scott B Hansen, Zoran Radic, Todd T Talley, Brian E Molles, Tom Deerinck, Igor Tsigelny, and Palmer Taylor “Tryptophan fluorescence reveals conformational changes in the acetylcholine binding protein” *J Biol Chem.* 2002 Nov 1;277(44):41299-302.

I thank Dr. Zoran Radic who first showed ligand binding to the acetylcholine binding protein quenched the intrinsic tryptophan fluorescence in the protein. Fluorescent kinetics experiments contained in this chapter were performed by Dr Radić. Electron micrographs where obtained by Tom Deerinck and Dr. Igor Tsigelny contributed the computational docking of gallamine in the binding protein. I thank Dr Todd T Talley for discussion in designing oligonucleotides for AChBP cDNA synthesis and for expressing and purifying protein used in the stopped-flow kinetics experiments. I thank Dr. Brian Molles for general lab instruction including molecular biology and protein expression.

F. References

1. Karlin, A. (2002) *Nat Rev Neurosci* **3**(2), 102-14.
2. Corringer, P. J., Le Novère, N., and Changeux, J. P. (2000) *Annu Rev Pharmacol Toxicol* **40**, 431-58
3. Brejc, K., van Dijk, W. J., Klaassen, R. V., Schuurmans, M., van Der Oost, J., Smit, A. B., and Sixma, T. K. (2001) *Nature* **411**(6835), 269-76.
4. Smit, A. B., Syed, N. I., Schaap, D., van Minnen, J., Klumperman, J., Kits, K. S., Lodder, H., van der Schors, R. C., van Elk, R., Sorgedrager, B., Brejc, K., Sixma, T. K., and Geraerts, W. P. (2001) *Nature* **411**(6835), 261-8.
5. Taylor, P., Osaka, H., Molles, B., Keller, S. H., and Malany, S. (2000) in *Neuronal Nicotinic Receptors* (Clementi, F., Fornasari, D., and Gotti, C., eds) Vol. 144, pp. 79-100, Springer-Verlag, Berlin ; New York
6. Itakura, K., Hirose, T., Crea, R., Riggs, A. D., Heyneker, H. L., Bolivar, F., and Boyer, H. W. (1977) *Science* **198**(4321), 1056-63.
7. Lackowicz, J. R. (1999) in *Principles of Fluorescence Spectroscopy*, 2 Ed., pp. 185-210, Kluwer Academic/Plenum Publishers, New York
8. Lockless, S. W., and Ranganathan, R. (1999) *Science* **286**(5438), 295-9.
9. Radic, Z., and Taylor, P. (2001) *J Biol Chem* **276**(7), 4622-33.
10. Sussman, J. L., Harel, M., Frolow, F., Oefner, C., Goldman, A., Toker, L., and Silman, I. (1991) *Science* **253**(5022), 872-9.
11. Galzi, J. L., Bertrand, D., Devillers-Thiery, A., Revah, F., Bertrand, S., and Changeux, J. P. (1991) *FEBS Lett* **294**(3), 198-202.
12. Xie, Y., and Cohen, J. B. (2001) *J Biol Chem* **276**(4), 2417-26.
13. Beene, D. L., Brandt, G. S., Zhong, W., Zacharias, N. M., Lester, H. A., and Dougherty, D. A. (2002) *Biochemistry* **41**(32), 10262-9.
14. Zhong, W., Gallivan, J. P., Zhang, Y., Li, L., Lester, H. A., and Dougherty, D. A. (1998) *Proc Natl Acad Sci U S A* **95**(21), 12088-93.
15. Colquhoun, D., and Sakmann, B. (1985) *J Physiol* **369**, 501-57.

16. Figl, A., Labarca, C., Davidson, N., Lester, H. A., and Cohen, B. N. (1996) *J Gen Physiol* **107**(3), 369-79.
17. Bouzat, C., Barrantes, F., and Sine, S. (2000) *J Gen Physiol* **115**(5), 663-72.
18. Prince, R. J., and Sine, S. M. (1998) *Biophys J* **75**(4), 1817-27.
19. Salamone, F. N., Zhou, M., and Auerbach, A. (1999) *J Physiol* **516**(Pt 2), 315-30.
20. Grosman, C., and Auerbach, A. (2001) *Proc Natl Acad Sci U S A* **98**(24), 14102-7.
21. Wang, H. L., Auerbach, A., Bren, N., Ohno, K., Engel, A. G., and Sine, S. M. (1997) *J Gen Physiol* **109**(6), 757-66.
22. Unwin, N., Miyazawa, A., Li, J., and Fujiyoshi, Y. (2002) *J Mol Biol* **319**(5), 1165-76.
23. Wenningmann, I., and Dilger, J. P. (2001) *Mol Pharmacol* **60**(4), 790-6.
24. Weiland, G., Georgia, B., Lappi, S., Chignell, C. F., and Taylor, P. (1977) *J Biol Chem* **252**(21), 7648-56.
25. Brockes, J. P., and Hall, Z. W. (1975) *Biochemistry* **14**(10), 2092-9.
26. Wang, G. K., and Schmidt, J. (1980) *J Biol Chem* **255**(23), 11156-62.
27. Flanagan, S. D., Barondes, S. H., and Taylor, P. (1976) *J Biol Chem* **251**(3), 858-65.
28. Mandell, J. G., Roberts, V. A., Pique, M. E., Kotlovyi, V., Mitchell, J. C., Nelson, E., Tsigelny, I., and Ten Eyck, L. F. (2001) *Protein Eng* **14**(2), 105-13.

Chapter IV

Structural and Ligand Recognition Characteristics of an Acetylcholine Binding Protein from *Aplysia californica*

A. Abstract

I generated an acetylcholine binding protein from *Aplysia californica* by synthesis of a cDNA found in existing databases and expression in mammalian cell culture. Its subunit assembly and ligand recognition behavior were compared to the binding protein previously derived from *Lymnaea stagnalis*. The secreted proteins were purified by elution from columns of attached antibodies directed to the FLAG epitope encoded in the expression construct. Although the sequences of the two proteins from marine and fresh water mollusks exhibit the characteristic features of the extracellular domain of the nicotinic receptor, they only possess 33% amino acid identity. Both assemble as stable pentamers with five binding sites per pentamer, yet they show distinguishing features of stability and sensitivity to epitope tag placement. Both proteins exhibit changes in tryptophan fluorescence upon ligand binding; however, the magnitude of the changes differs greatly. Moreover, certain ligands show marked differences in dissociation constants for the two proteins and can be regarded as distinguishing or signature ligands. Hence, the two soluble proteins from mollusks, which can be studied by a variety of physical methods, become discrete surrogate proteins for the extracellular domains of distinct subtypes of nicotinic acetylcholine receptors.

B. Introduction

Nicotinic acetylcholine receptors are prototype molecules for the large superfamily of pentameric ligand-gated ion channels (1-3). Owing to their abundance in

the electric organs of *Torpedo sp.* and the finding that peptide toxins from elapid venoms bind with high affinity to the receptor (4,5), the acetylcholine receptor became the first neurotransmitter receptor to be characterized as a molecular entity (6). The receptor from *Torpedo*, similar to the receptor found in skeletal muscle throughout the fish and mammal phyla, assembles as a pentamer composed of four distinct subunits with only one of the subunits being expressed as two copies. The two binding sites, which in the muscle receptor are not identical in recognition characteristics, reside at the interface of the α and its partnering subunits. At least 12 nicotinic receptor subunits from mammalian neuronal tissues have been isolated, and they assemble in selected permutations of α and β subtypes. The simplest subtypes structurally are the homomeric pentamers of α subunits such as such as those from the $\alpha 7$ subtype (1,7).

To function as gated channels, the receptor protein must span the membrane multiple times. The four transmembrane spans on each of the five subunits create a substantial region of hydrophobicity that precludes facile crystallization of this protein. Recent electron microscopy reconstruction analysis has led to a structure of the transmembrane region resolved to 4 Å, and a description of the extracellular domain at somewhat lower resolution (8). An additional specialization of nature has led investigators to a high-resolution structure of the extracellular domain of the receptor. The fresh water snail, *Lymnaea stagnalis*, produces a soluble protein, termed the acetylcholine binding protein (AChBP) that binds acetylcholine (9,10). Characterization of its ligand recognition characteristics shows similar ligand specificity to the nicotinic acetylcholine receptor (10,11). The *Lymnaea* binding protein is also pentameric, and

composed of identical subunits, most closely resembling the extracellular domain of the $\alpha 7$ receptor found in neurons.

Recently, I constructed a cDNA encoding the *Lymnaea* AChBP by ligating a series of chemically synthesized oligonucleotides into an expression construct. The encoded protein was expressed to study its ligand recognition properties and structure in solution (11). Other potential sequences of candidate AChBPs exist in databases of invertebrate species. Herein, I describe the expression and properties of a distinct binding protein from a salt-water mollusk, *Aplysia californica*. Although its sequence shares the hallmark features characteristic of the *Lymnaea* protein, as well as the nicotinic receptor itself, the two binding proteins come from evolutionary distant species and show only 33% amino acid residue identity. Upon purification, the *Aplysia* protein revealed structural and ligand recognition properties distinct from the *Lymnaea* protein enabling us to analyze comparatively two subtypes of binding proteins.

C. Experimental Procedures

1. Construction of an Expression Vector cDNA

The cDNA encoding the A-AChBP was synthesized using the nucleotide coding sequence found in an *Aplysia* database. Briefly, oligonucleotides extending up to 100bp and containing triplet codons with frequent mammalian codon usage (12) were ligated into a p3xFLAG-CMV-9 expression vector (Sigma) containing a preprotrypsin leader peptide followed by an N-terminal 3xFLAG epitope and a C-terminal six-histidine (His) tag. Three alternative expression plasmids were synthesized and compared to the corresponding plasmids from the *Lymnaea* sequence. One had an N-terminal 3X FLAG but was devoid the C-terminal (His) tag. The two others contained a 1X FLAG tag on the

C-terminus or N-terminus. Restriction sites were also engineered into the coding sequence at convenient locations to allow for formation of removable cassettes for subsequent mutagenesis studies.

Conditions for protein expression paralleled that of the *Lymnaea* AChBP (11). Briefly, HEK cells were transfected with A-AChBP cDNA along with a companion neomycin acetyltransferase gene and selected for stable expression using G418. Media containing the secreted A-AChBP was collected at 2 to 3 day intervals and cells replenished with fresh media. Collected media was preserved prior to purification with 0.02% NaN₃. A-AChBPs were purified by adsorption onto a flag antibody column followed by elution with the 3xFLAG peptide.

2. Fast Protein Liquid Chromatography.

Gel filtration was carried out using a Pharmacia LCC 500 plus FPLC with a Superdex 200 gelfiltration column. Fifty μ L of A-AChBP protein at 100 μ g/mL protein concentration in Tris HCl buffered saline (TBS) (20mM Tris HCl, 150mM NaCl, pH 7.4)+ 0.02% azide was loaded on the column at a rate of 0.5 mL/min. Protein in the eluent was monitored by absorption at 280 nm.

3. Sedimentation Equilibrium Analysis

Analytical ultracentrifugation was conducted in a Beckman/Coulter XL-I centrifuge equipped with UV absorption optics using a 60 Ti rotor. Protein solutions of 100 μ g/mL were used in a six-channel charcoal-filled epon centerpiece loaded with 110 μ L of sample and 125 μ L of reference buffer (20mM Tris HCl, 150 mM NaCl, pH 7.4). Individual samples were centrifuged at 20 °C for 16 hours at 10,000 and 12,000 rpm. Equilibrium was attained as judged by overlay of the last three sequential scans. Data

were recorded in step mode with a Δr of 0.001 cm, and 5 replicate absorption measurements were performed at each step every two hours. A partial specific volume, $\bar{v}= 0.71$, for AChBPs was calculated using Sednterp software (ver. 1.06) accounting for total sugar composition. Molar masses of the proteins were calculated using XL-A/XL-I Data Analysis Software version 4.0 based on Origin™ program.

4. Estimation of Binding Parameter from Fluorescence Signals

Equilibrium fluorescence was monitored using a Tecan Sapphire fluorescence plate reader (Tecan, USA) in 96 well UV plates (Costar, USA). AChBP was excited at 280nm and emission intensity monitored at 340nm using an excitation and emission slit widths of 7.5nm in a bottom read mode at room temperature.

AChBP, 50-100nM in binding site concentration, was equilibrated with half log dilutions of ligand. Data were normalized, and K_i 's were calculated by fitting to a sigmoidal dose-response curve with variable slope in Prism GraphPad 3.0. $Y = \text{Min} + (\text{Max} - \text{Min}) / (1 + 10^{((\text{LogEC}_{50} - X) * \text{HillSlope})})$; where X is the log of concentration. Y is the fractional binding. K_i is calculated from $Y_{50} / (1 + ([\text{ligand}] / K_d))$.

To determine ligand stoichiometries, AChBP at 400nM-650nM in binding sites, estimated from protein concentration, was titrated with sequentially increasing concentrations of epibatidine or methyllycaconitine. The concentration of binding sites greatly exceeded the K_d of the ligand. Accordingly, quenching was essentially linear with concentration until the binding sites were saturated and no further quenching was apparent.

5. pH Stability of AChBPs

AChBP at a concentration of 0.5nM binding sites was mixed with 0.1 mg/ml of beads for the PVT copper His-Tag scintillation proximity assay, according to manufacturers' recommendations (Amersham Bioscience, USA). The beads were suspended in 0.01M phosphate/pyrophosphate buffer between pH 5.0 and 11. [³H]-epibatidine at 20nM was added to the 200uL reaction and allowed to equilibrate at room temperature at the respective pH for 1hr or the designated time and then read on a Beckman LS 6500 scintillation counter.

6. Stopped-flow Kinetics

Stopped-flow measurements were obtained using an Applied Photophysics SX.18MV (Leatherhead, UK) stopped-flow spectrofluorometer. AChBP was excited at 280nm and emission was monitored above 305nm using a cut off filter. Changes in fluorescence emission intensity were fit to a first order equation and resulting rates plotted versus ligand concentration. Association and dissociation were estimated from the slope and ordinate intercept. In addition, dissociation rate constants were estimated by monitoring the dissociation of the ligand-AChBP complex by addition of excess gallamine and following the increase in fluorescence. Sufficient gallamine was used to ensure that the rate was limited by the dissociating ligand rather than the scavenging of free ligand by gallamine.

D. Results

1. Expression of the Acetylcholine Binding Protein from a Synthetic Gene

Using the published sequence of AChBP from *Lymnaea stagnalis*, a blast search of the Entrez pub med protein database yielded a sequence from *Aplysia californica* (A-AChBP) that shared 33% amino acid identity with *Lymnaea*. It contained internal

sequence features suggesting it was a soluble binding protein rather than a truncated receptor sequence. Given that *Aplysia* and *Lymnaea* are evolutionarily distant mollusks, I reasoned that A-AChBP might be an ortholog with distinct pharmacological properties. Figure IV.1 shows an alignment of soluble binding proteins with the N-terminal domains of transmembrane spanning heteromeric $(\alpha 1)_2\beta\gamma\delta$ nicotinic receptor in muscle and the homomeric $\alpha 7$ neuronal receptor. A-AChBP lacks a transmembrane spanning region. Furthermore, the cysteine loop region between residues 127 and 140 (*Aplysia* numbering), is highly conserved among binding proteins, but distinct from that of nAChR's, where it is also highly conserved among the receptor molecules. This region is thought to interact and link with the transmembrane domain of the receptor (7,13), but reveals a hydrophilic surface in the case of the binding proteins.

HEK 293 cells, transfected with the A-AChBP gene and selected as stable transfectants, secreted the encoded protein into the media. Typically between 1 and 3 milligrams of A-AChBP could be purified from a liter of media. A cDNA encoding A-AChBP, isolated from a sensory cell *Aplysia* library, when placed in our viral expression vector, was found not to express active secreted protein. When sequenced it was found to differ by valine being substituted to alanine at residues 43 and 138. A sequence with the two valine residue substitutions was not found in the *Aplysia* database.

2. Characterization of the Binding Protein

Due to variable aggregation of initial preparations of A-AChBP, I investigated the role played by a C-terminal 6x His tag and several FLAG tags of variable length at both the N- and C- termini of the AChBP coding sequence (Figure IV.2). Table IV.1 shows the typical expression achieved after purification for four constructs for both *Lymnaea*

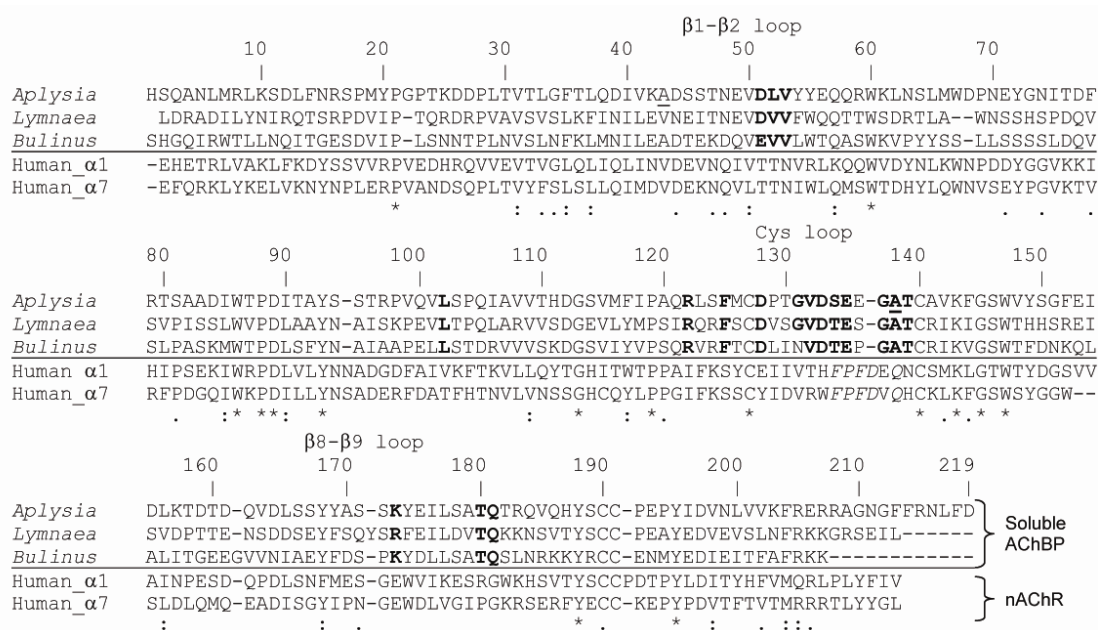


Figure IV.1: Protein sequence alignments. Three soluble binding proteins from *Lymnaea stagnalis*, *Aplysia californica* and *Bulinus truncatus* (22) are aligned with the first 210 amino acid residues of human nicotinic acetylcholine receptors $\alpha 1$ and $\alpha 7$ subunits. Numbering corresponds to *Aplysia* beginning with the first synthesized residue in the cDNA sequence and a probable start site based on consensus sequences. Asterisks indicate identity among the receptor family while colons and periods indicate limited conservation in the series. Bold residues are conserved among soluble AChBP's, but are distinct from transmembrane spanning receptors. Underscored alanines 43 and 138 were found to be valines in a sensory cell *Aplysia* cDNA library.

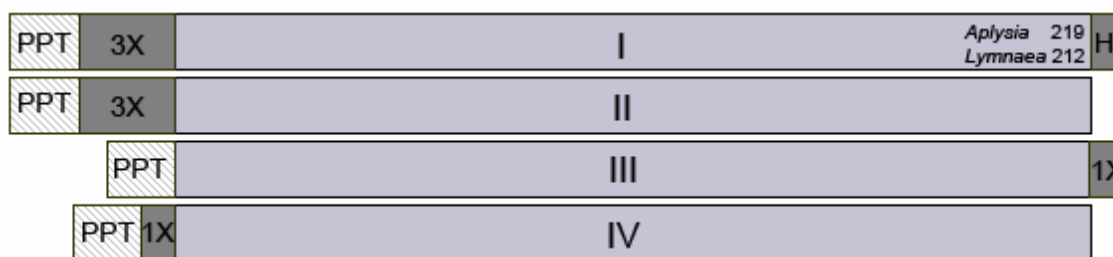


Figure IV.2: AChBP cDNA constructs used to characterize the acetylcholine binding protein. PPT indicates a preprotrypsin leader peptide. Dark shading indicates a purification tag (3x or 1x= FLAG epitope and H= 6x histidine). Equivalent constructs were made with both *Aplysia* and *Lymnaea*. The numbers indicate the respective amino acid residues in the assembled gene products coming from the sequences in Figure IV.1.

Table IV.1
Properties of the acetylcholine binding proteins from *Lymnaea* and *Aplysia*

Construct	Peptide MW ¹	Peptide MW ¹	Location of Purification Tags	Aggregation ³		Oligo- saccharide	Yield ⁴ (mg/L)
	(<i>Lymnaea</i>)	(<i>Aplysia</i>)		<i>Aplysia</i>	<i>Lymnaea</i>		
I	27,586	28,941	3xN-FLAG/C-6xHis	+	+/-	+	2-3
II	26,551	27,905	3xN-FLAG	-	-	+	2-3
III	24,834	26,074	1xC-FLAG	-	-	-	0.5-1
IV	24,834	26,187	1xN-FLAG	-	-	+	3-4

Summarized are the constructs with their corresponding purification tag, molecular weight, expression and physical properties. ¹Molecular weights designate calculated values for the mature peptide only. ²Large additional peaks at heavier apparent molecular weights, as observed by gel filtration, were interpreted as aggregation. ³Positive for oligosaccharide indicates extensive glycosylation processing with multiple bands; all forms contain N-linked oligosaccharides. ⁴Expression is shown as a range from several preparations, quantified as mg of protein purified to apparent homogeneity per liter of harvested media.

and *Aplysia* genes. Purified protein for each construct was analyzed by SDS-PAGE and gel filtration. A 6X histidine tag on the C-terminus resulted in extensive aggregation or oligomerization in the *Aplysia* cDNA following purification. The aggregation varied from a small shoulder slightly larger than the pentameric 190 kDa to an aggregate peak in the void volume upon gel filtration (Figure IV.3C-D). The presence of the larger oligomers accumulated rapidly at room temperature and 4° C. By contrast, the *Lymnaea* protein showed minimal aggregation initially, but formed higher order oligomers over a period of several months when stored at 4° C. Expression from constructs encoding both *Lymnaea* and *Aplysia* protein without the 6X-His tag yielded minimal aggregation over several months (Figure IV.3A-B). Both eluted at an apparent molecular weight of 190,000.

Constructs modified at the N-terminus showed variable glycosylation evident in the multiple bands on SDS-PAGE (Figure IV.4). Only the construct with a single C-terminal FLAG tag (III) migrated as a single, but broad band. Its expression yields however, were lower than those of the N-terminally tagged constructs (Table 1). Neither initial aggregation nor heavy glycosylation were observed to influence ligand binding parameters, although the aggregated proteins were not studied in detail. Analytical ultracentrifugation yielded profiles that fit to a molecular weight estimate of $155,100 \pm 1,400$ for A-AChBP and $151,700 \pm 800$ for L-AChBP (Figure IV.5), values expected for a glycosylated pentamer.

I examined protein stability in 0.01M phosphate/pyrophosphate buffer between pH 5.0 and 11 (Figure IV.6). In addition, solutions were kept at room temperature in the dark and stability monitored over a month (data not shown). [³H]-epibatidine sites were

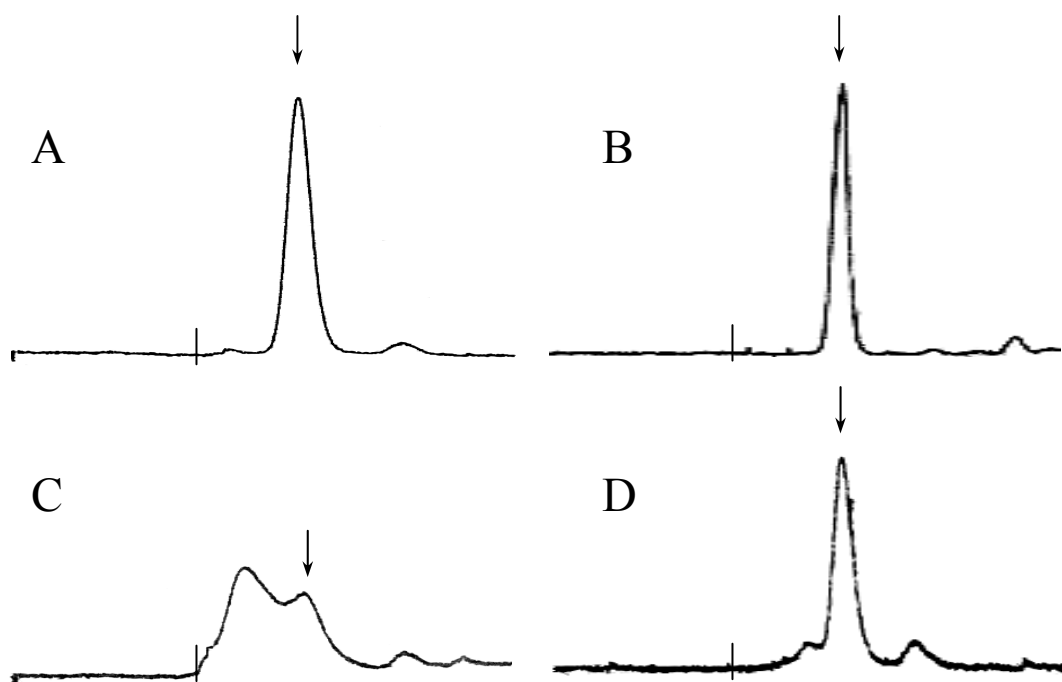


Figure IV.3: FPLC of AChBPs A, Non-His tagged A-AChBP (II); B, Non-His tagged L-AChBP (II); C and D, His tagged A-AChBP (I). The Roman numerals designate the constructs in Figure IV.2. Panel C contains ~50% aggregated protein while panel D is mostly properly assembled pentamer with a small shoulder of aggregate. Arrows indicate an apparent 190,000 MW pentamer peak and vertical lines indicate the void volume. Purified AChBP 0.1 mg/ml in 20mM Tris HCl 150mM NaCl, pH 7.4, was applied to a Superdex 200 size exclusion column.

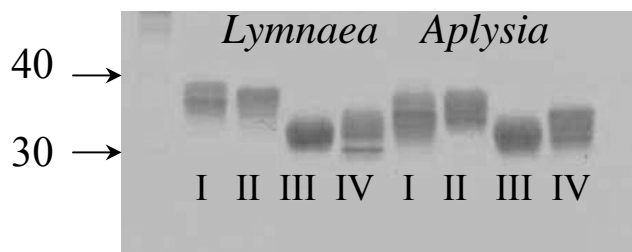


Figure IV.4: SDS-PAGE of the purified acetylcholine binding proteins. Lanes 1-4 are *Lymnaea* proteins and lanes 5-8 are *Aplysia* proteins. Size and glycosylation are distinct among tags and seem roughly similar between species. Purified protein (1.5 μ g) was spotted on each lane and run on 16% acrylamide gels. Roman numerals denote the constructs described in Figure IV.2.

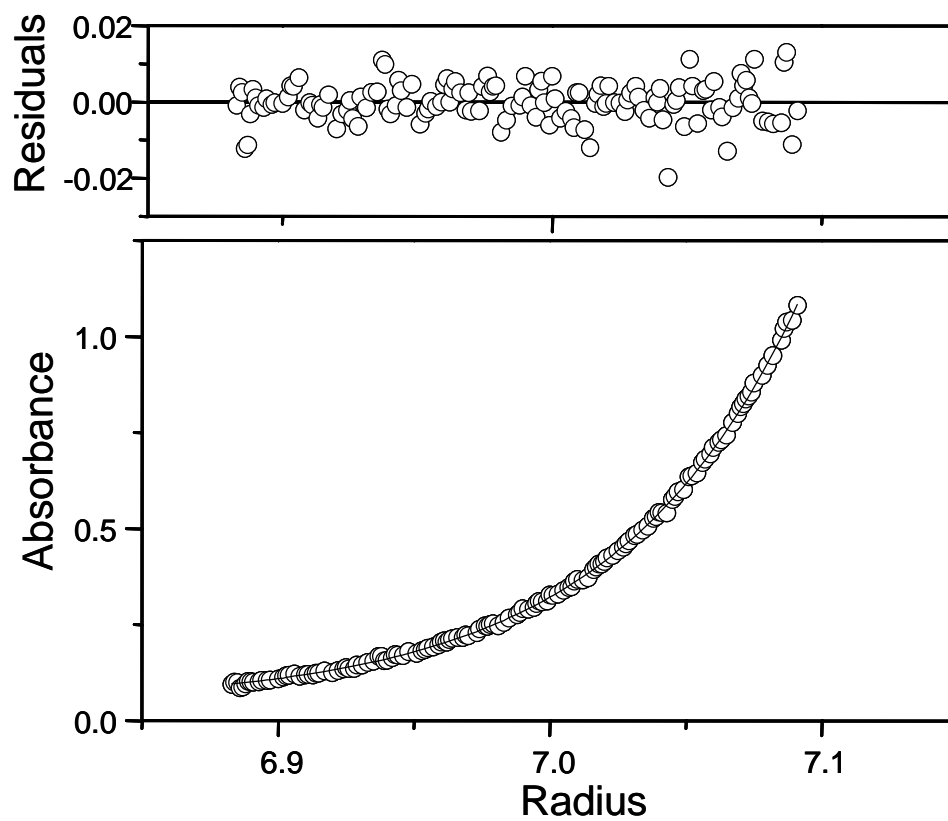


Figure IV.5: Analytical ultracentrifugation of *Aplysia* AChBP. Samples of 100 $\mu\text{g/mL}$ A-AChBP in (20mM Tris HCl, 150 mM NaCl, pH 7.4) was sedimented at 12,000 rpm until a constant profile was established. The curve is fit to a molecular weight of 153,000 with the other variables fixed as described in the text.

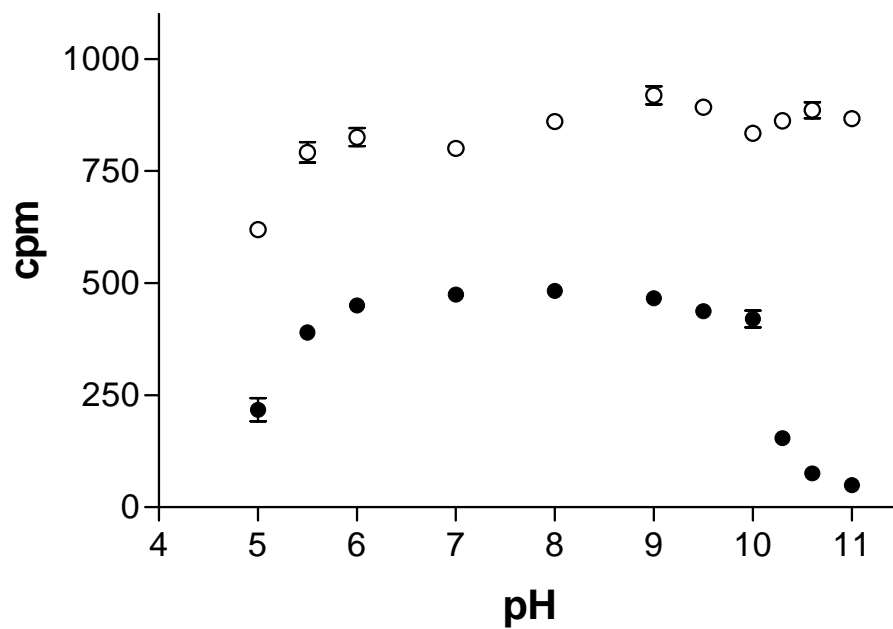


Figure IV.6: pH Stability of the AChBP's Samples of 0.5 nM AChBP binding sites was incubated with 20nM [^3H]-epibatidine for 1 hour and monitored using a scintillation proximity assay. The pH was varied between 5.0 and 11 using a 100mM phosphate/pyrophosphate buffer. \circ L-AChBP, \bullet A-AChBP

not lost during the 1hr incubation for *L*-AChBP between pH 5.5 and pH 11, whereas *A*-AChBP rapidly lost activity above pH10. Above pH 8, *L*-AChBP was stable for 6 days but showed some loss of signal after one month. *A*-AChBP showed little binding above pH 8.0 after 6 days but was completely stable between pH 6.0 and 7.0 for the observed period.

3. Ligand Binding Properties

To determine ligand recognition properties of *A*-AChBP, I employed an equilibrium-binding assay using intrinsic tryptophan fluorescence of AChBPs. Figure IV.7 shows typical mass action curves of both *L*-AChBP and *A*-AChBP. Surprisingly, while only gallamine was found to enhance tryptophan fluorescence for *L*-AChBP, small cholinergic agonists such as choline, acetylcholine and carbachol enhance fluorescence emission of *A*-AChBP in addition to gallamine. Agonists, such as nicotine and epibatidine, containing ring nitrogens markedly quench fluorescence of both AChBPs.

Binding of ligands with K_d 's below 100 nM was monitored using stopped-flow spectrometry and fluorescence detection (Table IV.3). Table IV.2 shows a summary of dissociation constants determined from tryptophan fluorescence either by equilibrium titration for lower affinity ligands or by kinetic analysis for the high affinity ligands. Interestingly α -bungarotoxin (bgtx) has 100 fold lower affinity for *A*-AChBP than *L*-AChBP, but the smaller peptide, α -conotoxin ImI, has an affinity for *A*-AChBP that is more than 4 orders of magnitude greater than that for *L*-AChBP. Higher affinity of α -

Conotoxin ImI for *Aplysia* arises primarily from its slower dissociation rate (Table 3). The slow binding, high affinity ligands appear to show a second unimolecular phase of low amplitude for tryptophan fluorescence quenching. This is being

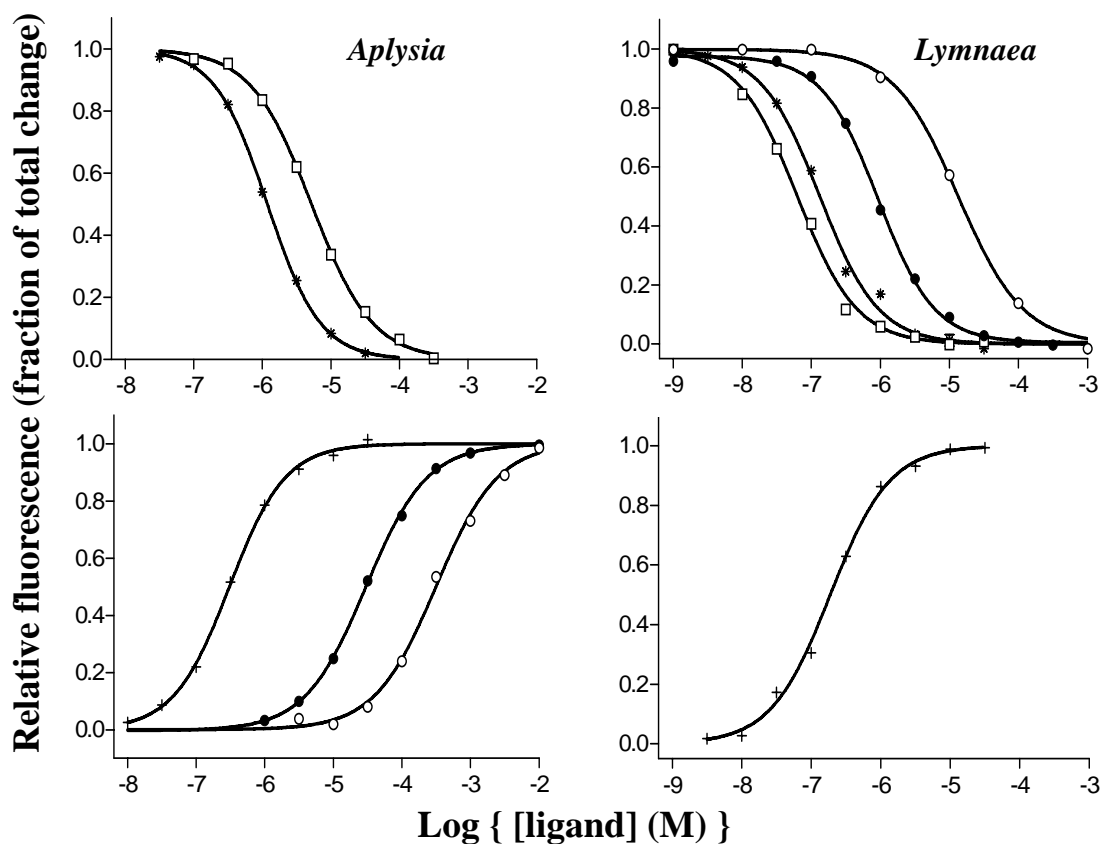


Figure IV.7: Steady state of ligand binding to AChBP's. Ligand binding was monitored in a 96 well fluorescent plate reader. Samples were excited at 280nm and intrinsic tryptophan fluorescence emission monitored at 340nm. (\circ carbachol, \bullet acetylcholine, $+$ gallamine, $*$ dansylcholine C_6 , \square nicotine). Dissociation constants from experiments as this are shown in Table 2. Left panels are *Aplysia* AChBP and right panels are *Lymnaea* AChBP.

Table IV.2
Dissociation constants for ligand binding to the *Aplysia*
and *Lymnaea* acetylcholine binding proteins

Ligand	<i>Aplysia</i> K _d (nM)	<i>Lymnaea</i> K _d (nM)	K _d Ratio L/A
α-Conotoxin ImI	0.88 ¹	14,000 ¹	16,000
Methyllycaconitine	2.8 ¹	0.41 ³	0.14
Epibatidine	14 ¹	0.16 ³	0.011
Strychnine	15 ¹	23 ¹	1.5
Gallamine	120 ²	140 ³	1.2
(-)-Nicotine	245 ²	86 ³	0.35
α-Bungarotoxin	250 ²	1.8 ³	0.0071
Dansylcholine C ₆ ⁴	1,600 ²	110 ³	0.069
Acetylcholine	33,000 ²	890 ²	0.027
Carbachol	240,000 ²	5,600 ²	0.023

⁴ 5-dimethylaminonaphthylsulfonamidoethyltrimethylammonium

K_d's for high affinity ligands¹ (K_d's <100nM) were determined from the ratio of association and dissociation rates by monitoring intrinsic tryptophan quenching with stopped-flow spectrofluorometry. Low affinity ligands² were measured using equilibrium fluorescence quenching in a 96 well fluorescent plate reader. All constants are either an average of two values or the mean of three or more. Values varied by less than 20%. ³Previously reported in reference (11)

Table IV.3
Kinetic constants for association (k_1) and dissociation (k_{-1}) of
various ligands for the acetylcholine binding proteins

Ligand	k_1 ($\times 10^8$ $M^{-1}s^{-1}$)		k_{-1} (s^{-1})	
	<i>Aplysia</i>	<i>Lymnaea</i>	<i>Aplysia</i>	<i>Lymnaea</i>
α -Conotoxin ImI	0.16	0.014	0.01	19
Epibatidine	2.5	1.7	3.4	0.027
Strychnine	3.0	0.93	4.6	2.2
Methyllycaconitine	0.44	0.13	0.12	0.005
Gallamine	2.5	2.5	65	36
α -Bungarotoxin	0.010	0.009	0.32	0.001
(-)-Nicotine	2.3	1.5	49	5.7

Kinetic constants were determined using stopped-flow spectrofluorometry. Samples were excited with 280nm light and emission monitored above 305nm. Slow dissociation rates of high affinity ligands were measured by competition. Addition of gallamine, induces an enhancement of fluorescence in formation of its complex. Data are averages of two measurements or means of three or more measurements.

investigated in relation to overall mechanism. We reported previously *L*-AChBP to have five binding sites per pentamer (11). Equilibrium titrations of *A*-AChBP at concentrations above its K_d likewise reveal 5 sites per pentamer (Figure IV.8). Titration profiles are very similar to that reported for the *L*-AChBP.

E. Discussion

The discovery of an acetylcholine binding protein from the fresh water mollusk *Lymnaea stagnalis*, and the elucidation of its structure by X-ray crystallography have added a new dimension to the study of the structure and ligand binding properties of the family of nicotinic acetylcholine receptors and related pentameric ligand gated ion channels (9). Moreover, linking structural details of the extracellular domain from crystallography at 2.8 Å resolution to electron microscopy reconstruction analysis of the transmembrane domain of the nAChR at 4 Å has yielded a more comprehensive structural perspective of the nicotinic receptor as an integral unit (2,7-9).

The multiplicity of the family of nicotinic receptor subunits and the diversity of subtypes that can be achieved through subunit assembly allow one to rank order selective ligands with respect to receptor subtype. The very size of the nAChR family exceeds the discrimination capacity of its ligands precluding a receptor subtype classification based solely on ligand specificity. Nevertheless, ligand selectivity of receptor subtypes does allow studies of subtype distribution in regional tissue areas and during developmental processes (14). Developing a complement of AChBPs with distinct specificities would enable one to add a structural dimension to the analysis of the determinants of ligand specificity, since the soluble proteins and their complexes can be analyzed in far more structural detail.

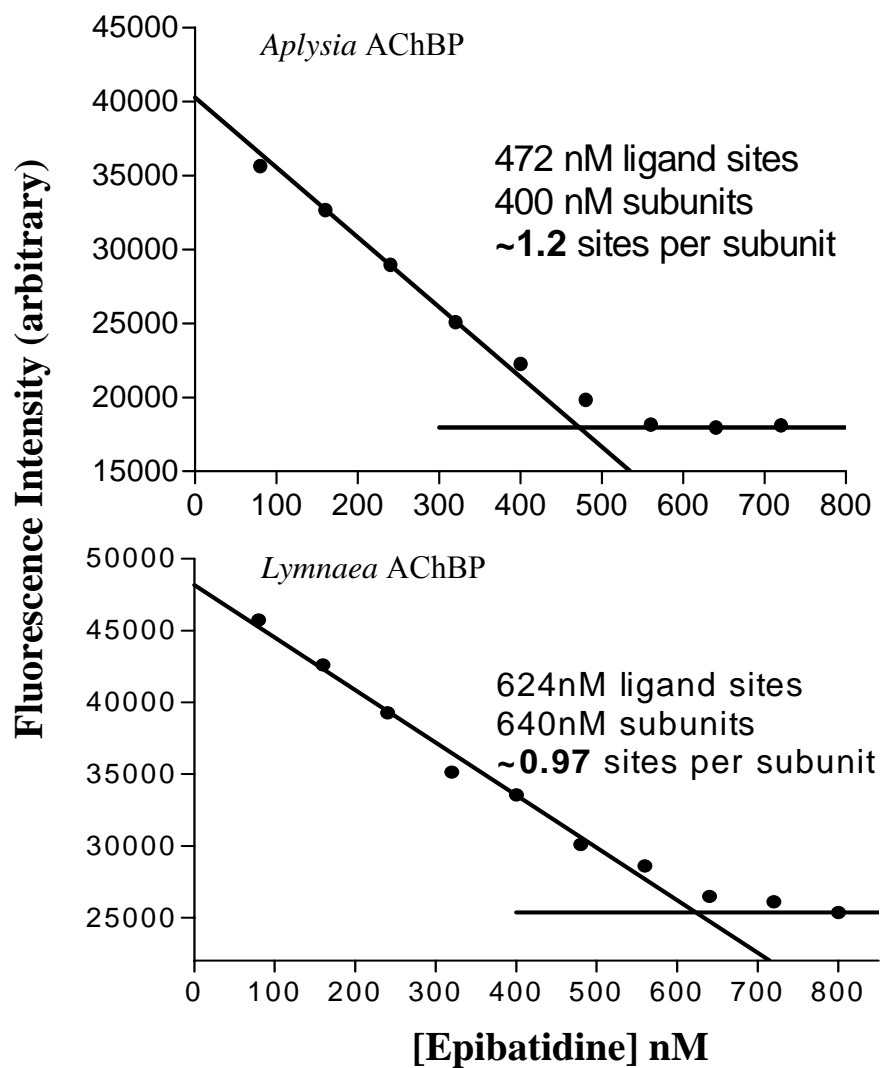


Figure IV.8: Titration of ligand stoichiometry. Using excess ligand binding sites over K_d and monitoring intrinsic tryptophan fluorescence quenching of AChBP at 340nm, binding site titration with [^3H]-epibatidine was used to estimate the total number of binding sites. Saturation occurs at approximately 5 sites per pentamer (*Aplysia* AChBP top, *Lymnaea* AChBP bottom).

To this end, I have synthesized a cDNA encoding an AChBP from *Aplysia californica* and demonstrated that it assembles as a pentamer, has a stoichiometry of one ligand binding site per subunit or five per pentamer, and exhibits a general profile of ligand binding affinities characteristic of the nAChR. The capacity of the expressed *Aplysia* subunit to assemble as a stable pentamer has been compared with *Lymnaea*. Moreover, I have identified a signature ligand for the *Aplysia* AChBP ortholog where α -conotoxin ImI has 16,000-fold greater affinity for *Aplysia* over the *Lymnaea* protein. Other naturally occurring ligands of peptidic or alkaloid composition also show preferential affinities for the one or the other AChBPs. α -Conotoxin ImI is produced by the cone snail, *Conus imperialis*, a worm hunting cone snail (15). This conotoxin is known to be a selective ligand for the $\alpha 7$ subtype among the nAChR's (16) suggesting the possibility that ligand specificity of the *Aplysia* AChBP more closely mimics the $\alpha 7$ receptor subtype than *Lymnaea*. Since the *Aplysia* and *Lymnaea* AChBPs only show 26 and 24% amino acid residue identity with the extracellular region of $\alpha 7$, neither binding protein would be a precise replicate homomeric mammalian receptor. However, they present a potential structural template for substitution of mammalian residue determinants of specificity.

1. Synthesis, Assembly and Stability of the Acetylcholine Binding Protein.

Using a mammalian expression system and cDNAs constructed from oligonucleotides designed to introduce restriction sites at strategic locations and weighted towards a mammalian codon abundance gives rise to expression and export of AChBP into the culture medium in quantities of several milligrams per liter. To increase the

surface area of attached cells, I have employed multilayer 100cm² flasks, but the expression system should be applicable to other adhesion attachments for cell growth. Multiple media changes and replenishment allow for continuous production from single plating for up to a month.

As might be anticipated, expression levels of protein differ substantially between experimental constructs depending on the nature of the recognition tag and where it is placed on the construct. I have employed a FLAG epitope for purification and a His tag for both purification and development of a radioactive assay for the soluble protein. Expression can be achieved with both tags, but stability of the protein and the extent of glycosylation processing differ as evidenced by migration on SDS-PAGE. The products of the expression constructs also differ in their capacity to assemble as pentamers as evidenced by size exclusion chromatography and sedimentation analysis. I routinely examine our preparations to insure that they are virtually devoid of monomeric species and higher orders of assembly or aggregates prior to analyzing binding parameters.

Both AChBPs can be purified in quantities of several milligrams offering the potential for physical investigations of their overall structure in relation to their ligand recognition properties. The purified proteins appear to be quite robust and retain their assembled structure and ligand binding properties for extended periods of time. Of the two, the *Lymnaea* protein appears to assemble more facily under the many conditions employed and exhibit the greater stability as measured at extreme pH values. The extent of glycosylation appears dependent on the placement of the recognition tag for purification. Glycosylation also appears to be an important factor in the ease of crystallization of the two binding proteins (S. B. Hansen, unpublished).

2. Determinants of Ligand Specificity

Since the pioneering findings of Karlin and colleagues (17), who demonstrated the importance of vicinal cysteines, now identified in the $\beta 9$ - $\beta 10$ linker, in the recognition characteristics of the nAChR, elucidating the determinants of recognition for the receptor for the variety of natural and synthetic ligands has become a major endeavor. Studies with site-directed irreversible inhibitors, chemical cross-linking and site-directed mutagenesis all have identified three non-contiguous segments on the face of the α -subunit and four on the opposing face of adjacent subunit of the circular pentamer that harbor the side chain determinants governing ligand specificity (18,19). Identification of these regions and delineation of the characteristics of the residues involved has benefited greatly from the comparison of specificity of homologous subunits, generation of subunit chimeras and site-directed residue substitutions from the homologous or orthologous subunits (18). This approach is now possible with residue substitutions in the homomeric *Lymnaea* and *Aplysia* pair.

The rate constants for association of α -bungarotoxin are far slower than the other ligands suggesting that initial binding of this toxin induces a slow change in conformation or the α -toxin binds to a conformation of low abundance. The uniquely slow rates of α -toxin association with the receptor have been known for many years (20,21). For both α -conotoxin ImI and α -bungarotoxin, differences in affinity for the two AChBP's are reflected primarily in the dissociation rates.

The two AChBP's also differ in several other properties that bear further experimental investigation. For example, the *Aplysia* protein has three tryptophans while

Lymnaea contains an additional tryptophan at position 53 (corresponding to 55 in *Aplysia*). This is a region in the muscle receptor shown to govern ligand specificity differences seen between the respective binding sites at the $\alpha\gamma$, the $\alpha\varepsilon$, and the $\alpha\delta$ subunit interfaces (18,19). Given the steric requirements for placement of a large indole ethyl side chain, tryptophan at this position becomes a candidate determinant of the distinct affinities found between the *Aplysia* and the *Lymnaea* AChBP's. Moreover, I have shown previously that many ligands quench the tryptophan fluorescence of the *Lymnaea* protein upon binding; these signals might be exploited further to monitor binding kinetics and ascertain binding orientation of the ligands.

F. Acknowledgements

This chapter is material as it appears in:

Scott B Hansen, Todd T Talley, Zoran Radic, and Palmer Taylor “Structural and ligand recognition characteristics of an acetylcholine binding protein from *Aplysia californica*” *J Biol Chem.* 2004 Jun 4;279(23):24197-202

I thank Dr. Igor Tsigelny for first pointing out that a homolog of the *Lymnaea* binding protein exists in *Aplysia*. I thank Dr. Todd T. Talley for assistance in designing oligonucleotides for cDNA synthesis of the *Aplysia* AChBP. Dr Talley also first employed the scintillation proximity assay (SPA) in our lab which I used to show pH stability of the AChBP in this chapter. I thank Dr. Zoran Radić for assistance in designing experiments for stopped flow kinetics and for discussion of all fluorescent measurement in this chapter. I am grateful to Dr. Kelsey Martin at UCLA for providing us with a sensory cell cDNA library from *Aplysia californica*.

G. References

1. Corring, P. J., Le Novere, N., and Changeux, J. P. (2000) *Annu Rev Pharmacol Toxicol* **40**, 431-458
2. Karlin, A. (2002) *Nat Rev Neurosci* **3**, 102-114
3. Sixma, T. K., and Smit, A. B. (2003) *Annu Rev Biophys Biomol Struct* **32**, 311-334
4. Chang, C. C., and Lee, C. Y. (1963) *Arch Int Pharmacodyn Ther* **144**, 241-257
5. Lee, C. Y. (1963) *Showa Igakkai Zasshi* **23**, 221-229
6. Changeux, J. P., Kasai, M., and Lee, C. Y. (1970) *Proc Natl Acad Sci U S A* **67**, 1241-1247
7. Kash, T. L., Jenkins, A., Kelley, J. C., Trudell, J. R., and Harrison, N. L. (2003) *Nature* **421**, 272-275
8. Miyazawa, A., Fujiyoshi, Y., and Unwin, N. (2003) *Nature* **424**, 949-955
9. Brejc, K., van Dijk, W. J., Klaassen, R. V., Schuurmans, M., van Der Oost, J., Smit, A. B., and Sixma, T. K. (2001) *Nature* **411**, 269-276
10. Smit, A. B., Syed, N. I., Schaap, D., van Minnen, J., Klumperman, J., Kits, K. S., Lodder, H., van der Schors, R. C., van Elk, R., Sorgedrager, B., Brejc, K., Sixma, T. K., and Geraerts, W. P. (2001) *Nature* **411**, 261-268
11. Hansen, S. B., Radic, Z., Talley, T. T., Molles, B. E., Deerinck, T., Tsigelny, I., and Taylor, P. (2002) *J Biol Chem* **277**, 41299-41302
12. Nielsen, H., Engelbrecht, J., Brunak, S., and von Heijne, G. (1997) *Protein Eng* **10**, 1-6
13. Unwin, N., Miyazawa, A., Li, J., and Fujiyoshi, Y. (2002) *J Mol Biol* **319**, 1165-1176
14. Zoli, M. (2000) in *Handbook Exp. Pharm* (Clementi F, F. D., and Gotti C, ed) Vol. 144, pp. 213-246, Springer-Verlag Berlin
15. McIntosh, J. M., Santos, A. D., and Olivera, B. M. (1999) *Annu Rev Biochem* **68**, 59-88

16. Johnson, D. S., Martinez, J., Elgoyhen, A. B., Heinemann, S. F., and McIntosh, J. M. (1995) *Mol Pharmacol* **48**, 194-199
17. Silman, I., and Karlin, A. (1969) *Science* **164**, 1420-1421
18. Taylor, P. (2000) in *Handbook Exp. Pharm* (Clementi F, F. D., and Gotti C, ed) Vol. 144, pp. 79-100, Springer-Verlag Berlin
19. Sine, S. M. (2002) *J Neurobiol* **53**, 431-446
20. Lee, C. Y. (1972) *Annu Rev Pharmacol* **12**, 265-286
21. Weiland, G., Georgia, B., Lappi, S., Chignell, C. F., and Taylor, P. (1977) *J Biol Chem* **252**, 7648-7656
22. Smit A. B., Sixma T. K. (2001) *World Intellectual Property Organization*, WO 01/58951 A2

Chapter V

Insights into Intrinsic Tryptophan Fluorescence of the Acetylcholine Binding Protein

A. Abstract

The acetylcholine binding protein (AChBP) undergoes changes in intrinsic tryptophan fluorescence upon binding of ligand. The ligand binding site at the subunit interface is characterized by a cluster of aromatic residues that reside internally to the C loop. This loop extends across the external perimeter of the subunit boundary to be in apposition with the neighboring subunit in the pentameric molecule (See Figure V.2). The two proteins differ in that one of the two tryptophans in this aromatic cluster at the 53 position in *Lymnaea* is replaced by a tyrosine in the *Aplysia* protein. This residue change is important for small agonist binding such as acetylcholine and nicotine. Quenching of intrinsic tryptophan fluorescence is also affected. In the case of the *Lymnaea* protein, all alkaloid antagonists studied, except for the trisquaternary ligand, gallamine, appear to quench the fluorescence. By contrast in *Aplysia*, quenching is seen with the alkaloid antagonists, the agonists in which the nitrogen is in a ring system, but not the flexible choline containing agonists. The crystal structure of apo *Aplysia* Y55W resolved at 2.7Å shows the tryptophan to occupy the same position and relative space as the tyrosine side chains in the wild type protein. Fluorescence data, combined with crystallographic coordinates, suggest that the positions of the ligand and possibly the vicinal cysteines in the C loop likely govern enhancement vs. quenching of intrinsic tryptophan fluorescence upon ligand binding.

B. Background

Ligand-gated ion channels, including nicotinic acetylcholine receptor, are composed of five subunits, each of which traverses the membrane four times (1,2); their hydrophobicity and size preclude conventional studies such as X-ray crystallography, nuclear magnetic resonance spectrometry, and fluorescence spectroscopy. The acetylcholine binding proteins (AChBP) are a structural(3) and functional(4-6) surrogates for the ligand binding domain of the prototypic nicotinic acetylcholine receptor. In previous chapters, I have shown that *Lymnaea* and *Aplysia* AChBP undergo changes in intrinsic tryptophan fluorescence upon binding of ligand(6,7). However, the mechanism by which fluorescence was enhanced or quenched is not understood. There are five tryptophans in *Lymnaea* AChBP and four in *Aplysia* AChBP. Here, I investigate the role played by these tryptophans in governing ligand specificity and fluorescence characteristics of the AChBP as determined by mutagenesis, steady-state fluorescence emission and X-ray crystallography.

C. Methods

1. Mutagenesis

Wild-type AChBP from *Aplysia californica* was expressed from a cDNA synthesized from oligonucleotides selected for mammalian codon usage, described in Chapter II. Briefly, the AChBP gene was inserted into a p3xFLAG-CMV-9 expression vector (Sigma) containing a preprotrypsin leader peptide followed by an amino-terminal 3xFLAG epitope. Mutant AChBPs were generated by polymerase chain reaction-mediated standard mutagenesis procedures, and cassettes containing the mutation were subcloned into the wild-type vector and verified by double-stranded sequencing.

2. Expression and Purification of AChBP

Wild-type and mutant AChBP-transfected HEK-293 cells were selected with G418 to generate stably expressing cell lines. Dulbecco's modified Eagle's medium (MediaTech CellGro) containing 3% fetal bovine serum was collected at 3-day intervals from multiter flasks maintained for up to 4 weeks. Adsorption onto a FLAG antibody column followed by elution with the 3xFLAG peptide yielded purified protein in quantities between 2 and 5 mg/liter. Proteins were concentrated to 1-10 mg/ml using a centricon spin column with a pore size of 50,000 MW (Millipore.) Purity and assembly of subunits as a pentamer were assessed by SDS-PAGE and fast protein liquid chromatography on Sephadex 200 size exclusion column (Amersham.)

3. Radioligand Binding Assays

A scintillation proximity assay (SPA, Amersham Biosciences) was adapted for use in a soluble radioligand binding assay. In 100- μ l reaction vessels, AChBP (0.5 nM binding sites) was incubated with increasing concentrations of either 125 I-labeled α -bungarotoxin or (+)-epibatidine in a solution of 1 mg/ml anti-IGg mouse SPA beads and 5nM anti FLAG antibody. In competition assays, 125 I-labeled α -bungarotoxin was held constant at 10 or 20 nM and epibatidine was added in variable concentrations (1-20nM). Radioactivity was measured on a Beckman LS 6500 liquid scintillation counter.

4. Fluorescence Emission

AChBP 100nM binding sites in 0.1 phosphate buffer, pH 7.0, was mixed with and without ligand to a final volume 50-100 μ l in 96 well fluorescent plate. Samples were incubated 10 min and read on a Tecan Sapphire plate reader. Ligand and instrumental backgrounds were subtracted, and emission intensities normalized to that of unliganded AChBP.

5. Crystallization

Crystallization of apo A-AChBP Y55W was achieved by vapor diffusion at 18°C using a protein-to-well ratio of 1:1 in 1 µl hanging drops. The well solutions comprised: 12-14% PEG-4000 (Fluka), 0.1 M sodium citrate, pH 5.6, and 20% isopropanol. The crystals were flash-cooled in liquid nitrogen after successive short soaks into well solutions supplemented with 18 to 23% PEG and 3 to 5% glycerol. Data were processed with HKL2000 (8)

6. Structure Refinement

Aplysia Y55W AChBP structures were solved by molecular replacement with AMoRe (9) using, as search model, the structure of apo *Aplysia* AChBP (PDB code 2BYP). Manual adjustments were made with the graphics programs Xtalview v4.1 (10). Refinement was achieved with REFMAC (11) using the maximum likelihood approach and incorporating bulk solvent corrections, anisotropic F_{obs} versus F_{calc} . Random sets of reflections were set aside for cross validation purposes.

D. Results

1. Tryptophan Mutations

AChBP from *Lymnaea stagnalis* contains 5 tryptophans (Figure V.1 and 2). Three tryptophans are located peripheral to the interfacial binding pocket and two are located within the binding pocket (Figure V.2). One of the tryptophans in the pocket is a tyrosine in *Aplysia* AChBP. All five tryptophans of *Lymnaea* AChBP were individually mutated by site directed mutagenesis. Peripherally located tryptophan mutants 58, 65, 82 were transfected into HEK 293 cells and tested for expression by western blot with the FLAG antibody and by the scintillation proximity assay. Protein was detected in cell

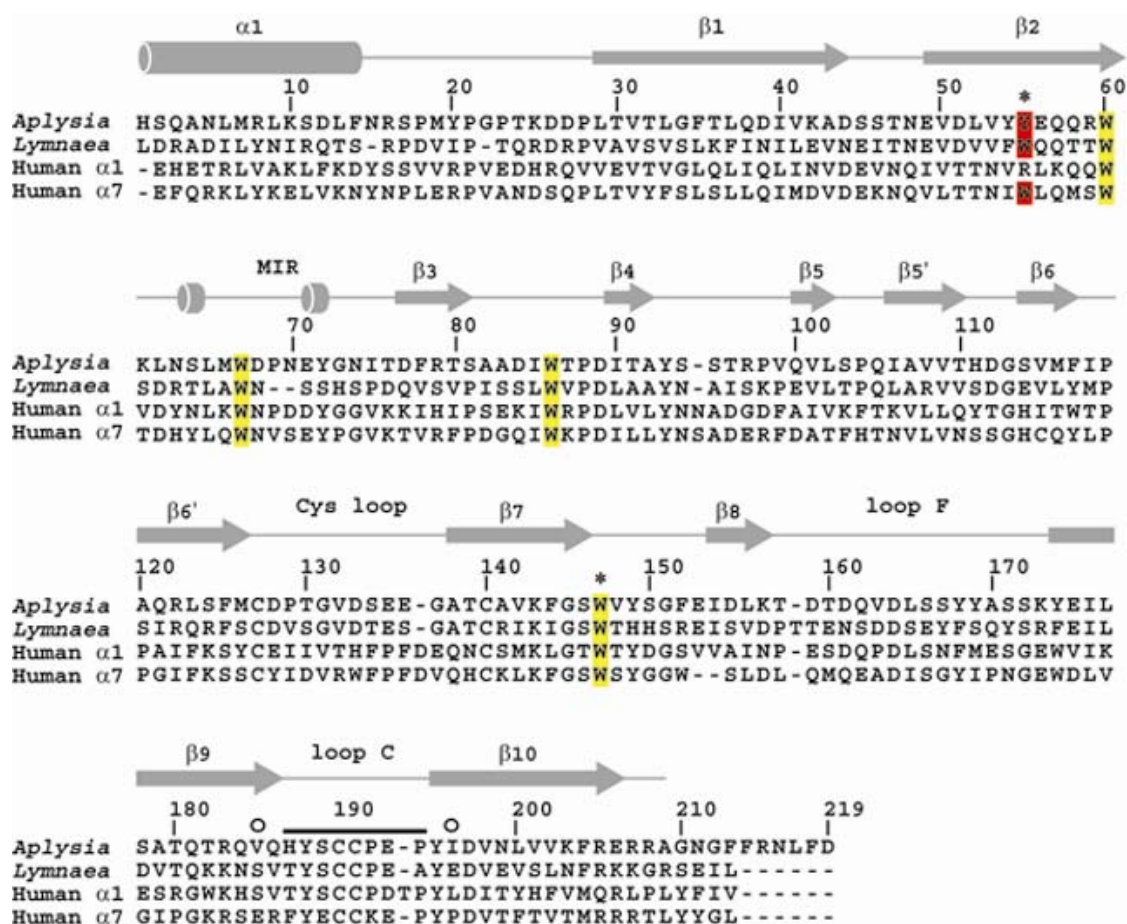


Figure V.1: Sequence alignment showing tryptophans. Tryptophans on yellow and red background are conserved and not conserved respectively between *Lymnaea* and *Aplysia* AChBP. An asterisk indicates tryptophans in the binding pocket. The two binding pocket tryptophans are on opposite subunit surfaces at the interface (see figure V.2).

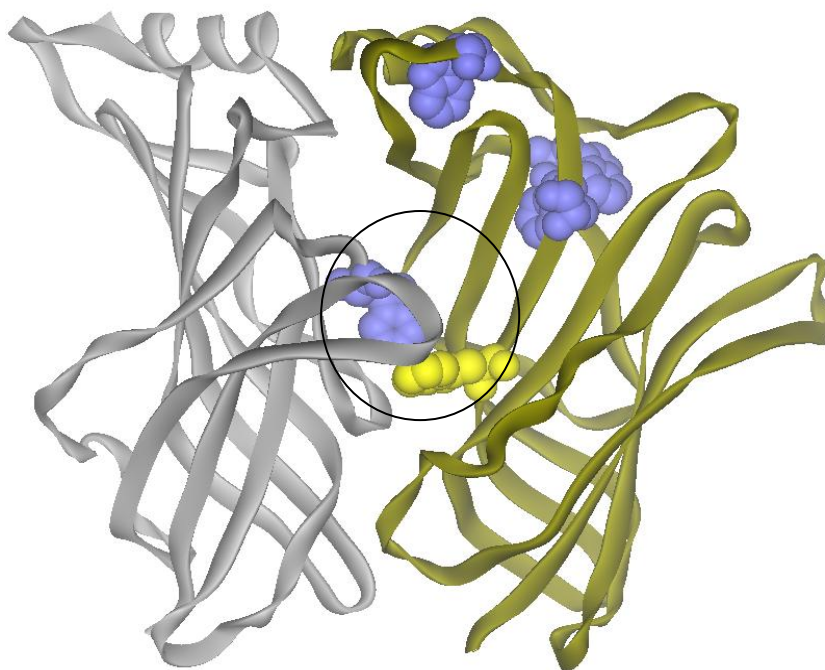


Figure V.2: Location of *Lymnaea* AChBP tryptophans. Of the five tryptophans found in *Lymnaea* AChBP, two are in the ligand binding pocket (highlighted with a circle) and 3 are in the periphery. Tryptophan 53 in the binding pocket (yellow) is not conserved between *Aplysia* and *Lymnaea* AChBPs.

lysates but not in the medium (Table V.1). Secreted protein was also not detected in stably selected cell lines from their transfected cells. In contrast, control wild type AChBP secreted most of the expressed protein in the medium. Only the mutant AChBPs with the tryptophans in the binding pocket substituted by tyrosine expressed appreciable binding protein when mutated (Table V.1). AChBP was expressed at levels similar to wild type when W53 was mutated to a tyrosine as found in *Aplysia*. FPLC analysis of the secreted mutant and wild-type proteins showed a mono-disperse species at the appropriate molecular weight of a pentamer. The reverse Y55W in the *Aplysia* protein likewise expressed similar to wild type (Table V.1). When Trp 143 was mutated to a Phe or a Tyr AChBP expressed and secreted protein was purified from the medium. However, the majority of the protein from this mutant appeared to be aggregated and eluted close to the void volume when analyzed by FPLC.

2. Radioligand competition assays

A scintillation proximity assay (SPA, Amersham Biosciences USA) was employed to measure ligand binding. Typical curves are shown for wild-type *Aplysia* titrations with [³H] epibatidine and [¹²⁵I] α -bungarotoxin (Figure V.3A) and dose-response curves with typical nicotinic ligands in competition with [³H] epibatidine (Figure V.3B). Dissociation constants are listed in Table V.2. Small cholinergic agonist all increase affinity 3-10 fold when a tryptophan is present at position 53/55 in the binding pocket. α -Conotoxin ImI was not significantly affected but most other antagonist show a slightly increased affinity when both tryptophans were present in the binding pocket (Table V.2).

3. Emission of Intrinsic Tryptophan Fluorescence

Table V.1
Expression of AChBP tryptophan mutants in HEK 293 cells.

Mutation	Expression ¹
<i>Lymnaea</i>	
W58F	not detected
W65F	not detected
W65L	not detected
W82F	not detected
W143F	aggregated
W143Y	aggregated
W53Y	pentamer
<i>Aplysia</i>	
Y55W	pentamer

1. Constructs were transfected into HEK 293 cells. Below dashed line are residues located in the ligand binding pocket. Aggregation yields a protein of greater molecular size than the pentameric molecule. In the aggregated expression cases, the majority of the protein absorbance appeared at the exclusion volume

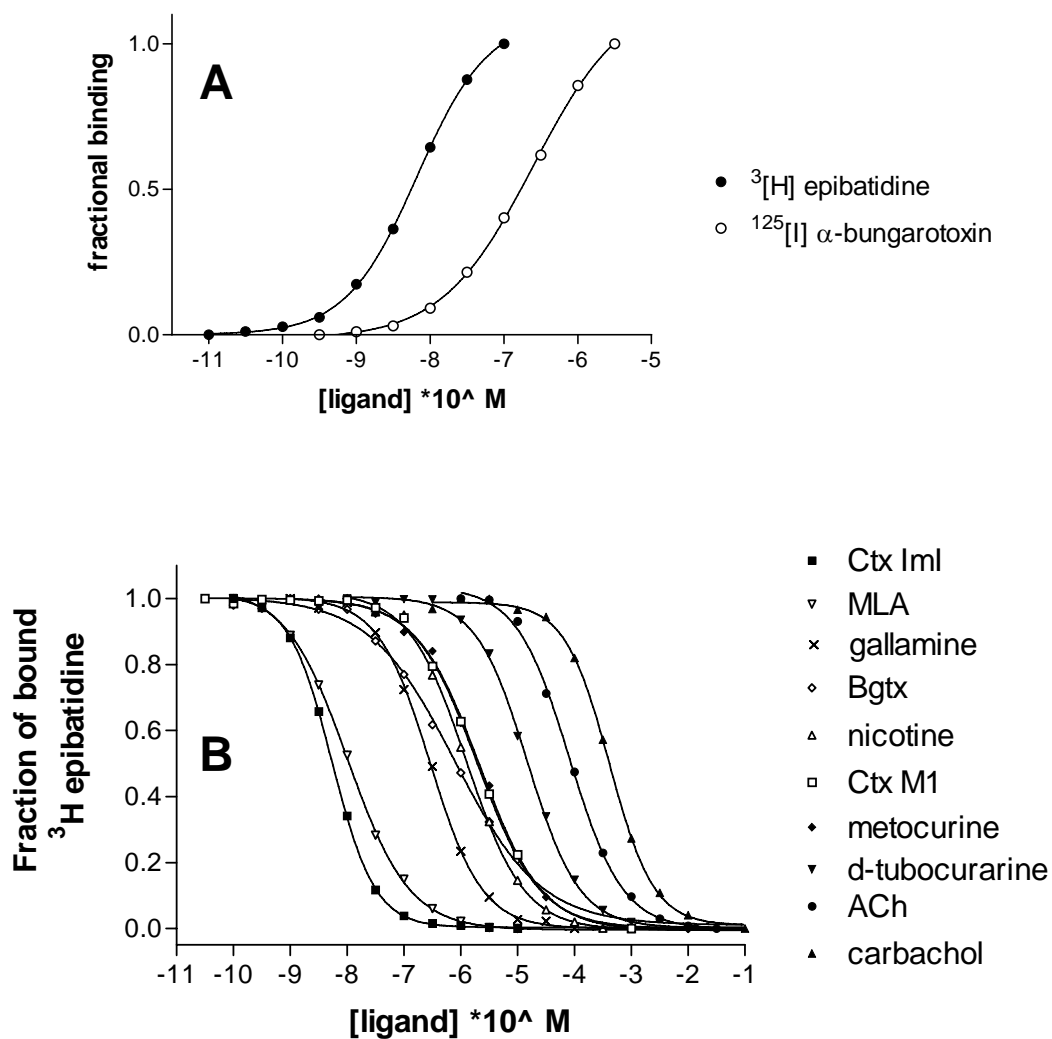


Figure V.3: Scintillation proximity assay of wild type *Aplysia* AChBP. **A**. Titration of *Aplysia* AChBP with [³H] epibatidine or [¹²⁵I] α-bungarotoxin **B** Concentration dependence for nicotinic agonists and antagonists in competition with [³H] epibatidine bound *Aplysia* AChBP

Table V.2
Dissociation constants for various ligands with wild-type and mutant AChBP

Ligand	<i>Aplysia</i> Wt nM	<i>Aplysia</i> Y55W nM	<i>Lymnaea</i> W53Y nM
α -Conotoxin ImI	1.5	3.5	825
Methyllycaconitine	2.8	0.50	1.4
Epibatidine	5.9	0.48	0.58
Gallamine	96	450	760
d-Tubocurarine	187	78	48
α -Cobratoxin	197	-	-
α -Bungarotoxin	216	59	1.2
Nicotine	270	59	147
Metocurine	461	-	-
α -Conotoxin M1	556	-	-
Dansylcholine C6	2200	-	-
Waglerin	4300	-	-
Dansylcholine C2	20000	9900	420
Acetylcholine	29100	3690	3700
Carbachol	106000	32000	36000
Serotonin	204000	-	-
Choline	206000	-	-

Nicotinic agonists and antagonists were tested for their ability to quench or enhance fluorescence. In the case of the *Lymnaea* protein, all alkaloid antagonists studied, except for the trisquaternary ligand, gallamine, appear to quench the fluorescence (Figure V.4). By contrast in *Aplysia*, quenching is seen with the alkaloid antagonists, the agonists in which the nitrogen is in a ring system, but not choline or the flexible choline containing agonists acetylcholine and carbachol.

When *Lymnaea* AChBP is mutated to a tyrosine at position 53, fluorescence emission resembles that of *Aplysia*; gallamine still enhances but acetylcholine, choline and carbachol also clearly enhance tryptophan fluorescence (Figure V.5A) (Table V.3). Other antagonists and agonists behave similarly to wild-type. Mutating tyrosine 55 in *Aplysia* AChBP to that of a tryptophan resulted in tryptophan emission similar to wild-type *Lymnaea* AChBP but did not yield a complete reversal. Carbachol association showed slight quenching, but acetylcholine binding slightly enhanced fluorescence.

4. Crystal structure of Apo *Aplysia* Y55W AChBP

Crystals of *Aplysia* Y55W AChBP were obtained in PEG 4000 and citrate buffer pH 5.6; the same condition as APO wild-type AChBP (chapter VI). Tryptophan 55 occupies the same relative space and position as Y55 in wild-type (Figure V.6), and as in the agonist bound forms of wt *Aplysia* and *Lymnaea* (Figure V.7).

E. Discussion

AChBP undergoes substantial changes in intrinsic tryptophan fluorescence upon binding of ligand(6,7). The exact mechanism is unknown, but a nest of aromatic residues make up a hydrophobic ligand binding pocket of which tryptophans play a key role. Ligands

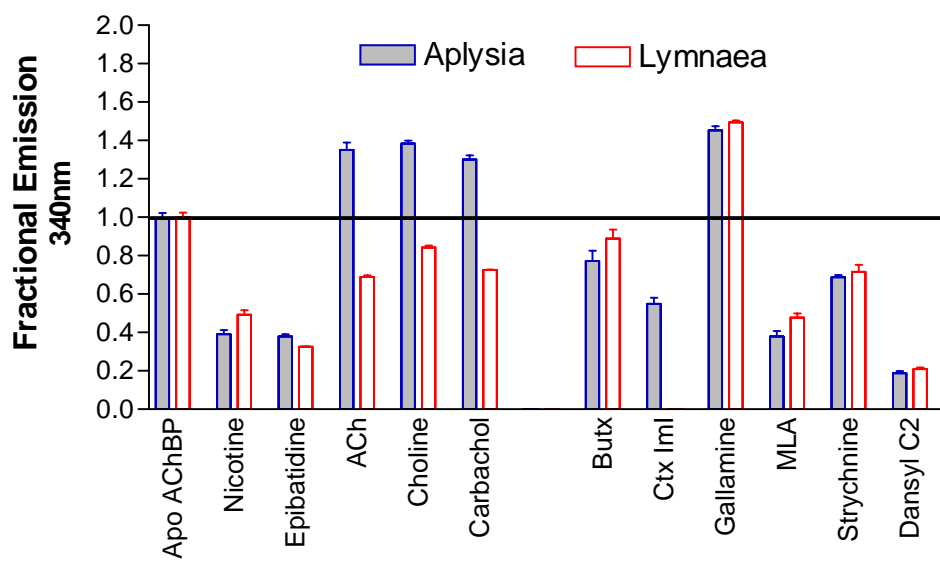


Figure V.4 Steady-state fluorescence emissions of wt *Aplysia* and *Lymnaea* AChBP

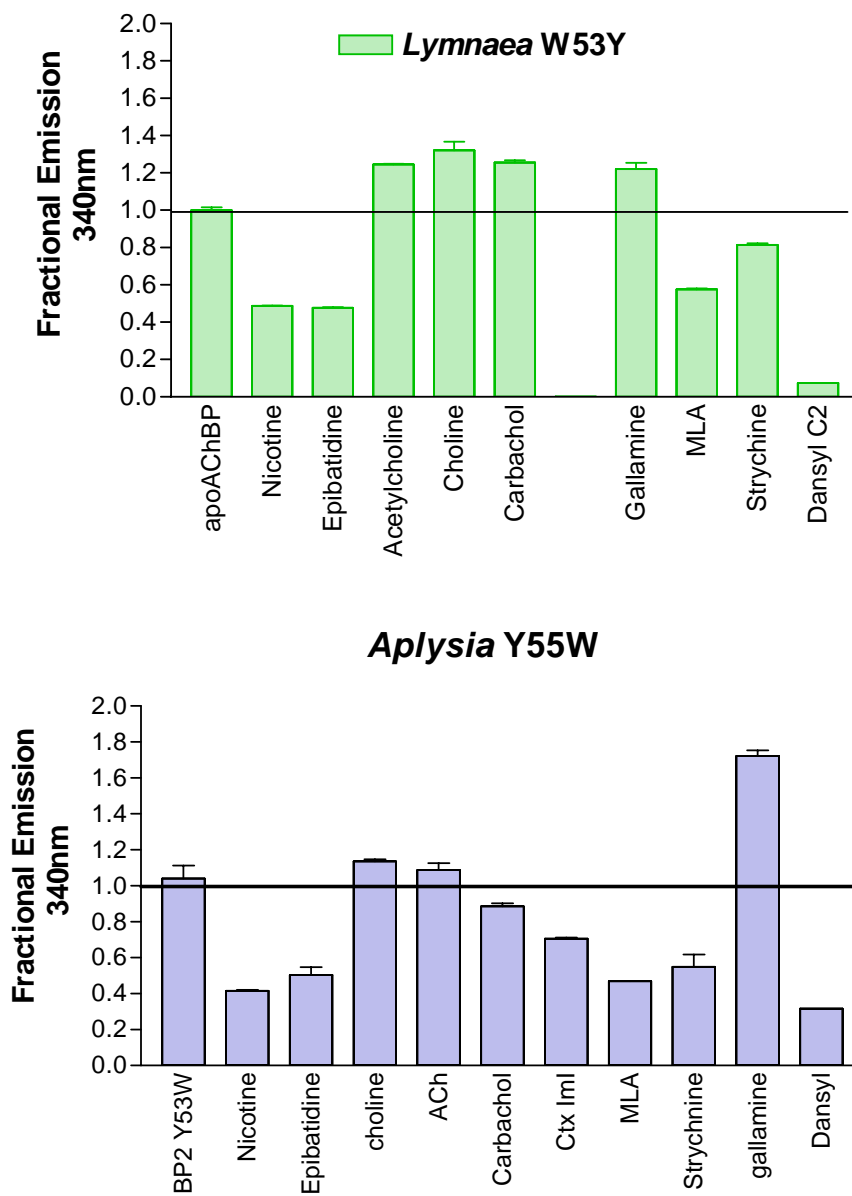


Figure V.5 Steady-state fluorescence emissions of mutant *Aplysia* and *Lymnaea* AChBP

Table V.3
 Fractional Fluorescence at 340nm of various ligand complexes
 with the acetylcholine binding protein

	<i>Aplysia</i>			<i>Lymnaea</i>			<i>Aplysia</i> Y55W			<i>Lymnaea</i> W53Y		
	340nm	SD	N	340nm	SD	N	340nm	SD	N	340nm	SD	N
Apo AChBP	0.99	0.05	3	1.00	0.05	5	1.04	0.13	3	1.00	0.03	4
Nicotine	0.39	0.04	3	0.49	0.04	3	0.42	0.01	2	0.49	0.01	2
Epibatidine	0.38	0.02	3	0.33	0.01	2	0.50	0.06	2	0.48	0.01	2
ACh	1.35	0.07	3	0.69	0.01	3	1.14	0.02	2	1.25	0.01	2
Choline	1.39	0.02	3	0.84	0.02	3	1.09	0.06	2	1.32	0.07	2
Carbachol	1.30	0.04	3	0.73	0.01	3	0.89	0.03	3	1.26	0.02	2
Gallamine	1.45	0.04	3	1.49	0.02	3	1.72	0.05	2	1.22	0.05	2
MLA	0.38	0.05	3	0.48	0.04	3	1.72	0.05	2	0.58	0.01	2
Strychnine	0.69	0.02	3	0.72	0.06	3	0.55	0.10	2	0.82	0.01	2
Dansyl C2*	0.19	0.02	4	0.21	0.01	3	0.32	0.00	1	0.07	0.01	2

*5-dimethyl aminonaphthyl sulfonamidoethyl trimethylammonium

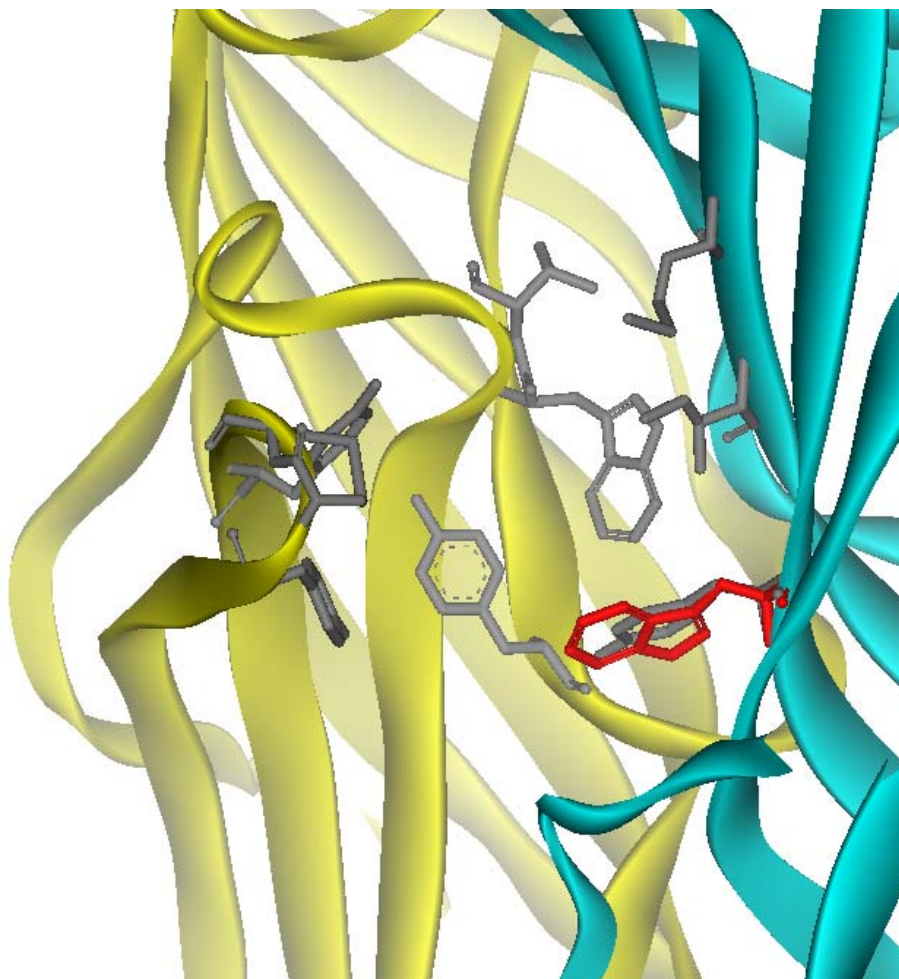


Figure V.6 Crystal structure of Apo *Aplysia* Y55W. Side chains contributing to the ligand binding pocket of Apo *Aplysia* AChBP are shown in grey. The Y55W mutant side chain is shown in red.

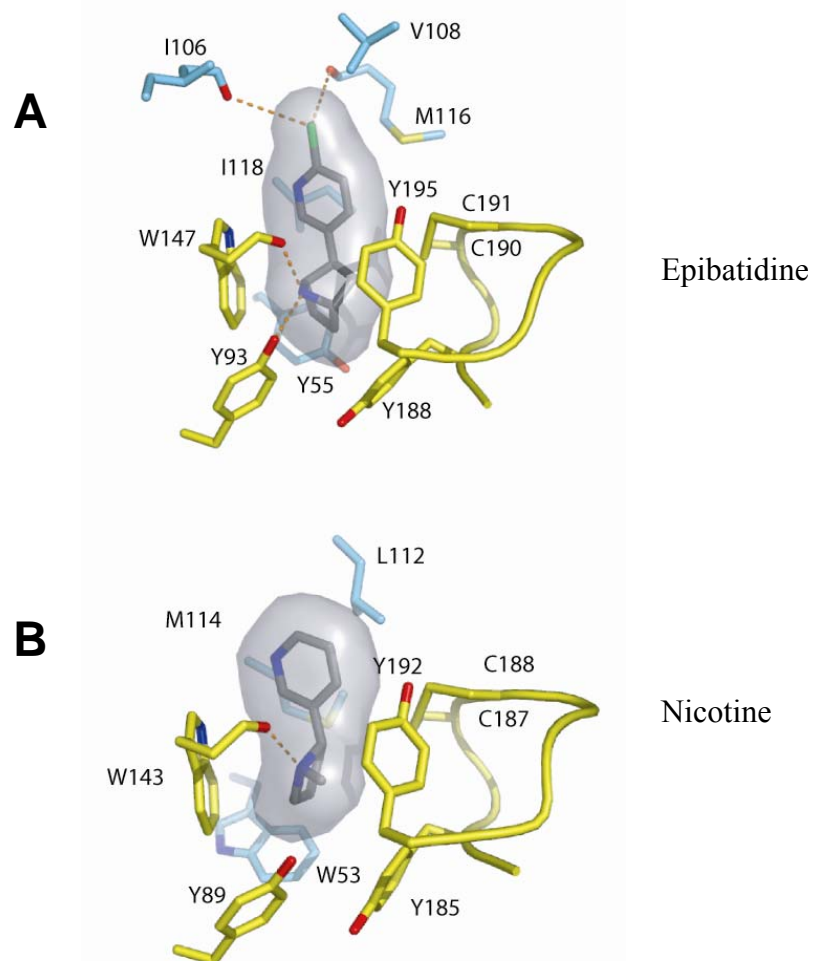


Figure V.7 Aromatic pocket with agonist bound to wild type (A) *Aplysia* and (B) *Lymnaea* (Y) AChBP, viewed from inside of the ion channel vestibule looking in a radial direction. Try55 in A occupies the same space and orientation as W53 in B.

with nanomolar to subnanomolar K_d values bind in the pocket with very few AChBP did not express. Located in the core of the protein, these residues are likely to be charged interactions. Developing a model that is not strictly charge dependent will be vital to successful computational analysis of AChBPs, nAChR, and their ligand interactions. Rational drug designs rely on atomic coordinates from experimental data and computation analysis of drug targets. Proper interpretations of atomic coordinates mandate sound theories for all types of interaction. Intrinsic tryptophan fluorescence is limited but valuable in that it is observable and may contain information about aromatic interaction as opposed to pure electrostatic interactions.

1. Expression of *Lymnaea* AChBP Tryptophan Mutants

To ascertain the role of tryptophan in ligand binding, I mutated individually all tryptophans in *Lymnaea* AChBP. Three peripheral tryptophans 58, 65, and 82 did not express suggesting they are important to protein folding and structure. Similar results were seen when mutants of the 5HT-3 receptor (12). Tryptophan 53 and 147 are located in the ligand binding pocket. Both tolerated mutations and secreted 1-3mg/ml protein into the medium. Upon mutation at the 53 position, AChBP assembly appeared identical to wild type, when analyzed by FPLC sized exclusion. However, mutations to Phe and Try at the 143 position resulted in aggregation. Analysis by FPLC showed a major peak at the void volume and a small peak at the proper pentamer volume. Aggregation does not always indicate a non-functional protein, but it was not possible to quantitate the fluorescence quenching by ligand. A histidine tag also results in similar aggregation(6) but ligands are still able to bind the larger protein aggregate (data not shown).

2. Ligand Binding of *Lymnaea* vs. *Aplysia* AChBP

Ligand binding is most affected by Trp143. [³H] Epibatidine did not bind at all with W143F or Y. α -Bungarotoxin (bgtx) is known to bind to subunit monomers or even peptides of the C loop but with lower affinity (13). Slight binding of ¹²⁵I labeled bgtx was observed and K_d determined to be >500nM, but the affinity was insufficient as a radiolabel for measuring displacement of competing ligand.

Wild type *Aplysia* AChBP has only one tryptophan in the binding pocket. Tyrosine in *Aplysia* is found at position 55, equivalent to Trp 53 in *Lymnaea*. Binding of small agonist such as nicotine, acetylcholine and epibatidine is about 10-fold less in *Aplysia* compared to *Lymnaea*. The Y55W increases binding of small agonists to affinities similar to those found in *Lymnaea* AChBP. Similar changes in ligand affinity were seen in *Torpedo* nAChRs when the equivalent tryptophan was mutated to a leucine. ACh affinity decreased by 20 fold (14). The affinity of smaller alkaloid antagonists are slightly reduced but the large peptide antagonist α -conotoxin ImI was not influenced significantly by this mutation. The *Lymnaea* W53Y mutation yields a protein with ligand recognition similar to that of wt *Aplysia* where most agonists have a decreased affinity.

Comparing the position of side chain at position 53/55 from crystal structures of *Lymnaea* and *Aplysia*, the tyrosine occupies the same relative position and space as a tryptophan. Crystal structures of the apo wild type and Y55W are identical (Figure V.6). Between species in the bound state Y55 is positioned similarly to W53 (Figure V.7). This suggests that the electron make up of the pocket dictates side chain conformations. Furthermore, a decrease in affinity is not steric or result from unfavorable contacts, but results from tyrosine's reduced aromaticity in the pocket.

3. Tryptophan Fluorescence

Changes in intrinsic tryptophan fluorescence varied between *Aplysia* and *Lymnaea*. In the case of the *Lymnaea* protein, all alkaloid antagonists studied, except for the trisquaternary ligand, gallamine, appear to quench the fluorescence. By contrast in *Aplysia*, quenching is seen with the alkaloid antagonists, the agonists in which the nitrogen is in a ring system, but not the flexible choline containing agonists with torsional movement of the cationic group. Mutagenesis interpreted with crystallography suggests that tryptophan 143 is responsible for the majority of change in fluorescence upon ligand binding. Tryptophans 58, 65 and 82 do not interact directly with bound ligand and do not appear to change conformation upon binding of ligand (15,16). Tryptophan 53/55 influences quenching, but for many ligands, equivalent quenching occurs in the absence of the second tryptophan. This is true for both wt *Aplysia* and the *Lymnaea* W53Y. The mechanism leading to changes in fluorescence has at least two contributing factors. First, direct quenching of tryptophan likely occurs by cation-quadrupole interaction and second a decrease in exposure to polar solvent normally enhances fluorescence. When *Lymnaea* AChBP is mutated to a tyrosine at residue 53 fluorescence is not quenched for the small choline containing agonists. Crystal structures are not available of bound ligand that enhances tryptophan fluorescence. However, apo *Aplysia* structures of wild type tryptophan and mutant tyrosine at the 55 position are very similar. This suggests that observed differences in tryptophan fluorescence is more likely to result from different modes of ligand binding than conformational changes of the aromatic side chains in the ligand binding pocket. This idea is further supported by gallamine binding. Gallamine enhances in both proteins and with the Tyr to Trp substitution. Therefore the component of ligand binding giving rise to quenching is missing in gallamine. Gallamine contains

three triethylammonio moieties, so that at least two of the quaternary groups are removed from the binding center.

F. Conclusions

The observed quenching and enhancement of tryptophan fluorescence of AChBPs can be explained by a two part mechanism of opposing processes. First, enhancement arises from exclusion of solvent from the pocket. Structural data show that binding of ligand induces a capping of the pocket (see chapter VI) and very little solvent remains in the pocket. A second process likely involves quenching that depends on the ligand composition and binding orientation. Most quenching ligands contain nitrogen that binds in the pocket. Agonists cause the electron withdrawing vicinal disulfides to pack closer the aromatic pocket. From this mechanism I would predict gallamine to bind as an antagonist with the C loop displaced and the pyrogallol ring buried in the pocket and not the charged quaternary amine. Reorientations of the aromatic side chains may play a role but appears to be unlikely given structural rigidity of the binding pocket.

G. References

1. Karlin, A. (2002) *Nat Rev Neurosci* **3**, 102-114
2. Corringer, P. J., Le Novère, N., and Changeux, J. P. (2000) *Annu Rev Pharmacol Toxicol* **40**, 431-458
3. Brejc, K., van Dijk, W. J., Klaassen, R. V., Schuurmans, M., van Der Oost, J., Smit, A. B., and Sixma, T. K. (2001) *Nature* **411**, 269-276
4. Bouzat, C., Gumilar, F., Spitzmaul, G., Wang, H. L., Rayes, D., Hansen, S. B., Taylor, P., and Sine, S. M. (2004) *Nature* **430**, 896-900
5. Smit, A. B., Syed, N. I., Schaap, D., van Minnen, J., Klumperman, J., Kits, K. S., Lodder, H., van der Schors, R. C., van Elk, R., Sorgedrager, B., Brejc, K., Sixma, T. K., and Geraerts, W. P. (2001) *Nature* **411**, 261-268
6. Hansen, S. B., Talley, T. T., Radic, Z., and Taylor, P. (2004) *J Biol Chem* **279**, 24197-24202
7. Hansen, S. B., Radic, Z., Talley, T. T., Molles, B. E., Deerinck, T., Tsigelny, I., and Taylor, P. (2002) *J Biol Chem* **277**, 41299-41302
8. Otwinowski, Z., and Minor, W. (1997) *Methods in Enzymology* **276**, 307-326
9. Navaza, J. (1994) *Acta Crystallogr Sect. A* **50**, 157-163
10. McRee, D. (1992) *J. Molecular Graphics* **10**, 44-46
11. Murshudov, G. N., Vagin, A. A. & Dodson, E. J. (1997) *Acta Crystallogr D Biol Crystallogr* **53**, 240-255
12. Spier, A. D., and Lummis, S. C. (2000) *J Biol Chem* **275**, 5620-5625
13. Harel, M., Kasher, R., Nicolas, A., Guss, J. M., Balass, M., Fridkin, M., Smit, A. B., Brejc, K., Sixma, T. K., Katchalski-Katzir, E., Sussman, J. L., and Fuchs, S. (2001) *Neuron* **32**, 265-275
14. Xie, Y., and Cohen, J. B. (2001) *J Biol Chem* **276**, 2417-2426
15. Celie, P. H., Kasheverov, I. E., Mordvintsev, D. Y., Hogg, R. C., van Nierop, P., van Elk, R., van Rossum-Fikkert, S. E., Zhmak, M. N., Bertrand, D., Tsetlin, V., Sixma, T. K., and Smit, A. B. (2005) *Nat Struct Mol Biol* **12**, 582-588

16. Celie, P. H., van Rossum-Fikkert, S. E., van Dijk, W. J., Brejc, K., Smit, A. B., and Sixma, T. K. (2004) *Neuron* **41**, 907-914

Chapter VI

Structures of *Aplysia* AChBP Complexes with Agonists and Antagonists Reveal Distinct Binding Interfaces and Conformations

A. Abstract

Upon ligand binding, the extracellular domain of the nicotinic acetylcholine receptor undergoes conformational changes that allosterically trigger opening of the ion channel. The crystal structure of the soluble acetylcholine binding protein from the saltwater snail, *Aplysia californica*, in the apo form shows major differences from that from the freshwater snail, *Lymnaea stagnalis*, with a more open loop C and distinctive positions for other surface loops. The structures of complexes show that loop C further opens in a radial direction upon binding of the peptidic antagonist, α -conotoxin ImI, whereas it wraps around the bound agonists, lobeline and epibatidine. The structures also reveal extended and non-overlapping interaction surfaces for the two antagonists at the subunit interface, outside of the binding loci for the agonists. Hence, these structures provide a dynamic template for the various classes of ligands interacting with ligand-gated ion channels and for delineating further the conformational changes associated with channel gating.

B. Introduction

Nicotinic acetylcholine receptors (nAChRs) are well-characterized transmembrane allosteric proteins involved in rapid gating of ions elicited by acetylcholine. They belong to the 'Cys-loop' superfamily of ligand-gated ion channels (LGIC) that also includes GABA-A and -C, 5-HT₃ and glycine receptors (1-3). The nAChRs are homo- or

heteromeric pentamers of structurally-related subunits that encompass an extracellular N-terminal ligand binding domain (LBD), four transmembrane spanning regions that form the ion channel, and an extended intracellular region between spans 3 and 4. They exist in at least three conformational states with distinctive sensitivities to the nicotinic ligands that dictate channel gating and function: basal or resting (closed, but activatable), activated (open), and desensitized (closed, not activatable). Indeed, ligand binding triggers conformational changes that are transmitted to the transmembrane spanning region, leading to gating and changes in membrane potential. Because of their functional importance and structural and functional differences in numerous pathologies, the nAChRs have been thoroughly investigated at the pharmacological, biochemical, and structural levels. However, structural analyses of the nAChR are impaired by the large size, the transmembrane spans and, in most species, the low abundance and heteropentameric assembly.

The recent pharmacological and structural characterization of the soluble acetylcholine binding protein from the freshwater snail, *Lymnaea stagnalis* (*L*-AChBP) (4,5), has considerably increased our knowledge of the structure and recognition determinants of the nAChR. *L*-AChBP shows limited sequence identity with the nAChR LBD (Figure VI.1), but it assembles as a stable homopentamer and displays ligand recognition properties similar to those of the neuronal homopentameric $\alpha 7$ receptor subtype (4). The refined 4 Å resolution electron microscopy structure of the heteropentameric muscle-type, $(\alpha 1)_2\beta\gamma\delta$ nAChR in the basal state has elegantly illustrated considerable structural similarity of *L*-AChBP with the nAChR LBD (6). Moreover, coupling of *L*-AChBP, where three membrane-facing loops have been modified, with the transmembrane domain

of the 5-HT_{3A} receptor, yielded a chimeric receptor with lower affinity for acetylcholine, as expected for an activatable receptor, and the capacity to trigger opening of the ion channel (7). Therefore, *L*-AChBP is now considered a structural and functional surrogate of the nAChRs.

The initial structures of *L*-AChBP, in a HEPES-bound form and as two complexes with the small agonists, (-)-nicotine and carbamylcholine, bound in the ligand binding site, show minimal conformational differences and have been postulated to reflect the desensitized state of the nAChR (5,8). In turn, the structure of *L*-AChBP in complex with the large peptidic toxin and antagonist, α -cobratoxin (Cbtx), tightly inserted at the subunit interface, has revealed concerted large movements of loops C and F that line the binding interface, and has provided a potential template for a resting state conformation of the nAChR (9). However, these structures are likely to illustrate only a limited range of the many conformational states of the nAChR when either unliganded or associated with a variety of agonists and antagonists.

The recently characterized *A*-AChBP from the saltwater mollusk, *Aplysia californica*, shares only 33% amino acid identity with *L*-AChBP (10), but it also assembles as a soluble homopentamer and possesses all the functional residues identified in *L*-AChBP (11), including those that form the aromatic nest characteristic of the nAChR LBD (Figure VI.1A). Of the five aromatic residues present in the *L*-AChBP binding pocket, only the conservative Trp55Tyr substitution is found in *A*-AChBP. However, *A*-AChBP, similar to the nAChR, lacks the sixth aromatic residue present as Tyr164 in *L*-AChBP. It also displays an Ala194Pro substitution within loop C on the principal face (the (+) face) of the interface and an Arg108Val substitution on the complementary face (the (-) face),

that are both conserved in the human $\alpha 1$ and $\alpha 7$ subunits. As a result, *A*-AChBP displays distinctive binding affinities and specificities for the nicotinic agonists and antagonists compared with *L*-AChBP, exemplified by its lower affinity for acetylcholine but higher affinity for the small α -conotoxin peptides, the natural ImI (10) (Table VI.1) and the PnIA Ala10Leu variant (11), two $\alpha 7$ -specific antagonists.

I report the crystal structures of *A*-AChBP in the apo form and as four complexes with two natural antagonists, the peptidic α -conotoxin ImI and the alkaloid methyllycaconitine (MLA), and two alkaloid agonists, α -lobeline (LOB) and (+)-epibatidine (EPI) (Figure VI.1B; Table V.2). Compared to the HEPES-bound *L*-AChBP and *A*-AChBP structures, that of apo *A*-AChBP, devoid of a bound amine buffer, reveals a distinctive conformation that may better reflect the basal or resting state than the desensitized state of the nAChR. Structural analysis of the four complexes reveals, at the subunit interface and outside of the primary competitive binding site, unpredicted anchoring surfaces that contribute non-overlapping binding loci for the antagonists, and enables one to visualize the distinctive conformational changes associated with agonist *versus* antagonist binding. Hence these structures, by defining non-overlapping binding regions for the agonists and antagonists and revealing a range of conformations that may resemble those adopted by the LBD of the nAChR, provide distinctive templates for predicting selectivity of various classes of ligands for the individual nAChR subtypes, and for delineating further the conformational changes associated with channel gating.

C. Results and Discussion

1. Determination and Quality of the Structure

Attempts to solve a structure from crystals obtained from the highly N-glycosylated and non-homogeneous *A*-AChBP expressed from a standard HEK cell line (10) were unsuccessful. However, expression from a glycosylation-deficient cell line (12) resulted in a homogenous protein with a shorter glycan chain as assessed by electrophoresis (Figure VI.1) and mass spectrometry analyses, yielding crystals suitable for structural studies.

The structures of the homopentameric *A*-AChBP in the apo form (Figure VI.3) and as complexes with the antagonists, α -conotoxin ImI and MLA, and the agonists, EPI and LOB (Figures VI.4 and VI.5), were solved in the 1.96-3.4 Å resolution range from crystals grown from different pH conditions and in distinctive space groups, leading to different packing geometries (cf. Materials and Methods; Table VI.2). Yet, each of the four complex structures, including the lower resolution EPI complex, shows well-defined electron density indicative of a high occupancy and a single binding orientation for each of the five ligand molecules bound at the subunit interfaces, along with unambiguous positioning of all side chains in the pentameric complex. Hence these structures, and their comparison with those of *L*-AChBP bound to HEPES (5), to the small agonists nicotine and carbamylcholine (8), and to the large antagonist Cbtx (9), reveal structural and functional determinants unique to *A*-AChBP along with a variety of conformations associated with ligand binding at the subunit interfaces.

2. Structure of *A*-AChBP in the Apo Form

The structure of apo *A*-AChBP shows the same homopentameric assembly of tightly associated subunits as found in structures of the HEPES-bound *L*-AChBP (5) and *A*-AChBP (11), and in microscopy images of the muscle-type, $(\alpha 1)_2\beta\gamma\delta$ nAChR from

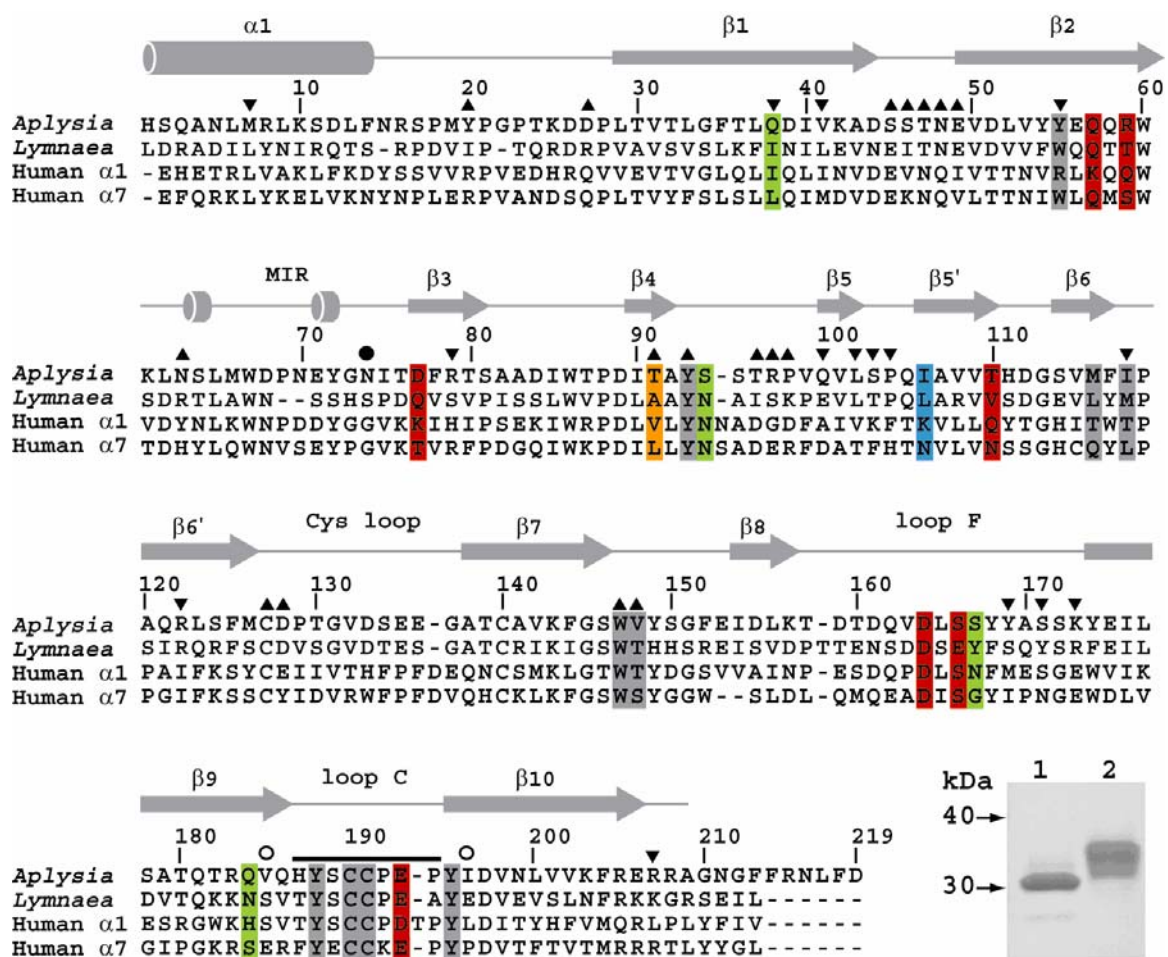


Figure VI.1: Sequence alignment of A-AChBP (A) Structural alignment of the subunit sequences of A-AChBP (Hansen et al., 2004) and L-AChBP (4) with those of the human $\alpha 1$ and $\alpha 7$ LBDs (LGIC database). The A-AChBP sequence reported in Celie et al. (2005) differs by Val substitutions at positions 43 and 138 and an N-terminal two-residue deletion. Secondary structure elements are indicated. The bar and asterisks above the A-AChBP sequence indicate the loop C tip and hinge regions, respectively. The solid circle denotes the glycosylated Asn74. Tip up and down triangles denote A-AChBP residues from the (+) and (-) faces that are within a 3.5 Å radius of interaction at the subunit interface in the apo conformation. A-AChBP residues whose side chains interact within 4.5 Å with all four ligands are on a grey background. Residues specific for the antagonists, α -conotoxin ImI and MLA, are on a red and a green background and those specific for the agonists, LOB and EPI, on an orange and a blue background, respectively. *Inset*: SDS-PAGE analysis (16% gel) of A-AChBP expressed from GnTI (lane 1) and standard HEK cells (lane 2). The protein expressed in GnTI cells migrate faster and as a thinner band indicative of a smaller size and greater homogeneity in oligosaccharide structure.

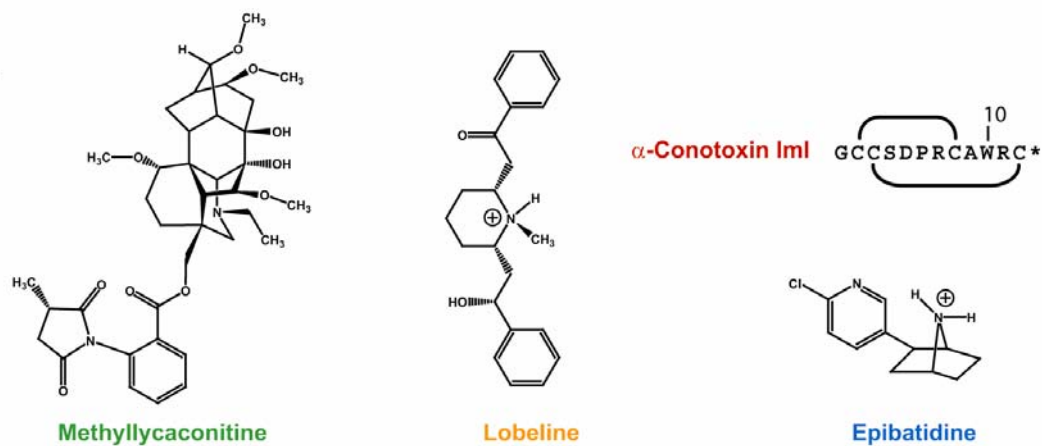


Fig VI.2 Schematic view of the organic ligands, MLA (the lycoctonine ring is at top and the N-ethylpiperidine ring at the bottom), EPI and LOB. *Top right*: sequence and disulfide bonding of α -conotoxin Iml; the carat denotes C-terminal amidation.

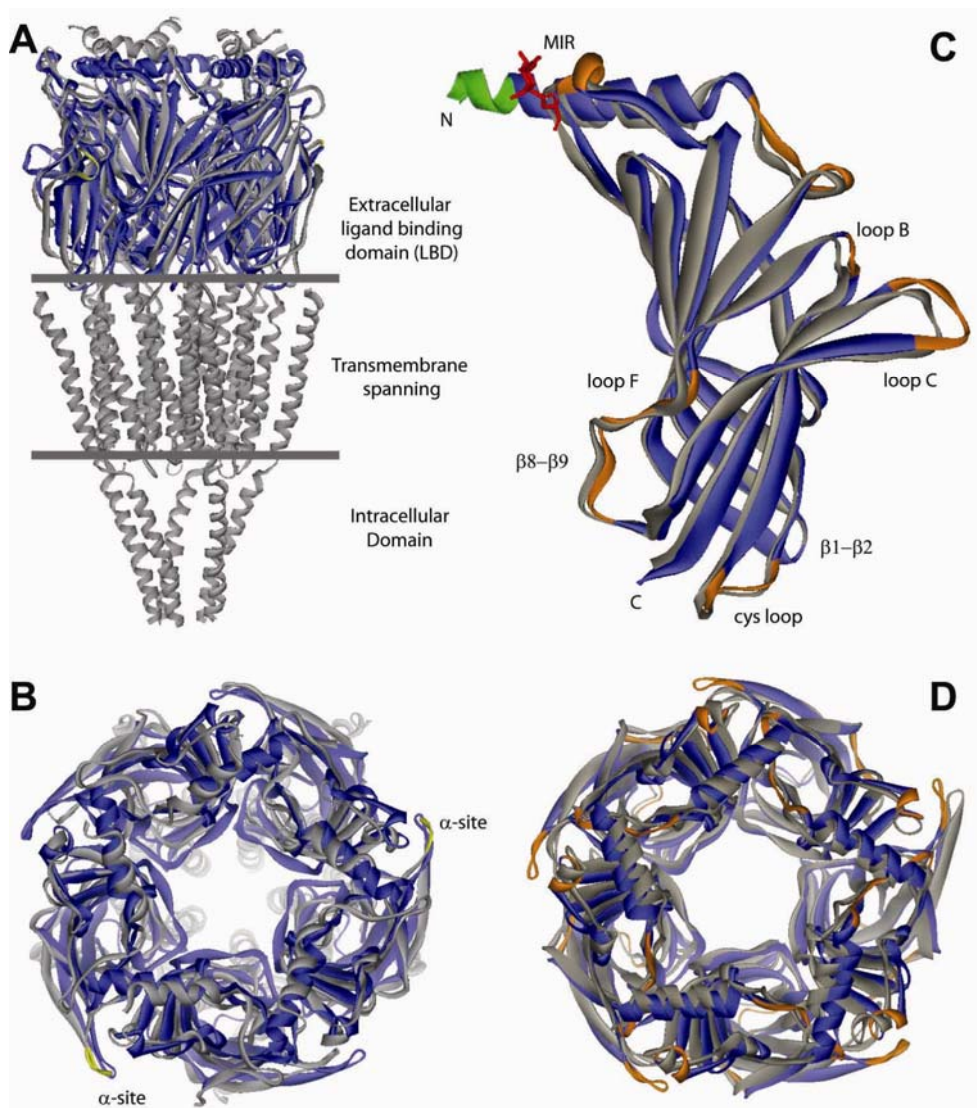


Figure VI.3: Overall view of the Apo A-AChBP structure and structural comparisons. (A) Side view and (B) apical view of apo A-AChBP (blue) overlaid with the muscle-type nAChR (grey) (Unwin, 2005). The tip of loop C in the nAChR α subunits is colored yellow. Loop C in apo A-AChBP overlays most closely with loop C in the α subunit. (C) Side view and (D) top view of the apo A-AChBP subunit and pentamer (blue) overlaid with those of HEPES-bound A-AChBP (grey). In apo A-AChBP, the Asn74-linked glycan is in red and the FLAG epitope that prolongs helix α 1 in green. The ‘MIR’ and loops where there is a large departure in position or conformation are shown in orange. In four of the five HEPES-bound A-AChBP subunits, loop C is closed whereas in the fifth subunit, devoid of a bound buffer, it is more extended than in apo A-AChBP.

Table VI.1
Ligand dissociation constants for the two AChBP species

Ligand	A-AChBP	L-AChBP	A/L Kd ratio
ACh	30 000 ³	890 ²	34
(-)-Nicotine	245 ³	86 ²	2.8
(+)-Epibatidine (EPI)	14 ³	0.16 ²	88
α -Lobeline (LOB)	0.3	30	0.01
Methyllycaconitine (MLA)	2.8 ³	0.41 ²	6.8
α -Bungarotoxin (Bgtx)	250 ³	1.8 ²	139
α -Cobratoxin (Cbtx)	191	3.2 ³	60
α -Conotoxin ImI	0.88 ³	14 000 ³	0.00006
α -Conotoxin MI	1000	2800	0.36

Dissociation constants (nM) are average (n = 2) or means (n > 2) of individual data that differ by less than 20%. ² From Hansen et al., 2002 ³ From Hansen et al., 2004

Table VI.2.
Data collection and refinement statistics

	Apo	ImI	MLA	LOB	EPI
Data collection					
Beamline	APS / 19-ID	ALS / 8.2.1	ESRF / ID29	ALS / 8.2.1	ESRF / ID14-EH3
Wavelength (Å)	0.97934	0.97623	0.97563	0.97623	0.931
Space group	C222 ₁	I222	P2 ₁	P1	I23
a, b, c (Å)	144.1, 146.8, 143.3	130.3, 140.0, 153.4	67.3, 126.8, 147.3	75.8, 85.7, 117.3	200.9, 200.9, 200.9
$\alpha / \beta / \gamma$ (°)			- / 99.5 / -	89.9 / 97.3 / 106.6	
Pentamer / asymmetric unit	1	1	2	2	1
Resolution range ¹	50 - 2.02 (2.09 - 2.02)	50 - 2.07 (2.14 - 2.07)	72 - 2.45 (2.51 - 2.45)	58.3 - 2.05 (2.16 - 2.05)	30 - 3.4 (3.49 - 3.4)
R _{merge} (%) ^{1,2}	5.8 (47.4)	8.5 (54.8)	7.9 (48.4)	6.2 (26.5)	19.8 (59.4)
Observations	603 776	433 003	356 687	333 038	64 112
Unique reflections	97 846	86 601	95 739	168 545	18 257
Completeness (%) ¹	98.5 (90.5)	99.9 (99.8)	100.0 (100.0)	95.8 (95.4)	97.6 (97.6)
Redundancy ¹	6.2 (5.7)	5.1 (3.8)	3.7 (3.8)	2.0 (2.0)	3.5 (3.5)
$\langle I/\sigma \rangle$ ¹	13.6 (3.8)	29.5 (2.2)	11.3 (2.5)	13.9 (2.5)	8.3 (2.0)
B-factor from Wilson plot (Å ²)	32.4	33.5	45.4	25.6	42.3
Refinement					
Resolution range (Å)	40 - 2.02 (2.07 - 2.02)	20 - 2.07 (2.12 - 2.07)	20 - 2.45 (2.51 - 2.45)	48 - 2.05 (2.1 - 2.05)	30 - 3.4 (3.49 - 3.4)
Protein atoms	8515	8411	16762	16324	8521
Solvent / ligand atoms	882 / 82	1043 / 469	560 / 490	1561 / 250	- / 70
R _{cryst} (%) / R _{free} (%)	16.8 (20.8) / 20.2 (25.2)	17.3 (23.1) / 21.4 (28.2)	19.3 (27.7) / 23.2 (33.8)	21.6 (30.8) / 25.8 (33.7)	18.3 (24.9) / 25.4 (33.1)
Free reflections	2980	1700	1916	5025	929
R.m.s. 1-2 bond distances (Å)	0.013	0.013	0.008	0.008	0.01
R.m.s. 1-3 bond angles (°)	1.41	1.42	1.37	1.16	1.5
Mean main / side chain B (Å ²)	39.3 / 41.9	39.29 / 41.03	45.3 / 46.4	39.6 / 40.6	45.4 / 46.6
Mean B solvent / ligand (Å ²)	43.8 / 62.6	43.56 / 35.26	36.8 / 40.4	36.6 / 31.9	- / 38.58
Main / side chain ΔB for bonded atoms (Å ²)	0.99 / 1.66	1.03 / 1.60	1.14 / 1.14	0.89 / 1.08	1.11 / 1.35
PDB accession code	2BYN	2BYP	2BYR	2BYS	2BYQ

¹ Values in parentheses are for the highest resolution shell.

² $R_{\text{merge}} = \frac{\sum_i \sum_l |I_{hkl_i} - \langle I_{hkl_i} \rangle|}{\sum_i \sum_l \langle I_{hkl_i} \rangle}$; $R_{\text{cryst}} = \frac{\sum ||F_o| - |F_c||}{\sum |F_o|}$

Torpedo (6) (Figure VI.3). Each A-AChBP subunit consists of an N-terminal, 20-residue α -helix, that includes the FLAG epitope, two short α_{310} helices and a 10-strand β -sandwich core made of an inner β -sheet of six strands (β_1 , β_2 , β_3 , β_5 , β_6 , β_8) and an outer β -sheet of four strands (β_4 , β_7 , β_9 , β_{10}). Apart from flexible surface loop regions, residue positions in the five subunits within the pentamer are very similar (rmsd values in the 0.3-0.35Å range for 211 C α atoms). A second apo structure, solved from a different crystal form grown at pH 8.5 instead of 5.6, was virtually identical (not shown); this indicates that the protonation state of the A-AChBP residues does not influence the overall conformation of the pentamer.

The subunit interface, which is made of six loops (loops α_1 - β_1 , β_1 - β_2 , β_3 - β_4 , β_4 - β_5 (or A), β_6 '- β_7 (Cys loop) and β_7 - β_8 (B)) from the (+) face and of secondary structure elements (helix α_1 and strands β_2 , β_3 , β_5 , and β_6) from the (-) face (Figure VI.1), buries, to a 1.6 Å probe radius, a surface area of ~ 1400 Å² on each subunit, in agreement with the HEPES-bound L-AChBP structure (5) (Figure VI.3). The interface, which is dominated by apolar residues, encompasses several polar contacts involving residues Asn48, Glu49, Arg97 and Glu153 from the (+) face and Gln3, Gln38, Tyr55, Arg79, Arg122 and Lys173 from the (-) face, which are weakly conserved. Only nine solvent molecules mediate direct contacts between residues from each subunit, an observation that emphasizes the requirement of a high surface complementarity between subunits in the nAChR to propagate allosteric movements. Of the several loops that emerge from the β -sandwich core, five (loops A, B, β_9 - β_{10} (or C), β_8 - β_9 (F), and the conserved Cys-loop)

have been shown to be critical for nAChR function with several of their residues being involved in both subunit assembly and ligand binding (3).

The architecture of the ligand-binding pocket, with the aromatic nest made of Tyr93, Trp147, Tyr188 and Tyr195 from the (+) face of the interface and Tyr55 from the (-) face, is highly conserved between the available crystal structures of AChBPs. Yet, in *A*-AChBP, compared to *L*-AChBP, major rearrangements are observed within the (-) face that may arise from replacement of Trp53 by Tyr55, as often found in the GABA-A and -C LBDs, and of the bulky Arg104 by Val108 (Figure VI.1). In fact, residue Arg79, which originates from a different region in *A*-AChBP, positions its guanidinium group close to that of Arg104 in *L*-AChBP. Near the pocket entry, two small *A*-AChBP residues, Thr36 and Ser167, replace the bulkier *L*-AChBP Lys34 and Tyr164. The large opening movement of loop C (Val183 to Tyr193 with deviation up to 6.5 Å at position Cys190) in apo *A*-AChBP compared to the HEPES-bound form (rmsd values: 0.46 Å and 0.57 Å for 194 and 201 C α atoms on the (+) and (-) face, respectively) markedly enlarge ligand access and reduce contribution to the subunit interface.

3. Apo *A*-AChBP vs. the Muscle-type α 1 Subunit

Structural overlays of the *A*-AChBP and *L*-AChBP subunits with the muscle-type α 1 subunit (6) show larger positional differences with the *L*-AChBP subunit (rmsd value: 1.7 Å for 130 C α atoms) but reveal a similar orientation of the ‘untwisted’ loop C with positional differences of only 0.7 Å and 1.6 Å for the two sulfur atoms from the vicinal Cys190-Cys191 residues (Figure VI.3). Loop β 1- β 2, which in the muscle-type nAChR is thought to control the displacement of the transmembrane, pore-lining span 2, adopts in

A-AChBP a conformation similar to that in the $\alpha 1$ subunit. Although the curvature of the inner β -sheet is roughly conserved between the *A*-AChBP and $\alpha 1$ subunits, the direction of the outer β -sheet markedly differs from that in the *L*-AChBP subunit.

In the muscle-type nAChR, the main immunogenic region (MIR) is a reactive epitope in autoimmune *Myasthenia gravis* (13). This region, which is localized within loop $\beta 2$ - $\beta 3$ apical in the $\alpha 1$ subunit, is separated from the N-terminal helix by a cleft that contributes to the major antibody-binding site (6). In the AChBPs, the corresponding region, that encompasses residues Trp67 to Glu71, is weakly conserved (Figure VI.1). In *A*-AChBP, compared to *L*-AChBP, loop $\beta 2$ - $\beta 3$ is longer by two residues and displays a large positional change that exposes the side chains of Asp68 and Glu71 to the solvent. These residues correspond to the immunoreactive Asn67 and Asp71 in the $\alpha 1$ subunit. However, while in the $\alpha 1$ subunit the N-terminal helix is solvent-exposed (6), in the *A*-AChBP subunit, it tightly packs against the β -sandwich core in a conformation that may restrict antibody access.

4. Antagonist Binding

a. The α -Conotoxin ImI-AChBP Complex

Certain conotoxin peptides, from the venom of marine snails of *Conus sp.*, are amongst the most selective nAChR ligands. The largest family of α -conotoxins has been divided into the structural $\alpha 3/5$, $\alpha 4/3$, $\alpha 4/6$ and $\alpha 4/7$ subfamilies based on the number of residues between the second and third Cys residues (loop I) and the third and fourth Cys residues (loop II). In the $\alpha 4/3$ family, the dodecapeptides ImI and ImII are the smallest α -conotoxins yet identified. They are $\alpha 7$ and $\alpha 3\beta 2$ nAChR selective, with lower affinity for

ImII (14). These two peptides, that differ by three residues (Gly1Ala, Pro6Arg and Ala9Arg), appear to bind non-overlapping sites on the $\alpha 7$ nAChR (15). Moreover, ImI, with a 14,000 fold preference for *A*-AChBP compared to *L*-AChBP as found by direct binding experiments (Table VI.1), in contrast to the 125-fold difference found in a competition assay (11), is the most selective of the nAChR ligands.

The ImI-*A*-AChBP complex structure (Figures VI.4A and VI.5A) shows bound ImI that adopts a rigid scaffold as found in solution. The peptide folds around two compact loops, made of a α_{310} -helical region followed by a β -turn, that are defined by the two disulfide bridges, Cys2-Cys8 (loop I) and Cys3-Cys12 (loop II), and are separated by a deep cleft (16,17). However, the conformations of the two disulfide bonds markedly differ from those for the free peptide, indicating subtle conformational rearrangement upon binding. The resulting rmsd value (0.87 Å for 12 C α atoms) is significantly greater than the averaged value (0.15 Å) between the best 20 energy-minimized conformers of the free ImI structure (16).

In the complex, the bound ImI, inserted under *A*-AChBP loop C, entirely fills the ligand-binding pocket where it buries 71% of its solvent-accessible surface area (Figures VI.4A and VI.5A). Only residues Gly1, Ser4, and Arg11 and the C-terminal amine group remain solvent-exposed. At the (+) face of the interface, the Asp5-Pro6-Arg7 tripeptide in ImI loop I is deeply anchored on the ‘membrane’ side of the pocket. This tripeptide represents a major binding determinant, consistent with earlier mutagenesis data showing dramatic affinity decreases upon residue substitution (18,19). Indeed, ImI Asp5, as a key residue, stabilizes the loop I conformation by establishing contacts with the ImI Arg7

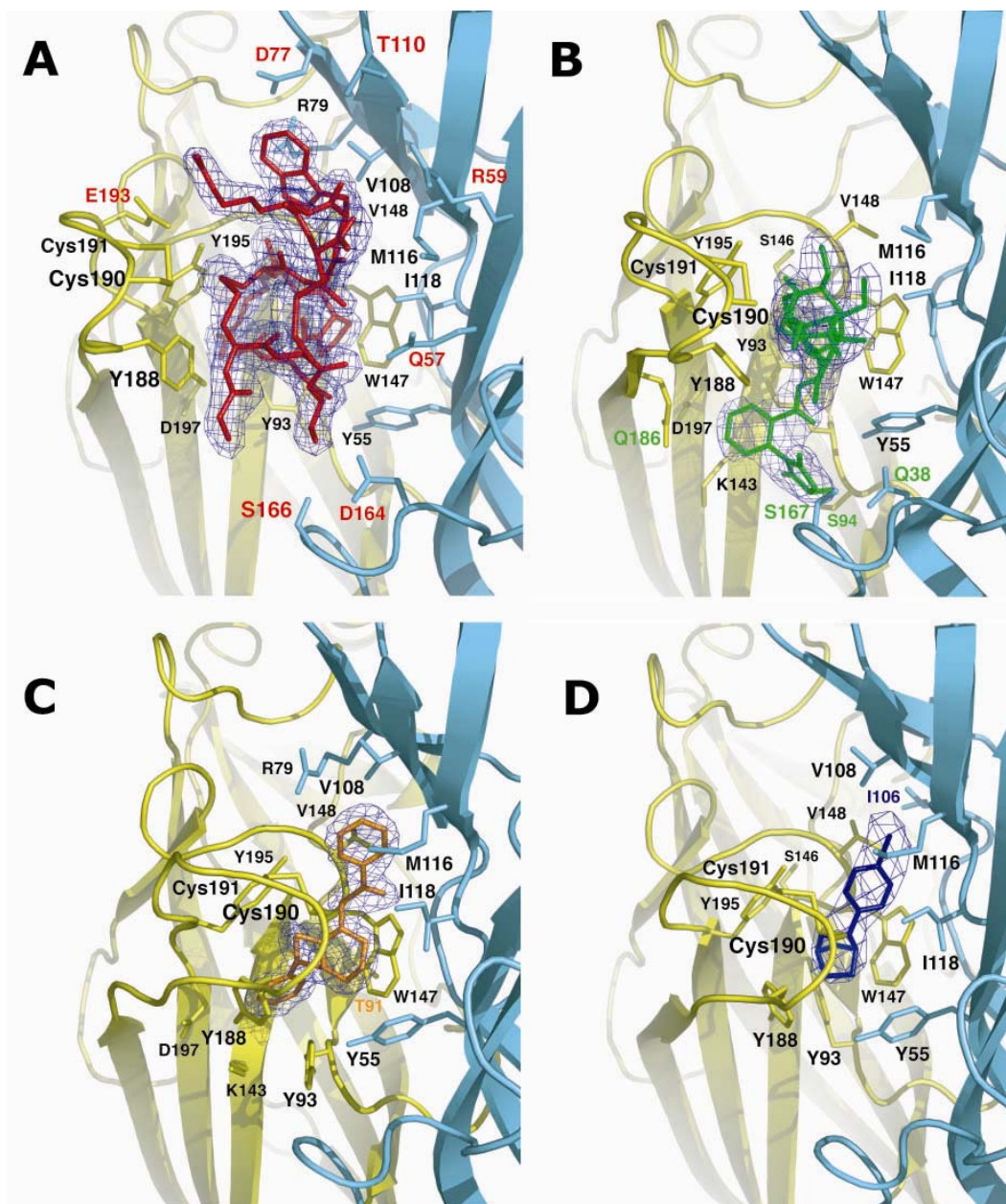


Figure VI.4: The A-AChBP subunit interface in the antagonist and agonist complexes. Side views of the bound antagonists (A) ImI, buried under loop C, and (B) MLA (same orientation), and of the bound agonists (C) LOB and (D) EPI in similar orientations. The 2.0-3.4 Å resolution omit $2F_0 - F_c$ electron density maps contoured at 1.4σ are shown in blue. The main and side chains from the (+) and (-) faces of the subunit interface are in yellow and cyan, respectively. Those side chains that interact specifically with ImI, MLA, LOB, and EPI are labeled red, green, orange, and blue, respectively.

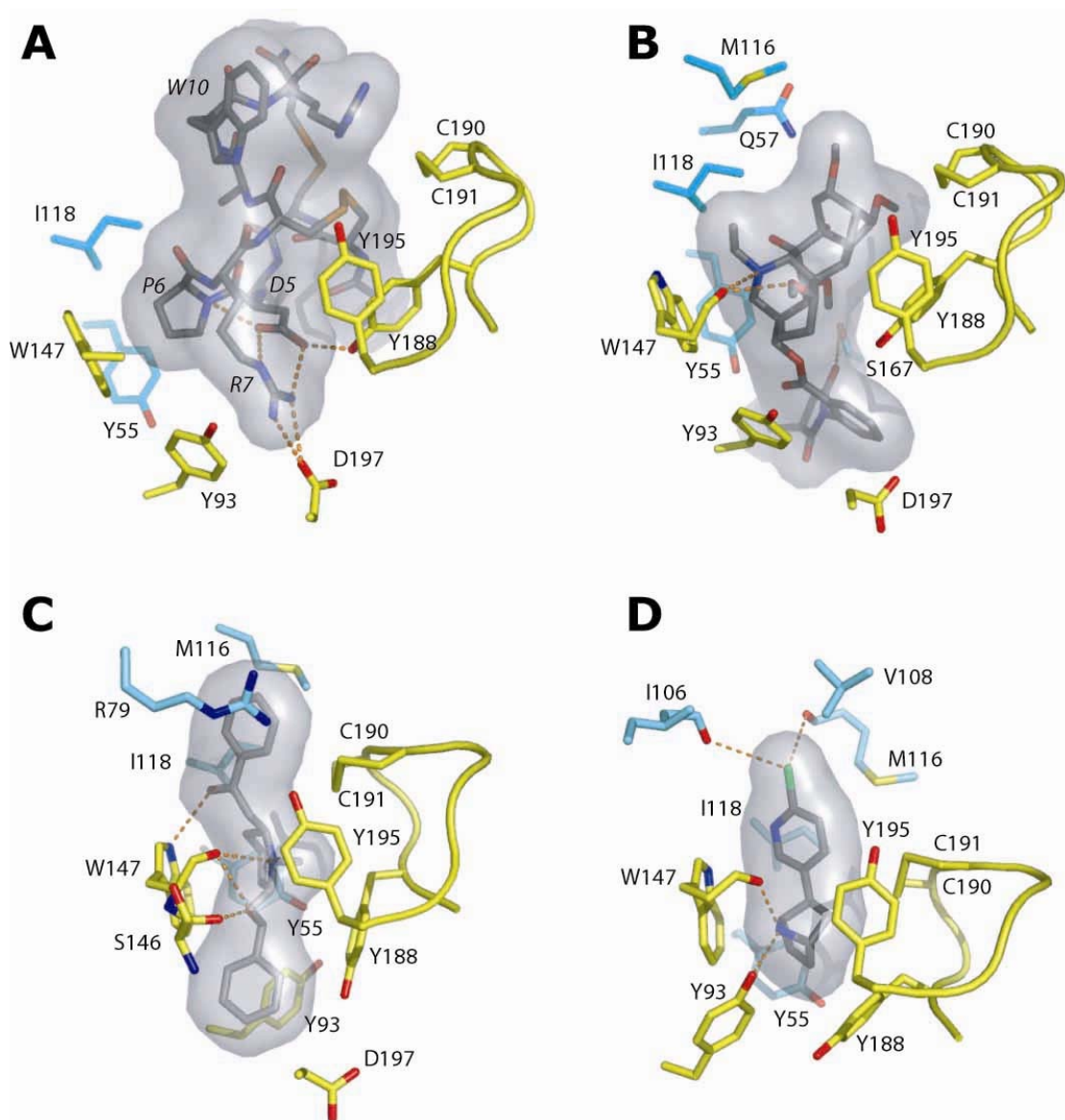


Figure VI.5: Expanded views of the bound ligands. Hydrogen bonding of key residues for the bound (A) ImI, (B) MLA, (C) LOB, and (D) EPI, viewed from inside of the ion channel vestibule looking in a radial direction. Ligands are bound between the Cys190-Cys191 disulfide on the left and Trp148 on the right. Labels for the ImI residues are italicized. The molecular surfaces of the ligands are in grey. Subunit coloring is identical to that in Figure VI.3.

guanidinium group and backbone nitrogen and with A-AChBP Tyr188 in loop C. ImI Pro6 is located deep in the pocket and in an edge-to-face aromatic interaction with the 4.1 Å distant A-AChBP Trp147. The ImI Arg7 guanidinium group establishes a salt-bridge with the invariant A-AChBP Asp197 in loop C and contacts the Tyr93 hydroxyl and the Ile196 carbonyl oxygen.

Moreover, the ImI Cys2-Cys8 disulfide bridge faces the 4 Å-distant A-AChBP Cys190-Cys191 disulfide and interacts with Tyr188 and Tyr195 in loop C. At the (-) face, ImI Ala9 contributes van der Waals contacts with A-AChBP Met116 and Ile118, and ImI Trp10 establishes extensive interactions with A-AChBP Arg79, Val108, Met116 and Arg59, consistent with its key role for ImI binding to the $\alpha 7$ nAChR (18,19) (Figures VI.4A and VI.5A). At the complex interface, only eight ordered solvent molecules are found, indicating a high degree of surface complementarity that is consistent with the nM dissociation constant of ImI for A-AChBP (10) (Table VI.1). Overall, the bound ImI buries, to a 1.6 Å probe radius, equivalent surface areas of 357 Å² and 343 Å² on the (+) and (-) faces of the A-AChBP subunit interface. The number of residues involved in the resulting interfacial area is consistent with the ImI large preference for A-AChBP, compared to L-AChBP (Table VI.1). Compared to ImI, the PnIA Ala10Leu/Asp14Lys variant, of the $\alpha 4/7$ family, is bound ~ 1 Å deeper in the ligand-binding pocket of A-AChBP (11), due to the Pro residue that replaces the bulky Arg7 at the tip of ImI loop I. Yet, the conformation of loop I in the two peptides is similar, whereas large deviations occur in loop II, which in PnIA is longer (by four residues) and larger (in size) than in ImI. This argues for loop I being the major determinant to confer nAChR selectivity.

b. The Methyllycaconitine-AChBP Complex

The diterpene alkaloid MLA, the principal toxic component of the plants seeds from the *Aconitum* and *Delphinium* generi, is the most potent, non peptidic nAChR antagonist known. MLA is highly selective for the neuronal $\alpha 7$ receptor subtype (20). Yet, it displays similar affinities for the *A*- and *L*-AChBP species (Table VI.1). The MLA molecule consists of a bulky, oxygen-rich lycoctonine moiety lacking nicotinic potency and linked, *via* a carbonyl ester linkage, to an N-phenyl succinimide (2-methylsuccinimidobenzoyl) side chain (Figure VI.1). Hydrolysis of the ester bond to produce lycoctonine markedly diminishes MLA affinity for the α -bungarotoxin binding sites on rat brain preparations, suggesting that the N-phenyl succinimide moiety of MLA is a major determinant for $\alpha 7$ selectivity.

In the MLA-A-AChBP complex (Figures VI.4B and VI.5B), the long axis of the bulky and rigid lycoctonine skeleton, that resembles a 7 Å x 4 Å cylinder, is located at the subunit interface and abuts against *A*-AChBP residues Tyr188 and Tyr195 and the Cys190-Cys191 disulfide from the (+) face of the interface, and against Met116 and Ile188 from the (-) face. The key interaction is an edge-to-face stacking of the N-ethylpiperidine ring, in a chair conformation, with Trp147 at the ‘membrane’ side of the binding site pocket. This conformation ideally positions the lycoctonine tertiary amine within hydrogen bond distance to the Trp147 carbonyl oxygen, whereas the ethyl group makes van der Waals contacts with Trp147 and Val148 on the (+) face and with Ile118 on the (-) face. Yet, the lycoctonine ring makes limited polar contact with *A*-AChBP, with only one of its six oxygen atoms bound to the Trp147 carbonyl oxygen. This is consistent with the potent antagonistic properties retained by simplified MLA derivatives

that contain only an N-ethylpiperidine moiety linked to the succinimidoylanthranilate ester (21). Owing to the flexibility of the ester linkage, the carbonyl oxygen is ideally positioned to be hydrogen bonded to Tyr55 on the (-) face. The well-ordered succinimidoylanthranilate moiety partially occupies a cavity lined by Ser94, Met126, Lys143, Gln186 and Asp197 on the (+) face and Gln38 and Ser167 on the (-) face, with the methyl group at position 3 of the imide ring contributing van der Waals contacts. The three hinge regions in MLA are essential to complement the shape of the binding pocket, resulting in a near perpendicular orientation of the lycoctonine cylinder axis relative to the direction of the ester linkage, while within the succinimidoylanthranilate ester the succinimide and phenyl rings are twisted by 60°.

The structurally-related alkaloid aconitine, a voltage-gated Na⁺ channel activator, differs from MLA in the oxygen pattern and stereochemistry and by the presence of bulky benzoyl and acetyl functional groups. Moreover, the N-phenyl succinimide group linked to the lycoctonine portion of MLA is absent in aconitine, where it is replaced by an O-methyl ether. The MLA-A-AChBP complex structure reveals that all aconitine substituents could be easily accommodated in A-AChBP, consistent with observation that addition of an N-phenyl succinimide moiety to aconitine produces a compound with nicotinic potency comparable to that of MLA, but lacking Na⁺ channel activation properties (22).

5. Agonist Binding

a. The Lobeline-AChBP Complex

The lipophilic alkaloid LOB, isolated from the Indian tobacco plant, *Lobelia inflata*, has been described as a nicotinic agonist and mixed agonist/antagonist (23). Comparison of

the large, three ring LOB (Figure VI.1) with the chemically related but smaller nicotine and cytisine has suggested that the phenyl 2-keto-ethyl moiety, more than the phenyl 2-hydroxyethyl group, may be the primary functional determinant for LOB binding to the nAChR (24). Its 100-fold preference for *A*-AChBP over *L*-AChBP indicates its selectivity among the agonists (Table VI.1).

In the LOB-*A*-AChBP complex (Figures VI.4C and VI.5C), the LOB molecule adopts an extended conformation devoid of internal hydrogen bonding that differs from the highly flexible conformation observed by NMR (16) but favors its interaction with both faces of the subunit interface. The LOB central piperidine ring is in a stacking interaction with *A*-AChBP Trp147 that favors hydrogen bonding between the tertiary amine and the carbonyl oxygen of this residue, while the methyl group contributes van der Waals contacts with Cys190, Tyr188 and Tyr195. Within the binding pocket, the LOB carbonyl oxygen is bound to the Trp47 indole nitrogen and establishes a water-mediated contact with the Ile106 carbonyl and Ile118 nitrogen. At the ‘membrane’ side of the binding pocket, the LOB hydroxyl is bound to the Ser146 and Trp147 carbonyl oxygens, consistent with its hydrogen bonding potential. The phenyl 2-keto-ethyl moiety is enclosed at the binding pocket entrance where it interacts with the Cys190-Cys191 disulfide on the (+) face and with Arg79, Met116 and Ile118 on the (-) face. In contrast, the phenyl 2-hydroxyethyl moiety, distant from the other phenyl moiety by ~11 Å, is buried at the ‘membrane’ side of the binding pocket where it is exclusively lined by residues Tyr93, Lys143, Gly145, Trp147 and Asp197 from the (+) face. Consistent with the requirement of retaining both arms for optimal affinity (25), the high flexibility of the two arms appears essential for the tight fit of the large LOB molecule to the shape of the

binding pocket with a closed loop C conformation. In the complex, this results in the two distal phenyl rings being twisted and bent by $\sim 15^\circ$ from colinear planarity. Given the expended surface area that LOB occupies relative to smaller agonists, multiple residues contribute to its preference for *A*-AChBP over *L*-AChBP (Table VI.1).

b. The Epibatidine-AChBP Complex

The chlorine-containing alkaloid EPI, from the skin of the Ecuadoran frog, *Epipedobates tricolor*, displays high potency and efficacy for several neuronal nAChR subtypes (26,27). EPI displays a 90-fold lower affinity for *A*-AChBP than for *L*-AChBP (Table VI.1). However, substitution of *A*-AChBP Tyr55 for a Trp, as found in the *L*-AChBP and human $\alpha 7$ subunits (Figure VI.1), restores the higher affinity (S.B.H., unpublished results), suggesting that the nature or size of the aromatic side chain at this position is critical for EPI binding.

The mode of binding of EPI to *A*-AChBP closely resembles that of nicotine to *L*-AChBP (8) (Figures VI.4 D and VI.5D). EPI is sandwiched between the Trp147 side chain and the Cys190-Cys191 disulfide positioned at the mid-point of the two ring systems. The pyridine ring in the bound EPI is oriented similar to the pyridine ring in the bound nicotine, while the nitrogen-containing alicyclic skeleton (bridge ring) in EPI, which abuts on the Tyr55 ring, coincides with the slightly smaller pyrrolidine ring in nicotine, resulting in similar intra-nitrogen distances (4.5 Å in *A*-AChBP vs. 4.4 Å in *L*-AChBP). As a result, a similar network of hydrogen bonds is observed in the two complexes, with the pyridine amine bound to Ile118 and Trp147 *via* a solvent molecule while the bridge ring amine targets the Trp147 carbonyl oxygen. In three *A*-AChBP subunits in the pentamer, a second hydrogen bond is seen between the bridge ring amine

and Tyr93. The bulky bridge ring in EPI favors additional aromatic interactions with Tyr188, and the aromatic chloride ideally contributes polar contacts with the Ile106 and Val108 carbonyl oxygen from the (-) face of the interface in the apical region of the binding pocket. The mode of binding of EPI, with the chloride contribution and the large bridge ring that compensates for the *A*-AChBP smaller Tyr ring, compared to the *L*-AChBP Trp, is consistent with the mutagenesis data and provides an explanation for EPI's higher affinity than nicotine for *A*-AChBP (Table VI.1).

6. Conformational Fit for Antagonists and Agonists

The availability of an apo *A*-AChBP structure along with two antagonist and two agonist complexes permits a direct comparative analysis of the conformational changes induced differentially by antagonist and agonist binding. Structural comparisons of the five structures (rmsd values in the 0.55-0.65 Å range for ~1000 C α atoms) and of the subunits from each pentamer (rmsd values in the 0.35-0.55 Å for 210 C α atoms) indicate that the large conformational changes are localized to loops C and F with smaller changes arising in other regions and in the relative orientation of subunits within the pentamer. In contrast, attempts to overlay either of our five *A*-AChBP pentamers with the Hepes-bound or the PnIA-bound pentamer (11) were unsuccessful. This suggests that differences in the protein sequence (cf. legend to Figure VI.1) or its preparation may influence the relative orientation of the subunits within the pentamer.

The largest differences arise from the rigid-body motion of loop C, which swings as much as 11 Å between the two extreme positions observed in the ImI and EPI complexes (Figure VI.6A), around hinge regions defined within dipeptides Gln184-Val185

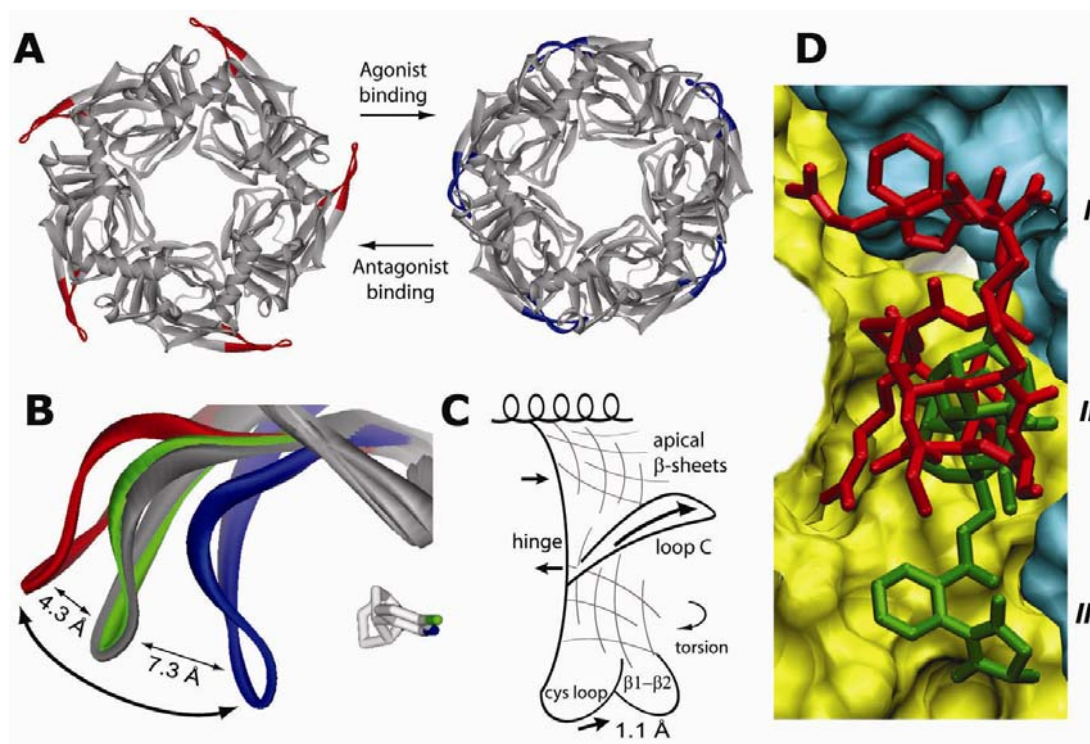


Figure VI.6: Conformational fit mechanism and ligand selectivity. (A) Top views of the ImI-bound (red loops C) and EPI-bound A-AChBP pentamers (blue loops C) showing the distinctive conformations for the antagonist and agonist complexes. (B) Overlay of loop C in apo A-AChBP (grey) and the ImI (red), MLA (green) and EPI complexes (blue); the bound EPI molecule is shown in light grey. The curved arrow denotes opening and closure of loop C upon antagonist and agonist binding. (C) Schematic profile of a single subunit showing the ligand-induced conformational changes. The thin arrows and their lengths denote direction and magnitude of movement upon agonist binding. The curved arrow on the right denotes subunit rotation. Agonist binding induces a large closure of loop C followed by a small rotation of subunit near the membrane and a slight puckering near the loop C hinge. A-AChBP, when viewed from the side, moves from an hour glass shape towards a slightly more cylindrical shape upon agonist binding. (D) Overlay of the A-AChBP-bound antagonists ImI (red) and MLA (green). The surfaces of the (+) and (-) faces of the subunit interface are shown in yellow and cyan, respectively. The common competitive binding site is at the center (labeled II); the two peripheral non-overlapping sites are distinguished by ImI Trp10 (I) and the MLA N-phenyl succinimide moiety (III).

and Tyr195-Ile196, respectively located in strands $\beta 9$ and $\beta 10$ (Figures VI.1 and VI.6). In fact, the loop C positions throughout the five structures cluster into three groups that contain i) the peptide antagonist-bound ‘open’ conformations (ImI complex); ii) the apo and organic antagonist-bound ‘intermediate’ conformations (apo and MLA complex); iii) the agonist-bound ‘closed’ conformations (LOB and EPI complexes) (Figure VI.5B). Indeed, A-AChBP in the apo conformation lies between the peptide antagonist- and the agonist-bound conformations. Loop C in the Cbtx-*L*-AChBP complex adopts a similar intermediate conformation as seen in the apo and the MLA-A-AChBP complex, but it is tangentially displaced by ~ 4 Å toward loop $\beta 7$ - $\beta 8$ (9), suggesting either a common mechanism for peptide toxin antagonism or that the Cbtx fingers lock loop C in a unique position. The slower ligand association rates observed for the peptide toxins (10,28), being well below the diffusion limitation, may be a consequence of the transition to the extended (open) loop C conformation.

Residues at the tip of loop C contribute to the subunit interface and wrap around the bound agonist, with Ser196 bound to Asp164 in loop F from the (-) face as seen for the *L*-AChBP-Hepes complex (5) (Figure VI.6). Hence, a series of local conformational changes specific to each ligand is observed, and loop C behaves as an induced-fit ‘sensor’ adapting its configuration to the structural characteristics of the ligand entering the binding pocket. Hence this motif may not only govern ligand specificity but also whether the ligand elicits channel opening events, *i.e.*, the efficacy of the ligand as an agonist. In the apo A-AChBP structure, the architecture of the binding pocket is reminiscent of the resting state of the nAChR (6) with low affinity for the nicotinic ligands. In contrast, the agonist-elicited closure of loop C is associated with substantial reorganization of the

recognition determinants, *e.g.* Gln186, Tyr188, Glu193 and Tyr195; this results in a binding pocket configuration that perhaps reflects the desensitized state of the nAChR. At two of the five subunit interfaces in the ImI-A-AChBP complex, loop F adopts two alternative conformations, indicating that this region also displays significant conformational flexibility when antagonists are bound.

7. Ligand Selectivity

The aromatic nest rich in Tyr and Trp residues that characterizes the ligand binding site of AChBP and of the nAChR LBD emphasizes the importance of cation- π interactions to stabilize the cation of the nicotinic ligands (2). Although several cation- π interactions are observed in the A-AChBP and L-AChBP complexes, the secondary amine in EPI and tertiary amines in LOB and MLA are located within 0.9-1.0 Å of the Trp147 carbonyl oxygen; this association contributes charge compensation to the cation (Figures VI.4B-D and VI.5B-D). In the ImI complex, the Arg7 nitrogen, distant by only 2 Å from the amine centroid position in the alkaloid ligands, serves as the cation (Figures VI.4A and VI.5A). Hence, the multiple ligand-bound A-AChBP structures largely support the previous assumption that a partial negative charge of the Trp147 carbonyl oxygen, mediated *via* the invariant Asp85, may favor interaction with the common cationic ammonium of the nicotinic ligands (8).

This comparative analysis also permits identification of the structural determinants required to accommodate specifically these chemically-diverse ligands. It has been suggested that the ligand may access the binding pocket from either the apical side or the ‘membrane’ side of loop C (5). The structure of the MLA-A-AChBP complex reveals an unpredicted binding pocket, located well below Trp147 at the ‘membrane’ side of the

agonist binding site and loop C, which accommodates the MLA N-phenyl succinimide moiety (Figure VI.4B, VI.5B, and VI.6D). In turn, the structure of the ImI-A-AChBP complex identifies a second binding region, located on the apical side of loop C, which accommodates ImI Trp10 and neighboring residues (Figure VI.4A, VI.5A, VI.6D). The residues that line these two distant functional sites are weakly conserved within the nAChRs and may confer subtype selectivity. In apo A-AChBP with its open loop C, these pockets at the subunit interface are freely accessible from the outside (Figure VI.3), whereas in the agonist complexes (closed loop C), access is impaired by the close proximity of the invariant Tyr188 and Lys143 residues (located on the ‘membrane’ side) and the tight packing of the Cys190-Cys191 disulfide (apical side) that act as barriers that isolate the competitive binding site (Figures VI.4, VI.5, panels C, D). In the LOB complex, subtle reorientations of side chains near the binding pocket, as seen for Tyr93, displaced by one of the LOB phenyl moieties, are required to accommodate a specific ligand (Figure VI.4C, VI.5C).

The mode of binding of ImI reveals that the critical Asp5-Pro6-Arg-7 triad, rather than Trp10 (16), is the primary region that targets A-AChBP (Figure VI.4A, VI.5A), a finding consistent with the low conformational flexibility of these residues in solution. I would anticipate that substitution of ImI Pro6 or Ala9 by a residue with a larger side chain as found in ImII would drastically impair ImI binding, whereas the binding contribution of Trp10 would be less sensitive to mutation. Based on these structural criteria, α -conotoxin EpI should bind A-AChBP; this would be consistent with data on binding to the $\alpha 7$ receptor (29). To some extent, the same rationale could apply to α -conotoxin PnIB, whereas α -conotoxin MII should not be a potent blocker, as is the case for MI (Table

VI.1). Overall, the crystalline ImI-A-AChBP complex provides a suitable template for designing synthetic peptides for further characterization of nAChR subtypes, and highlights the absolute requirement of a α_{310} helical region within loop I of the α -conotoxin to confer nAChR antagonism.

Previous structural analysis of the Cbtx-*L*-AChBP complex along with unpublished mutagenesis data led us to examine whether the lower affinity of Cbtx for *A*-AChBP (Table VI.1) could be enhanced, to approach that found for *L*-AChBP, by a His197Phe substitution that may eliminate electrostatic repulsion on the external face of loop C (9). In contrast to the large and flat Cbtx molecule, the smaller and globular ImI molecule binds deeper in the binding pocket, and residues that line the pocket are primary candidates for mutation. Docking of ImI onto *L*-AChBP, by superimposing the *L*-AChBP and *A*-AChBP coordinates from their respective Cbtx and ImI complexes, does not reveal steric occlusion except for a small overlap between ImI Trp10 and the side chain of *L*-AChBP Gln78. It therefore appears that ligand selectivity arises from subtle differences between *L*-AChBP and *A*-AChBP such as electrostatic repulsion, most particularly with residues in loop F at the (-) face of the subunit interface. Based on their structural similarity, the 3_{10} helical turn in ImI and the tip of loop II in Cbtx have been proposed to exhibit similar spatial organization upon binding to the α_7 receptor, with the ImI Trp10/Arg7 and Cbtx Phe29/Arg33 pairs mimicking each other and being deeply anchored within the binding pocket (30). However, comparative analysis of the respective complexes shows that these structural determinants are separated by 7 Å and rotated by 50° from each other. Hence the toxins may orient differently in targeting distinct nAChR subtypes.

D. Concluding Remarks

The structure of apo *A*-AChBP reveals several features not evident in those of the Hepes-bound *L*-AChBP and *A*-AChBP. First of all, the radial extension of loop C creates a portal for ligand access. Such a conformation in absence of a bound cationic ligand may reflect better the resting state of the nAChR than the open conformation previously observed for Cbtx-bound *L*-AChBP (9).

Agonists bind within a discrete site, as seen for the LOB- and EPI-*A*-AChBP and nicotine- and carbamylcholine-*L*-AChBP complexes. They elicit loop C closure, and this may be an essential feature of a conformational change linked to channel opening in the nAChR. It will be of interest to ascertain whether the small conformational changes observed in the loops proximal to the 'membrane' interface are also linked to channel opening.

Antagonists primarily use distinct non-overlapping regions of the subunit interface for stabilization of their complexes. They further distend loop C either radially (ImI-*A*-AChBP complexes) or tangentially (Cbtx-*L*-AChBP complex) to accommodate their disparate structures and mode of association, suggesting that loop C extension may be a common feature for all competitive antagonists. This also suggests that loop C extension and closure may be the distinguishing feature in the extracellular region between agonist and antagonist complexes with the nAChR.

E. Materials and Methods

1. Protein Expression and Purification

A-AChBP, flanked with a N-terminal FLAG epitope numbered (-8)DYKDDDDKL(0), was expressed from chemically synthesized cDNA (10) as a

soluble exported protein from stable HEK293S cells lacking the N-acetylglucosaminyltransferase I (GnTI) gene (12) and selected for G418 resistance. Culture media containing A-AChBP (6-8 mg/l) were collected at 24-36 h intervals, added with 0.02% NaN₃ and stored at 4°C. A-AChBP was purified on immobilized anti-FLAG antibody (28), and dialyzed against 50 mM Tris, pH 7.4, 150 mM NaCl, 0.02% NaN₃ and concentrated to 12 mg/ml by ultrafiltration (YM50 Centricon unit). Mass spectrometry analyses yielded a monoisotopic mass of 27,254 Da, *i.e.* 3.9% higher than the theoretical mass, and indicated the presence of a single pentasaccharidic Man₅GlcNAc₂ moiety linked to Asn74. Gel filtration FPLC on prepacked Superdex-200 (Amersham Biosciences) showed a single peak corresponding to a pentamer of subunits.

2. Ligand Binding

K_d's for the high affinity ligands (values < 100 nM) were determined from the ratio of dissociation to association rates by monitoring intrinsic Trp quenching with stopped-flow spectrofluorometry, while for the low affinity ligands (values > 100 nM) they were measured by equilibrium fluorescence quenching (10).

3. Crystallization and Data Collection

The peptidic α -conotoxin ImI, from *Conus imperialis* venom, was from the American Peptide Co. The organic ligand MLA and LOB were from Tocris and EPI from Sigma-Aldrich. Formation of each of the four A-AChBP complexes used a 1.1-fold molar excess of the ligand and 1h incubation at room temperature. Crystallization was achieved by vapor diffusion either at 18°C using a protein-to-well ratio of 1:1 in 1 μ l hanging drops, or at 20°C using a protein-to-well ratio of 2:1 in nanoliter sitting drops set-up with automated crystallization TECAN Genesis and Cartesian robots (31). The well solutions

were: for apo A-AChBP, 12-14% PEG-4000 (Fluka), 0.1 M sodium citrate, pH 5.6, 20% isopropanol, 5% glycerol; for the ImI complex, 11-14% PEG-4000, 0.1 M Tris, pH 7.5, 0.4 M MgCl₂; for the MLA complex, 21-22% PEG-4000, 0.1 M Tris, pH 7.5, 0.4 M MgCl₂; for the EPI complex, 18-22% PEG-3350 (Nextal Biotech.), 0.1 M Tris, pH 7.5, 0.2 M sodium citrate, and the crystals were improved by macroseeding; for the LOB complex, 25% PEG-4000, 0.1 M HEPES, pH 7.5. The crystals were flash-cooled in liquid nitrogen after successive short soaks into well solutions supplemented with 18 to 23% PEG and 3 to 5% glycerol. Data were processed with HKL2000 (32) and Mosflm (33), and all further computing carried out with the CCP4 program suite (34), unless otherwise stated.

4. Structure Determination and Refinement

The five structures were solved by molecular replacement with AMoRe (35) using, as search model, the structure of HEPES-bound *L*-AChBP (PDB code 1UX2, (8) for the apo A-AChBP structure, and the latter for each of the four complexes. The initial electron density maps were improved considerably using the automatic rebuilding procedure as implemented in ARP/wARP (36) and manual adjustment with the graphics programs Xtalview v4.1 (37) and TURBO-FRODO (38). All structures were refined with REFMAC (39) using the maximum likelihood approach and incorporating bulk solvent corrections, anisotropic F_{obs} versus F_{calc} scaling and TLS refinement. Random sets of reflections were set aside for cross validation purposes. NCS restraints were applied for refinement of the MLA, EPI and LOB complex structures. Automated solvent building was performed with ARP/wARP. Data collection and refinement statistics are reported in Table VI.2.

The final apo *A*-AChBP and MLA, LOB, and EPI complex structures comprise residues His1-Arg207/Arg208 in all five subunits. A partially ordered PEG molecule occupies the binding pocket in all five apo *A*-AChBP subunits. The final ImI complex structure comprises *A*-AChBP residues His1-Arg208 and Im1 residues Gly1-Cys12 in all five subunits and bound toxins. In all structures, most of the N-terminal FLAG epitope is clearly visible in most subunits, but weak electron density is associated with surface loop Asn15-Met19. A well-ordered GlcNAc moiety linked to Asn74 is visible in a single subunit in the apo and the ImI complex structures. The stereochemistries of the structures were analyzed with PROCHECK (40); no residues were found in the disallowed regions of the Ramachandran plot. Figures VI.3 and VI.6 were made with ViewerLite (Accelrys) and Figures VI.4 and VI.5 with PyMOL (DeLano Scientific LLC).

F. Acknowledgements

This chapter is material as it appears in:

Scott B Hansen, Gerlind Sulzenbacher, Tom Huxford, Pascale Marchot, Palmer Taylor, and Yves Bourne. “Structures of *Aplysia* AChBP complexes with agonists and antagonists reveal distinctive binding interfaces and conformations” in press *Embo J* 2005

This work was done in the laboratories of Drs. Yves Bourne and Pascale Marchot at the CNRS in Marseille, France and in the laboratory of Dr. Gourisanker Gosh, UCSD. I thank Yves and Pascale for their hospitality and allowing me to work in their labs. Gerlind Sulzenbacher did extensive work on the *Aplysia* Apo-AChBP structure and final atom placement of the crystal complexes described. Initial work including crystallization and data collection were carried out with Dr. Tom Huxford in the Gosh lab at UCSD. I thank Dr. Gosh for use of his laboratory and supplies.

We are grateful to the ESRF (Grenoble, France), ALS (Berkeley, CA) and APS (Argonne, IL) staff for assistance in data collection, and to G. Ghosh, N. Nguyen, C. Kim, S.S. Taylor, T.T. Talley and Z. Radic (UCSD) for support and fruitful discussions. Supported by USPHS grants R37-GM18360/GM07752 (to P.T.) and T32DK007233 (to T.H.), a Tobacco-Related Disease Research fellowship (to S.B.H.), and by the CNRS during S.B.H.’s work in Marseille (to Y.B. and P.M.).

G. References

1. Grutter, T., and Changeux, J. P. (2001) *Trends Biochem Sci* **26**, 459-463
2. Lester, H. A., Dibas, M. I., Dahan, D. S., Leite, J. F., and Dougherty, D. A. (2004) *Trends Neurosci* **27**, 329-336
3. Karlin, A. (2002) *Nat Rev Neurosci* **3**, 102-114
4. Smit, A. B., Syed, N. I., Schaap, D., van Minnen, J., Klumperman, J., Kits, K. S., Lodder, H., van der Schors, R. C., van Elk, R., Sorgedraeger, B., Brejc, K., Sixma, T. K., and Geraerts, W. P. (2001) *Nature* **411**, 261-268
5. Brejc, K., van Dijk, W. J., Klaassen, R. V., Schuurmans, M., van Der Oost, J., Smit, A. B., and Sixma, T. K. (2001) *Nature* **411**, 269-276
6. Unwin, N. (2005) *J Mol Biol* **346**, 967-989
7. Bouzat, C., Gumilar, F., Spitzmaul, G., Wang, H. L., Rayes, D., Hansen, S. B., Taylor, P., and Sine, S. M. (2004) *Nature* **430**, 896-900
8. Celie, P. H., van Rossum-Fikkert, S. E., van Dijk, W. J., Brejc, K., Smit, A. B., and Sixma, T. K. (2004) *Neuron* **41**, 907-914
9. Bourne, Y., Talley, T. T., Hansen, S. B., Taylor, P., and Marchot, P. (2005) *Embo J* **24**, 1512-1522
10. Hansen, S. B., Talley, T. T., Radic, Z., and Taylor, P. (2004) *J Biol Chem* **279**, 24197-24202
11. Celie, P. H., Kasheverov, I. E., Mordvintsev, D. Y., Hogg, R. C., van Nierop, P., van Elk, R., van Rossum-Fikkert, S. E., Zhmak, M. N., Bertrand, D., Tsetlin, V., Sixma, T. K., and Smit, A. B. (2005) *Nat Struct Mol Biol*
12. Reeves, P. J., Callewaert, N., Contreras, R., and Khorana, H. G. (2002) *Proc Natl Acad Sci U S A* **99**, 13419-13424
13. Richman, D. P., and Agius, M. A. (2003) *Neurology* **61**, 1652-1661
14. Ellison, M., Gao, F., Wang, H. L., Sine, S. M., McIntosh, J. M., and Olivera, B. M. (2004) *Biochemistry* **43**, 16019-16026
15. Ellison, M., McIntosh, J. M., and Olivera, B. M. (2003) *J Biol Chem* **278**, 757-764

16. Maslennikov, I. V., Shenkarev, Z. O., Zhmak, M. N., Ivanov, V. T., Methfessel, C., Tsetlin, V. I., and Arseniev, A. S. (1999) *FEBS Lett* **444**, 275-280
17. Rogers, J. P., Luginbuhl, P., Shen, G. S., McCabe, R. T., Stevens, R. C., and Wemmer, D. E. (1999) *Biochemistry* **38**, 3874-3882
18. Quiram, P. A., and Sine, S. M. (1998) *J Biol Chem* **273**, 11007-11011
19. Servent, D., Thanh, H. L., Antil, S., Bertrand, D., Corringer, P. J., Changeux, J. P., and Menez, A. (1998) *J Physiol Paris* **92**, 107-111
20. Ward, J. M., Cockcroft, V. B., Lunt, G. G., Smillie, F. S., and Wonnacott, S. (1990) *FEBS Lett* **270**, 45-48
21. Bergmeier, S. C., Ismail, K. A., Arason, K. M., McKay, S., Bryant, D. L., and McKay, D. B. (2004) *Bioorg Med Chem Lett* **14**, 3739-3742
22. Hardick, D. J., Cooper, G., Scott-Ward, T., Blagbrough, I. S., Potter, B. V., and Wonnacott, S. (1995) *FEBS Lett* **365**, 79-82
23. Terry, A. V., Jr., Williamson, R., Gattu, M., Beach, J. W., McCurdy, C. R., Sparks, J. A., and Pauly, J. R. (1998) *Neuropharmacology* **37**, 93-102
24. Barlow, R. B., and Johnson, O. (1989) *Br J Pharmacol* **98**, 799-808
25. Flammia, D., Dukat, M., Damaj, M. I., Martin, B., and Glennon, R. A. (1999) *J Med Chem* **42**, 3726-3731
26. Badio, B., and Daly, J. W. (1994) *Mol Pharmacol* **45**, 563-569
27. Gerzanich, V., Peng, X., Wang, F., Wells, G., Anand, R., Fletcher, S., and Lindstrom, J. (1995) *Mol Pharmacol* **48**, 774-782
28. Hansen, S. B., Radic, Z., Talley, T. T., Molles, B. E., Deerinck, T., Tsigelny, I., and Taylor, P. (2002) *J Biol Chem* **277**, 41299-41302
29. Nicke, A., Wonnacott, S., and Lewis, R. J. (2004) *Eur J Biochem* **271**, 2305-2319
30. Tsetlin, V. (1999) *Eur J Biochem* **264**, 281-286
31. Sulzenbacher, G., Gruez, A., Roig-Zamboni, V., Spinelli, S., Valencia, C., Pagot, F., Vincentelli, R., Bignon, C., Salomoni, A., Grisel, S., Maurin, D., Huyghe, C., Johansson, K., Grassick, A., Roussel, A., Bourne, Y., Perrier, S., Miallau, L., Cantau, P., Blanc, E., Genevois, M., Grossi, A., Zenatti, A., Campanacci, V., and Cambillau, C. (2002) *Acta Crystallogr D Biol Crystallogr* **58**, 2109-2115

32. Otwinowski, Z., and Minor, W. (1997) *Methods in Enzymology* **276**, 307-326
33. Leslie, A. (1992) in *Joint CCP4+ESF-EAMCB Newsletter on Protein Crystallography* Vol. 26
34. CCP4. (1994) *Acta Crystallogr D Biol Crystallogr* **50**, 760-763
35. Navaza, J. (1994) *Acta Crystallogr Sect. A* **50**, 157-163
36. Perrakis, A., Morris, R., and Lamzin, V. S. (1999) *Nat Struct Biol* **6**, 458-463
37. McRee, D. (1992) *J. Molecular Graphics* **10**, 44-46
38. Roussel, A., and Cambillau, C. (1989) *TURBO-FRODO*. Silicon Graphics Geometry Partners Directory (Committee, S. G., Ed.), Mountain View, California, Silicon Graphics
39. Murshudov, G. N., Vagin, A. A. & Dodson, E. J. (1997) *Acta Crystallogr D Biol Crystallogr* **53**, 240-255
40. Laskowski, R., MacArthur, M., Moss, D., and Thornton, J. (1993) *J Appl Cryst* **26**, 283-291

Chapter VII

Summary and Implications

A. Protein Expression

1. Gene Synthesis

A gene coding for *Lymnaea* AChBP was synthesized chemically (1) due to lack of a *Lymnaea* cDNA library. Commercial synthesis of the entire gene was cost prohibitive but advances in oligonucleotides allowed for gene assembly by sequential ligation described in chapter II. Since that time, inexpensive oligonucleotides have made commercial gene synthesis more reasonable. As a result the C-terminal half of the *Aplysia* AChBP was commercially made (Bio-nexus, USA). The N-terminus was generated as described for *Lymnaea* AChBP.

Designed into the genes are triplet codes reflecting mammalian codon usage, thereby increasing expression, and convenient enzyme restriction sites. The restriction sites use inexpensive and efficient enzymes. Properly spaced, they greatly facilitated the molecular biology in this study. New technologies using PCR have further decreased cost; as much as an 80% decrease over the period of this work, making commercial gene synthesis the preferred method for large amounts of gene manipulation.

2. Mammalian Expression and Glc-NAc Transferase I Deficient Cells

Large scale protein expression of AChBPs was carried out in an HEK 293 mammalian expression system as described in chapter II. AChBP was first expressed in a yeast system by Smit et al (2). For this study mammalian expression was selected because of the expertise in the lab. Expressing protein in yeast is less expensive but

apparently has some disadvantages given that the Smit et al., later used a baculovirus expression system (3) to express an AChBP from *Bulinus truncatus*. Apart from cost, mammalian expression and purification was very convenient. When the purification tag was properly placed (4), AChBP expressed 6-10 mg/liter. Immuno-purification with an antibody directed to the FLAG epitope is also expensive but very convenient. FLAG antibody specificity resulted in greater than 99% AChBP purity after a single column step followed by buffer exchange. Purification based on nickel affinity to six histidines was not successful. The metal column did not tolerate large amounts of mammalian media. A myc antibody system was also investigated but the capacity of the antibody column was one fifth that of FLAG (Lee Schroeder, unpublished data).

Glycosylation processing by mammalian cells yielded very heterogeneous set of oligosaccharides and yields a protein not necessarily amenable to crystallization. AChBP expressed in wild type HEK cells contained ~20,000 kDa of N-linked glycosylation per pentamer (1,4). Heterogeneity of N-linked glycosylation was overcome by the use of a Glc-NAc transferase I deficient (GnTI⁻) HEK 293 cell line (5) that decreased glycosylation to yield oligosaccharides of total mass of 6090 kDa (Jian Shi, unpublished data). GnTI⁻ cells were less robust than wt HEK but expressed large quantities of protein in about half the time. Stably transfected cell lines were also more difficult to obtain. However the homogeneity of GnTI⁻ expressed protein was crucial to crystallization and achieving high resolution diffraction patterns.

3. *Aplysia* vs. *Lymnaea* AChBP as a Surrogate

Lymnaea AChBP expressed approximate 25% more protein than *Aplysia* AChBP. *Aplysia* AChBP was more sensitive the nature of the conjugated tag and aggregation (4).

However, *Aplysia* AChBP was more amenable to crystallization. Robot screens (6) yielded crystals with 5-fold increase in number of parallel samples, many of which diffracted sufficiently for a structure to be solved. Already, more complexes have been solved with the *Aplysia* protein than with *Lymnaea*. Many of these complexes failed to yield diffracting crystals with *Lymnaea* protein. These include the apo form and antagonists complexes that yielded high resolution diffraction patterns (7).

B. Ligand Binding Assays

The acetylcholine binding protein is soluble and thus can not be assayed in the same manner as the nAChR. A key step in receptor assays is to separate bound and free ligand by pelleting membranes or collecting membrane fraction on a filter and then washing away free ligand. Smit et al who first assayed the *Lymnaea* AChBP immobilized the protein on a bead and followed traditional nAChR assay methods (2). This was not very effective and several ligand dissociation constants were shown to be incorrect (1,4). Later studies by the same group used microcalorimetry (3,7,8). However, this method lacked efficiency for comparing dissociation constants of AChBPs for larger numbers of assays and is limited in the types of ligands that can be accurately measured. My study outlines methods for accurately determining steady state, kinetic, and competition experiments.

1. Steady-state Equilibrium

Intrinsic tryptophan fluorescence was used to directly monitor ligand binding described in Chapter II. Most ligands quench fluorescence. Assays were set up in a plate reader format (96 well). Sensitivity was limited to ligands with dissociation constants less than 100nM and fluorescent ligands absorbing light at 280nm. Ligands that did not

change fluorescence were competed with gallamine, a strong enhancer of AChBP fluorescence, or with dansylcholine, a ligand that quenches fluorescence by FRET.

The scintillation proximity assay (SPA) adapted from Amersham Biosciences was the most sensitive assay for detection of ligand binding. Here AChBP was attached to a solid scintillate and radioligand binding was measured by its proximity to the solid scintillate. Radioactive free ligand was diffusely distributed and not measured by the solid scintillate. Sensitivity was ~ 100 picomolar concentration of AChBP sites and results were very reproducible.

2. Stopped-flow Fluorescence

Direct measurements of intrinsic tryptophan fluorescence have the advantage that the reaction can be monitored in real time. Stopped-flow can detect changes in the millisecond time frame which is sufficient to determine on and off rates of most ligands. Very fast equilibrating low affinity ligands such as carbamylcholine were not detectable.

C. Fluorescence Resonance Energy Transfer (FRET) to the dansylcholine acceptor.

Dansylcholine has spectral overlap for resonance energy transfer with tryptophan side chains in the ligand binding pocket. Very small volumes are needed to detect fluorescence. At equilibrium in a plate reader assay volumes of $2\mu\text{l}$ have a signal 20 fold over background (Figure VII.1). Similar results were seen with $1\mu\text{l}$ total volume suggesting that screens with nano liter volumes are feasible. Fluorescence competition is amenable to assay development when the competing drugs of interest are scarce or expensive. Figure VII.2B shows α -conotoxin ImI binding to *Lymnaea* AChBP. ImI affinity for *Lymnaea* is low and a high concentration was achieved by reducing the reaction volume to $2\mu\text{l}$.

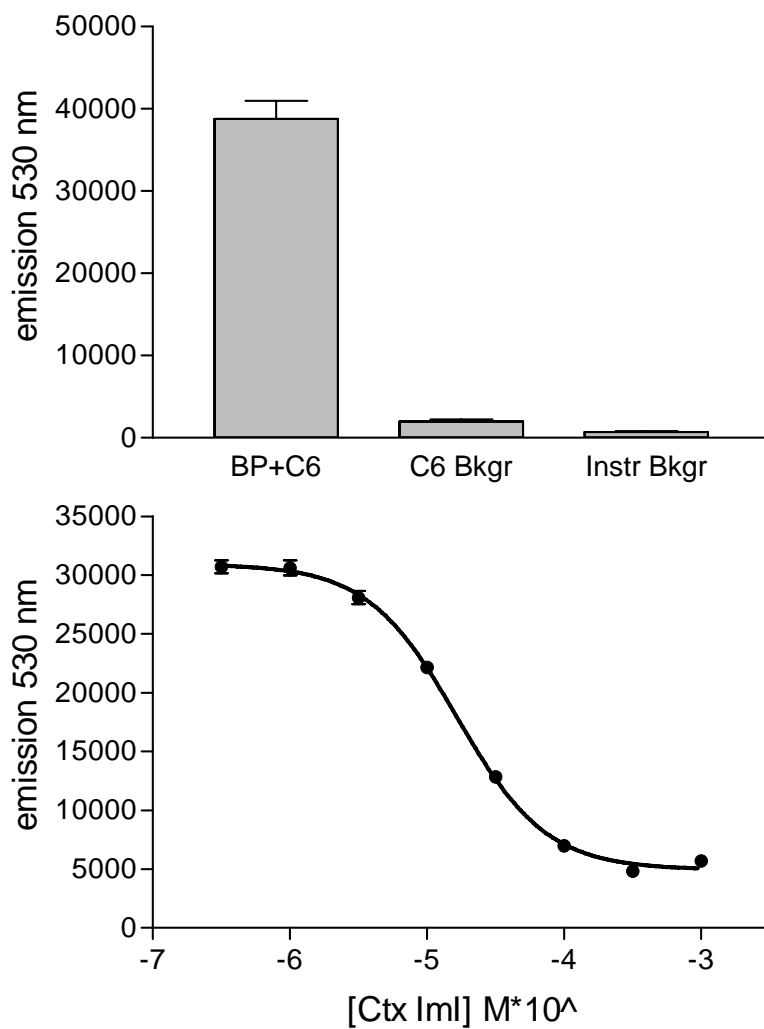


Figure VII.1 Fluorescence competition with limiting volumes.
Lymnaea AChBP 400nM sites in a 384 half well plate and a 2ul final reaction volume.
Dansylcholine C6 is the competing ligand with AChBP at 500nM sites.

D. Contributions to Receptor Knowledge

The acetylcholine binding protein is only a surrogate to the nAChR, and it is important to evaluate what insights can be applied to the nAChR. The structural fold published by Brejc et al has shed enormous clarity onto years of biochemical experiment of the receptor. Nigel Unwin recently refined an impressive structure of the full length nAChR at 4 angstrom resolution (9). The *Lymnaea* AChBP published by Brejc et al was used as a starting model and key to refinement. The transmembrane domain was solved independently (10).

Are more detailed studies of AChBP warranted? The coupling of AChBP to an ion pore and the capacity of AChBP to respond to acetylcholine and gate ions demonstrates that studies are warranted (11). Structural determinants that govern ligand binding and resulting conformational changes almost certainly have several parallels with the nAChR.

E. The nAChR as a Drug Target

For the nAChR to be an effective drug target, candidate ligands must be subtype selective. The first subclassification is to select between neuronal and muscle subtypes. Cross reactivity with muscle and ganglionic receptors is adverse to vital processes for chronic treatments of CNS manifestations such as neuro degeneration and pain. Current therapeutics are limited to short term muscle relaxation associated with anesthesia. More effective nicotinic therapeutic agents could be developed if selectivity were achieved. Many speculated that detailed understanding of α -bungarotoxin (bgtx) would yield selective molecules; given that bgtx binds selectively to muscle and just one neuronal receptor, $\alpha 7$. However, AChBP data suggests that most of α -bungarotoxin selectivity is

achieved through a solvent exposed surface on the C loop. Other nicotinic ligands do not contact this area. It is bgtx's large size and surface of interaction that allows for specificity. Such interactions may be difficult to mimic with a small molecule. Figure VII.2 is a sequence alignment of AChBPs and nAChR subtypes showing residues that interact with all ligands delineating the ligand binding pocket. Most of the residues are conserved that make up the ligand binding pocket. Two residues M116 and I118 (*Aplysia* numbering) are located on the apical side of the C loop (Figure VII.3). The membrane side of the pocket is closest to the F loop.

1. Structural Basis of Agonism and Antagonism

Structural data show C loop closure to pack tightly against agonist. This is the case for both structures from *Aplysia* and *Lymnaea* proteins (3,7,8,12). In the case of bound antagonist the C loop is pushed radially (13). To design subtype specific agonist the ligand must allow the C loop to close tightly. Antagonists fill the entire pocket and interact with various surfaces both on the 'membrane' side of the C loop, in the case of methyllycaconitine, and on the apical side of the C loop, in the case of α -conotoxin ImI. α -Conotoxin ImI reveals a large binding surface apical to the C loop where larger ligands might probe for selectivity. For all bound ligands little residual water remains in the binding pocket and most interactions are hydrophobic and not electrostatic.

This study reveals the detailed binding determinants of AChBP and by homology the nAChR (13). The nature of antagonism by the various peptide toxins and alkaloids indicate how a novel antagonist could be developed for the nAChR. The ligand needs to be relatively large and take up sufficient space in the ligand binding pocket to displace the C loop. There are distal non-overlapping domains that might serve as selective

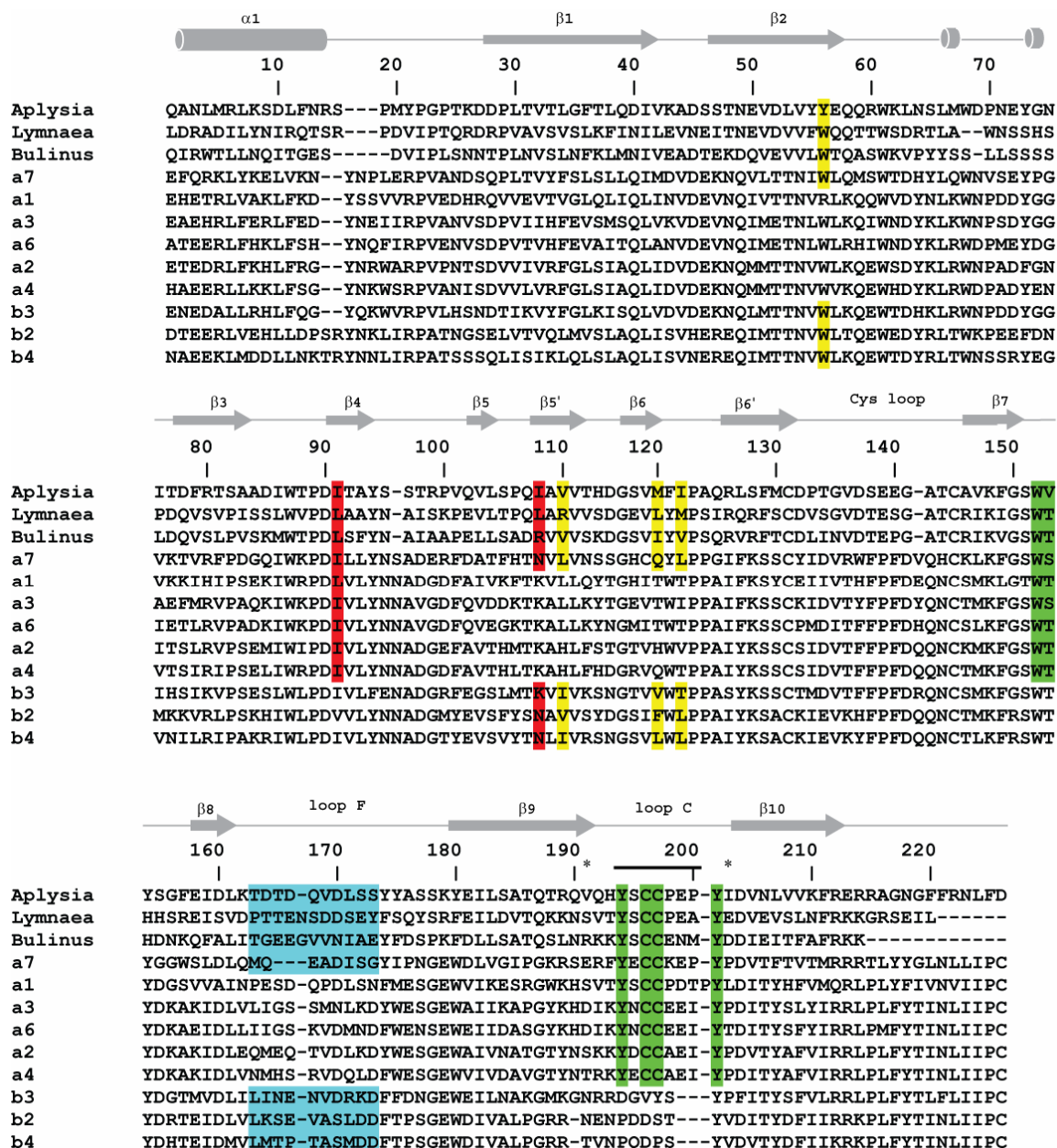


Figure VII.2: Alignment of nAChR subtypes with AChBP and potential selective residues. Conserved residues of the ligand binding pocket are on yellow and green background of the + and - subunit interface respectively. The residues on the F loops with potential to interact with the ligand binding pocket are highlighted in cyan. Red residues are agonist specific residue determinants for lobeline and epibatidine.

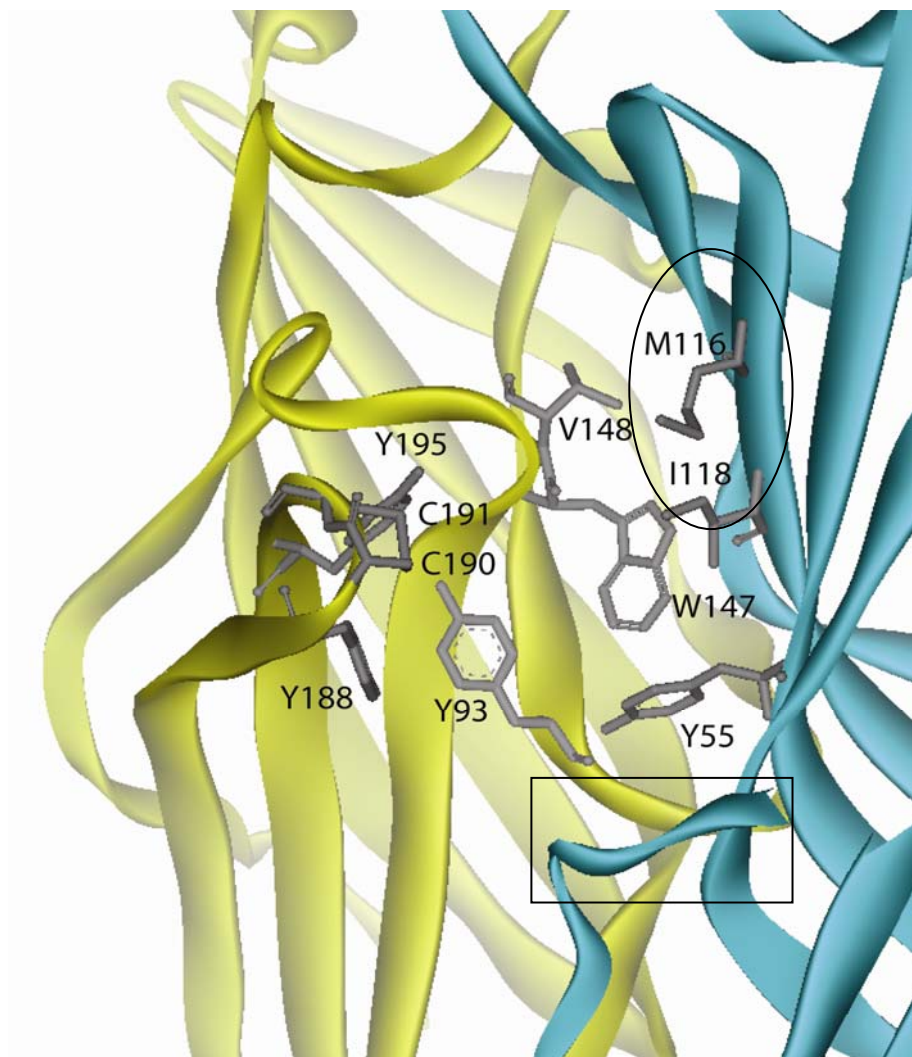


Figure VII.3: The competitive ligand binding pocket. Residues that are common to all competitive ligand binding are highlighted and numbered with *Aplysia* AChBP numbering. Residues in the binding pocket that are not well conserved are circled. Residues not in the pocket but that might be targeted for agonists are boxed.

determinants in nAChRs. α -Conotoxin ImI is selective for receptor subtype and future studies using mutagenesis will likely show which residues govern α -conotoxin ImI selectivity.

Agonism is also linked to a structural basis in that the C loop packs tightly on the ligand binding pocket to surround the ligand. Agonists must accommodate to limited space in the pocket. Most of the residues in the pocket are conserved among all subtypes. A few residues on the apical side of the C loop and the F loop have variability among the different species. These regions will likely play a large role in developing receptor subtype selective agonists. A recent structure of Anabaseine with the binding protein supports this hypothesis (Ryan Hibbs, unpublished data).

2. Competitive Ligand-Binding Pocket Energetics

Ligands that bind within the competitive pocket with picomolar K_d values reveal very few electrostatic interactions. Developing a model that is not strictly charge dependant will be vital to successful computational analysis of AChBPs, nAChR, and their ligand interactions. Structural-guided drug design based on atomic coordinates still requires the partitioning of energetics of ligand binding into electrostatic, hydrophobic and directed hydrogen bond components and mandates sound theories for all types of interaction, including hydrophobic ones.

F. Conformations and Receptor Activation

A ligand binding domain for an ion channel was solved for the first time in three conformational states; apo, agonist and antagonists bound states. Previous studies were limited to the conformation with agonist (12). The largest structural differences are found in the C loop (Figure VII.4). In the apo structure the C loop is 7.3 Å radially extended

from the position of agonists. Large peptide toxins, α -cobratoxin and α -conotoxin ImI, displace the C loop more radial than apo differing by up to 11 Å from its agonist bound position. A hinge region for the C loop was defined at residues V185 and I196 (*Aplysia* numbering). Other conformational differences were very small <1.0 Å. The cys loop is positioned in full length receptors to interact with the transmembrane domain. Measurement of pore diameter showed a small but statistically significant decrease of 1.0 Å at the cross section of the cys loop. Conformations simulated from altering between agonist and antagonist structures indicate a small torsion of the subunit. A summary of the conformational changes is depicted in Figure VII.5C. When viewed from the side the core beta sheets move from an hourglass shape to a slightly more cylindrical shape upon binding of agonist. These conformational changes correlate to a recent computational study of the $\alpha 7$ receptor modeled from AChBP (Taly et al. 2005). Agonist binding led to a bending at the subunit interface, torsion, and a pivot point at the Cys loop. The Cys loop moved slightly (<1.0 Å) toward the pore. Pivoting on the Cys loop, the transmembrane domain underwent large conformational changes resulting in an opening of the ion-channel (14). Combining these data, agonist binding results in a large radial closing of the C loop, torsion, and small movements at the Cys membrane loop. The transmembrane domain pivots about the Cys loop with torsion and large conformational changes opening the ion-channel.

G. Structural Basis of Partial Agonism

Rigid-body movements of the C loop make possible a structural model for partial agonism. A partial agonist must accommodate aspects of both agonists and antagonists. At least two possible mechanisms exist. One, the C loop might assume an intermediate

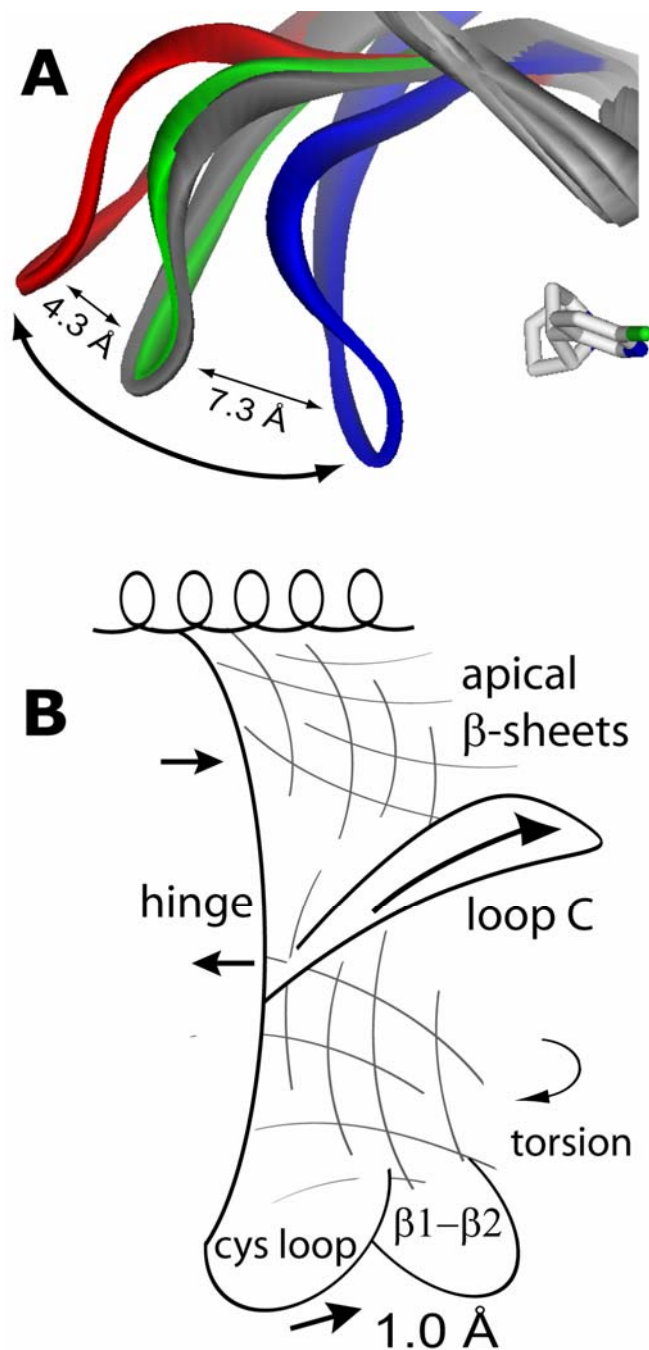


Figure VII.4 Residue and loop positions of AChBP. **(A)** The C loop caps the ligand binding pocket and is displaced up to 11 Å. **(B)** Cartoon of the positional changes found in the various domains of AChBP. Movements in the ligand binding domain upon binding of agonists are shown with arrows. The C loop moves inward causing the pore diameter at loop C to decrease by 1 Å. A slight counter clockwise torsion is observed and the beta sheets move from an hour glass shape to slightly more cylindrical.

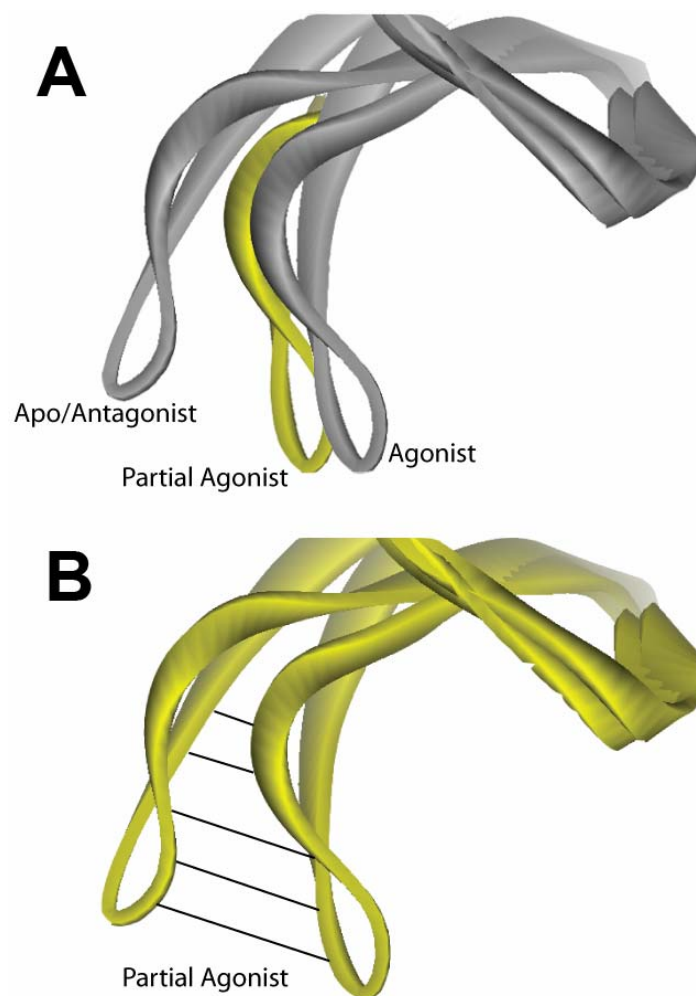


Figure VII.5 Model for partial agonism Possible loop C conformations of a partial agonist are shown in yellow. (A) A rigid partial agonist is shown at an intermediate position between apo/antagonists and agonists loop C conformations. Grayed C loops of apo/antagonists and agonists are shown for reference (B) Loop C conformations of a partial agonist that loosely associates with the C loop. Lines depict multiple conformations possible while a partial agonist is bound in the ligand binding pocket.

position between that of Apo and agonist (Figure VII.5A). Or two, the ligand might have high affinity for the subunit interface with relatively low affinity for the C loop allowing it to occupy multiple conformation with ligand bound (Figure VII.5B). The amount of agonism would be proportional to the probability that the C loop occupies the radially packed position. A small ligand could allow the C loop to close radially but not with such favorable C loop interactions as to always induce the closed C loop conformation. In this manner, 100% occupancy of the binding pocket results in only partial channel opening

H. Future Implications

The acetylcholine binding protein still has structural information waiting to be explored. The non-competitive site is yet to be defined. A crystal structure will likely reveal this site and given the ease of crystallization it will likely be generated with the *Aplysia* protein. Other investigations relate to molecular weight will benefit from the GnTI expressed proteins including hydrogen deuterium exchange, NMR, protein hydrodynamics, and time resolved fluorescence.

The acetylcholine binding protein has been the primary template for structural studies in the entire cys loop family of ligand gated ion channels including nAChRs, GABA, serotonin, and glycine receptors. It is likely that the ligand binding domains of these receptors will be generated as soluble entities in a manner similar to AChBP. If not, AChBP can be mutated to make the ligand binding pockets resembling each related protein. Once soluble the nAChR ligand binding domains will have unique recognition capacities and the knowledge gained from these studies will greatly facilitate expression, purification, and monitoring of ligand binding.

I. References

1. Hansen, S. B., Radic, Z., Talley, T. T., Molles, B. E., Deerinck, T., Tsigelny, I., and Taylor, P. (2002) *J Biol Chem* **277**, 41299-41302
2. Smit, A. B., Syed, N. I., Schaap, D., van Minnen, J., Klumperman, J., Kits, K. S., Lodder, H., van der Schors, R. C., van Elk, R., Sorgedragter, B., Brejc, K., Sixma, T. K., and Geraerts, W. P. (2001) *Nature* **411**, 261-268
3. Celie, P. H., Klaassen, R. V., van Rossum-Fikkert, S. E., van Elk, R., van Nierop, P., Smit, A. B., and Sixma, T. K. (2005) *J Biol Chem* **280**, 26457-26466
4. Hansen, S. B., Talley, T. T., Radic, Z., and Taylor, P. (2004) *J Biol Chem* **279**, 24197-24202
5. Reeves, P. J., Callewaert, N., Contreras, R., and Khorana, H. G. (2002) *Proc Natl Acad Sci U S A* **99**, 13419-13424
6. Sulzenbacher, G., Gruez, A., Roig-Zamboni, V., Spinelli, S., Valencia, C., Pagot, F., Vincentelli, R., Bignon, C., Salomoni, A., Grisel, S., Maurin, D., Huyghe, C., Johansson, K., Grassick, A., Roussel, A., Bourne, Y., Perrier, S., Miallau, L., Cantau, P., Blanc, E., Genevois, M., Grossi, A., Zenatti, A., Campanacci, V., and Cambillau, C. (2002) *Acta Crystallogr D Biol Crystallogr* **58**, 2109-2115
7. Celie, P. H., Kasheverov, I. E., Mordvintsev, D. Y., Hogg, R. C., van Nierop, P., van Elk, R., van Rossum-Fikkert, S. E., Zhmak, M. N., Bertrand, D., Tsetlin, V., Sixma, T. K., and Smit, A. B. (2005) *Nat Struct Mol Biol* **12**, 582-588
8. Celie, P. H., van Rossum-Fikkert, S. E., van Dijk, W. J., Brejc, K., Smit, A. B., and Sixma, T. K. (2004) *Neuron* **41**, 907-914
9. Unwin, N. (2005) *J Mol Biol* **346**, 967-989
10. Miyazawa, A., Fujiyoshi, Y., and Unwin, N. (2003) *Nature* **423**, 949-955
11. Bouzat, C., Gumilar, F., Spitzmaul, G., Wang, H. L., Rayes, D., Hansen, S. B., Taylor, P., and Sine, S. M. (2004) *Nature* **430**, 896-900
12. Brejc, K., van Dijk, W. J., Klaassen, R. V., Schuurmans, M., van Der Oost, J., Smit, A. B., and Sixma, T. K. (2001) *Nature* **411**, 269-276
13. Hansen, S. B. S., G.; Huxford, T.; Marchot, P.; Taylor, P.; and Bourne, Y. (2005) *Embo J* in press

14. Taly, A., Delarue, M., Grutter, T., Nilges, M., Le Novere, N., Corringer, P. J., and Changeux, J. P. (2005) *Biophys J* **88**, 3954-3965